

UC Berkeley

UC Berkeley Electronic Theses and Dissertations

Title

Characterizing Air Pollution Sources Through Speciated Measurements of Organic Carbon Across 15 Orders of Magnitude of Volatility

Permalink

<https://escholarship.org/uc/item/8wf301q3>

Author

Wernis, Rebecca A

Publication Date

2022

Peer reviewed|Thesis/dissertation

Characterizing Air Pollution Sources Through Speciated Measurements of Organic Carbon
Across 15 Orders of Magnitude of Volatility

By

Rebecca A Wernis

A dissertation submitted in partial satisfaction of the

requirements for the degree of

Doctor of Philosophy

in

Engineering – Civil and Environmental Engineering

in the

Graduate Division

of the

University of California, Berkeley

Committee in charge:

Professor Allen H. Goldstein, Chair

Professor Robert A. Harley

Professor Inez Fung

Summer 2022

Characterizing Air Pollution Sources Through Speciated Measurements of Organic Carbon
Across 15 Orders of Magnitude of Volatility

Copyright 2022

by

Rebecca A Wernis

Abstract

Characterizing Air Pollution Sources Through Speciated Measurements of Organic Carbon Across 15 Orders of Magnitude of Volatility

by

Rebecca A Wernis

Doctor of Philosophy in Civil and Environmental Engineering

University of California, Berkeley

Professor Allen H. Goldstein, Chair

Organic carbon in the atmosphere fuels the formation of ozone and comprises a large fraction of fine particulate matter, both of which are detrimental to human health. Particulate matter additionally is a source of uncertainty in radiative forcing predictions, hindering predictions of climate change impacts. Atmospheric organic carbon is complex, consisting of thousands of different compounds and covering more than 15 orders of magnitude in volatility (vapor pressure) and widely varying chemical reactivity. Many of these compounds serve as specific indicators of pollution sources or atmospheric chemical processes. In this work, two different advanced custom instruments for measurement of speciated volatile, intermediate volatility and semivolatile organic compounds (VOCs, IVOCs and SVOCs) are used to elucidate and profile the sources of pollution in distinct atmospheric environments. One of these instruments is introduced for the first time along with its design and development details.

Chapter 2 presents a suite of semivolatile markers of fresh biomass burning (BB) measured at a rural site in Amazonia, Brazil by the Semivolatile Thermal desorption Aerosol Gas chromatograph (SV-TAG), which specializes in hourly speciated measurements of IVOCs and SVOCs and their partitioning between the gas and particle phases. These 16 markers are found to comprise the majority of fresh BB organic aerosol. Despite much greater concentrations in the dry season versus the wet season, the BB markers comprise about the same fraction of total organic aerosol in both the dry and wet seasons. Composition of individual BB events and atmospherically aged air parcels were highly variable but provide a chemical profile of fresh BB in the Amazon.

By combining traditional speciated VOC measurement instrumentation with the SV-TAG, the Comprehensive Thermal desorption Aerosol Gas chromatograph (cTAG) is sensitive to a wider range of volatility of reactive organic carbon. cTAG joins a layered bed of adsorbents for VOC and IVOC collection and a reusable metal mesh filter for SVOC collection together before a single mass spectrometer, providing consistent quantification across the volatility range. Chapter 3 presents design and development details for cTAG, including VOC and IVOC collector design optimization, performance of a custom liquid evaporation system for VOCs and IVOCs, and verification that ozone removal is effective while not perturbing measured concentrations of nonreactive compounds. Potential applications of this instrument are presented using a brief analysis of field data.

Chapter 4 analyzes major sources of pollution in suburban Livermore, California using measurements of 123 VOCs, IVOCs and SVOCs collected by cTAG. Positive Matrix Factorization on the generated timelines yields 13 distinct factors representing different sources and processes in the atmosphere, including gasoline exhaust, consumer products, biomass burning, secondary oxidation, emissions from evaporative sources and more. Monoterpenoid mass was present in greater quantities in the consumer product factor than biogenic sources, consistent with recent observations in other urban contexts. Several factors contained significant mass from measurements on both channels of cTAG, indicating that the expanded volatility range afforded by cTAG led to more complete chemical characterization of those sources.

The final chapter notes directions for future research and explores measurement and analysis opportunities for cTAG.

Table of Contents

1	Introduction.....	1
1.1	Scientific background.....	1
1.2	Overview of this work.....	2
2	Diel and seasonal variability of semivolatile biomass burning markers in the dry and wet seasons in Amazonia.....	5
	Abstract.....	5
2.1	Introduction.....	5
2.2	Experimental methods.....	6
2.2.1	Green Ocean Amazon (GoAmazon 2014/5) field campaign: T3 site description.....	6
2.2.2	Deployment of a Semivolatile Thermal desorption Aerosol Gas Chromatograph (SV-TAG).....	7
2.2.3	Supporting measurements.....	9
2.3	Results and discussion.....	9
2.3.1	Biomass burning markers measured and quantified with SV-TAG.....	9
2.3.2	Seasonality.....	11
2.3.3	Strong agreement with AMS PMF BBOA factors.....	12
2.3.4	Diurnal variability.....	13
2.3.5	Variability in composition during BB events.....	15
2.4	Conclusion.....	15
2.5	Acknowledgments.....	17
3	Development of an in situ dual-channel thermal desorption gas chromatography instrument for consistent quantification of volatile, intermediate-volatility and semivolatile organic compounds.....	18
	Abstract.....	18
3.1	Introduction.....	18
3.2	Description of instrument.....	21
3.2.1	Inlet and I/VOC channel.....	21
3.2.2	SVOC channel.....	23
3.2.3	Miniature gas chromatographs.....	24
3.2.4	High resolution time of flight mass spectrometer.....	24
3.2.5	Calibration.....	25
3.2.6	Instrument operation.....	26
3.2.7	Data processing.....	27

3.3	System evaluation	27
3.3.1	I/VOC collector breakthrough tests	27
3.3.2	Dynamic dilution system testing.....	28
3.3.3	Limits of detection	31
3.3.4	Evaluation of ozone removal on the I/VOC channel	31
3.3.5	Region of sensitivity overlap.....	34
3.3.6	Measurements of ambient air	35
3.4	Summary and concluding remarks.....	40
3.5	Acknowledgments.....	41
4	Source apportionment of VOCs, IVOCs and SVOCs by positive matrix factorization in suburban Livermore, California	42
	Abstract	42
4.1	Introduction.....	42
4.2	Methods	44
4.2.1	Sampling site.....	44
4.2.2	cTAG measurements of VOCs, IVOCs and SVOCs	44
4.2.3	Positive matrix factorization	47
4.3	Results and discussion.....	48
4.3.1	Positive matrix factorization solution.....	49
4.3.2	Factor 1: Long-lived and continuously emitted compounds	55
4.3.3	Factor 2: Episodic petrochemical source	57
4.3.4	Factor 3: Gasoline	59
4.3.5	Factor 4: Oxidized urban and temperature-driven emissions.....	60
4.3.6	Factor 5: Consumer products	63
4.3.7	Factor 6: Primary biogenic and diesel.....	64
4.3.8	Factor 7: Parachlorobenzotrifluoride (PCBTF).....	65
4.3.9	Factor 8: Secondary oxidation and persistent personal care product emissions...	65
4.3.10	Factor 9: Biomass burning	67
4.3.11	Factor 10: Industrial and/or agricultural background and continuous combustion source	68
4.3.12	Factor 11: Early morning cooking/diesel event.....	68
4.3.13	Factor 12: Isoprene	69
4.3.14	Factor 13: Possible jet fuel event.....	70

4.4	Conclusion	71
4.5	Acknowledgments.....	72
5	Future work	73
	Appendix A: Miniature gas chromatograph development.....	75
	Appendix B: Supporting information for source apportionment of VOCs, IVOCs and SVOCs in Livermore	77
B.1	Precision uncertainty histograms.....	77
B.2	PMF evaluation of different factor solutions.....	79
B.2.1	Q/Q_{exp}	79
B.2.2	Beyond 13 factors: bootstrapping results	80
B.2.3	FPEAK rotation	80
B.3	Factor apportionment of VOCs, IVOCs and SVOCs	82
B.4	Isoprene to benzene emission factors in gasoline exhaust	83
	References	84

List of Figures

Figure 2.1. Stacked timeline of (a) dry and (b) wet season gas + particle measurements of the 16 reported biomass burning markers measured by SV-TAG.	11
Figure 2.2. (a) The particle phase only sum of the BB markers plotted against total OA measured by the AMS in the dry season (orange) and wet season (blue).	12
Figure 2.3. The particle phase only sum of the BB markers vs (a) the AMS LO-BBOA PMF factor from the dry season, (b) the AMS MO-BBOA PMF factor from the dry season and (c) the AMS BBOA PMF factor from the wet season.	13
Figure 2.4. Diel plots of gas + particle concentrations in ng m^{-3} of the 16 BB markers in the dry season.	14
Figure 2.5. (a) Mean composition of the 7 periods of fresh emissions vs that of the 4 periods of slightly aged and/or more oxidized BB emissions. (b) Composition of individual periods of fresh and aged emissions.	16
Figure 3.1. Schematic of cTAG.	22
Figure 3.2. Schematic of I/VOC collector.	23
Figure 3.3. Schematic of dynamic dilution system for VOC and IVOC calibration.	26
Figure 3.4. Calibration curves with R^2 values for (a) benzene, (b) o-xylene, (c) α -pinene and (d) β -caryophyllene	30
Figure 3.5. Results of evaluation of effectiveness of sodium thiosulfate filter in mitigating the effects of ozone on reactive analytes during collection of VOCs and IVOCs.	33
Figure 3.6. Bornyl acetate measured on the I/VOC and SVOC channels of cTAG during FIREX-AQ.	35
Figure 3.7. Example chromatograms from cTAG.	37
Figure 3.8. Concentration timelines for naphthalene, a primary emission from vehicle exhaust measured on cTAG's I/VOC channel, and the sum of phthalic anhydride and phthalic acid, secondary photooxidation products of naphthalene detected on cTAG's SVOC channel.	38
Figure 3.9. Pearson's R correlation matrix for a suite of petroleum-derived compounds observed by cTAG in Livermore, California between 11 April and 21 April 2018, ordered by volatility.	39
Figure 3.10. Timelines for characteristic species from each of the three main groupings of compounds evident in the correlation matrix.	40
Figure 4.1. 13 factor solution factor timelines.	54
Figure 4.2. 13 factor solution factor profiles.	55
Figure 4.3. Diurnal profiles of the factor timelines in the 13 factor solution.	56
Figure 4.4. (a) Time series of wind speed and direction, (b) time series of temperature (left axis) and ozone (right axis) measured at the Bay Area Air Quality Management District monitoring site, and (c) all factor timelines stacked.	57
Figure 4.5. Rose plots, showing the correlation of emissions and wind direction, of each factor using only data points where the concentration was elevated	58
Figure 4.6. Timelines of select alkanolic acids (left axis) and temperature (right axis) for the study period.	61
Figure 4.7. Timelines of nitrophenol isomers (left axis) and temperature (right axis) for the study period.	62
Figure 4.8. Correlation of isoprene and benzene between 22:00 and 05:30 LT	70

Figure A.1. Schematic and photo of miniature gas chromatographs.....	75
Figure A.2. Demonstration of reproducibility of temperature ramps on the miniature gas chromatographs.....	76
Figure B.1. Relative standard deviations of all internal standard ratios used in this study.	78
Figure B.2. Example distribution of relative ratios of internal standards	78
Figure B.3. (a) Q/Q_{exp} for different numbers of factors. (b) % reduction in Q/Q_{exp} as the number of factors is increased.	79
Figure B.4. Q/Q_{exp} for different values of the FPEAK parameter.	80
Figure B.5. Pearson's r for the cross correlation between every pair of factors in the 13 factor solution, along with the mean r for each FPEAK value.....	81
Figure B.6. (a) Fraction of average mass from each cTAG measurement channel in each factor. (b) Fraction of the average total mass of compounds measured on each channel found in each factor.	82
Figure B.7. The ratio of isoprene to benzene emission factors (EF) (mg (kg Fuel)^{-1}) for cold-start emissions for a wide range of vehicle classes	83

List of Tables

Table 2.1. Mean concentration and partitioning data for biomass burning markers measured by SV-TAG as well as NR-PM ₁ and OA	10
Table 3.1. Composition of different I/VOC collectors and corresponding breakthrough volumes for some of the most volatile target compounds.....	29
Table 3.2. Limits of detection (LOD) for a selection of linear, branched and aromatic hydrocarbons on the I/VOC channel of cTAG.....	32
Table 4.1. Compounds measured by cTAG and included in the PMF analysis.	49
Table B.1. Summary of internal standard assignments for normalization of ambient compounds in this analysis and the precision uncertainty incurred from each assignment.....	79

Acknowledgments

This work represents much more than the effort of one person. I'd like to thank the following people for their especially significant contributions to this work and my development as a scientist:

Allen Goldstein, for the years of guidance and mentorship he provided, and for providing me with the opportunity I wanted most: getting in the lab and building something new.

Nathan Kreisberg, who was basically a second adviser, mentor and friend to me for large portions of my tenure as a graduate student as cTAG became a reality.

Lindsay Yee, who taught me the nuts and bolts of gas chromatography – mass spectrometry analysis when I was just starting out as a graduate student, patiently mentored me in the operation of SV-TAG during GoAmazon and drank coconut water with me straight from the coconut.

Gabriel Isaacman-VanWertz, for his occasional mentorship, innovations on SV-TAG, and the analysis software he wrote to make it easier to deal with all that data. Not to mention for letting me move into his office before he had technically graduated.



Lindsay (left) and me preparing to drink coco gelado (chilled coconut water) at the GoAmazon field site.

1 Introduction

1.1 Scientific background

Atmospheric organic carbon exists in trace quantities but has a complex and disproportionate impact on human well-being and the environment. Reactive organic carbon (ROC), including volatile organic compounds (VOCs), lower volatility organic gases and organic particulate matter (PM) and excluding methane, causes adverse impacts on human health (Srivastava et al., 2005; Nurmatov et al., 2013; Brunekreef and Holgate, 2002; Nel, 2005; Pope and Dockery, 2006; Lippmann and Chen, 2009) and significantly impacts the planet's radiation balance, a crucial factor in predicting the effects of climate change (Kanakidou et al., 2005; Myhre et al., 2013; Shrivastava et al., 2017). Gas phase ROC consists of thousands of VOCs, intermediate volatility organic compounds (IVOCs) and semivolatile organic compounds (SVOCs), with the diversity of possible species increasing exponentially as the number of carbon atoms increases (Goldstein and Galbally, 2007). These compounds undergo oxidation reactions and condense to form secondary organic aerosol (SOA), by mass the largest type of PM in the atmosphere globally (Zhang et al., 2007; Heald and Kroll, 2020). With thousands of possible precursor compounds and a single organic compound able to form potentially thousands of oxidation products (Aumont et al., 2013), SOA is an exceedingly complex mixture, making it especially challenging to characterize or predict its effects on human health and the environment (Shrivastava et al., 2017).

IVOCs and SVOCs have recently been recognized as a likely source of substantial organic aerosol (OA) mass (Hodzic et al., 2010; Robinson et al., 2007a; Weitkamp et al., 2007) and have been demonstrated to have a high potential to form SOA (Chan et al., 2009a; de Gouw et al., 2011; Lim and Ziemann, 2009; Presto et al., 2010; Zhao et al., 2014). Moreover, they make up a significant fraction of ROC (Robinson et al., 2007a; Hunter et al., 2017). Due to their propensity to condense on surfaces inside instruments, measurement of IVOCs and SVOCs in the atmosphere is especially challenging (Goldstein and Galbally, 2007; Hunter et al., 2017; Isaacman-VanWertz et al., 2018; Heald and Kroll, 2020), and advancements in instrumentation have only recently occurred enabling their widespread comprehensive field measurement (Zhao et al., 2013; Isaacman et al., 2014; Lopez-Hilfiker et al., 2014; Martinez et al., 2016; Cropper et al., 2017; Ren et al., 2019). Temporally resolved field measurements of speciated IVOCs and SVOCs in a variety of atmospherically distinct environments are still needed and remain an active area of current research (Heald and Kroll, 2020).

In addition to advancing predictions of SOA formation, speciated IVOCs and SVOCs can serve as valuable marker compounds for specific pollution sources and atmospheric processes. For example, levoglucosan and its isomers are unique markers of biomass burning influence (Simoneit, 2002), a fact which underpins the analysis and interpretations in Chapter 2. While VOC markers of biomass burning exist, they are produced during other combustion processes as well and thus cannot serve as definitive biomass burning indicators without further context (Yokelson et al., 1997; Schauer et al., 1999a, b, 2001, 2002a; Akagi et al., 2011). Other primary IVOC and SVOC emissions mark specific sources such as sesquiterpenes from vegetation (Duhl et al., 2008), bis-(2-ethylhexyl) adipate and other phthalates from plasticizers (Liu and Little, 2012; Bui et al., 2016; Shi et al., 2018), or palmitic and stearic acids from cooking (Rogge et al., 1991; Nolte et al.,

1999; Schauer et al., 2002a). Secondary IVOCs and SVOCs serve as tracers for oxidation from specific precursors, such as phthalic acid for naphthalene oxidation (Wang et al., 2007; Chan et al., 2009a; Kleindienst et al., 2012) or myriad biogenic VOC oxidation products (Jaoui et al., 2005, 2007; Claeys et al., 2007, 2009; Chan et al., 2010). Quantification of tracer compounds can be used to assess the impact of different sources and inform the prioritization of pollution mitigation strategies.

Continuing and improving measurements of VOCs in addition to their lower volatility counterparts remains crucial to our understanding of pollution sources and SOA formation potential. VOCs are critical SOA precursors (Seinfeld and Pankow, 2003; Ervens et al., 2011) that are generally emitted in greater quantities than their less volatile counterparts on a specific compound basis (Fraser et al., 1997, 1998). Their oxidation governs the formation of tropospheric ozone (Atkinson and Arey, 2003). Furthermore, their abundance is closely linked with that of oxygenated IVOCs and SVOCs through atmospheric chemistry, so a complete snapshot of the atmospheric oxidation process requires measurement of VOCs as well. Additionally, in urban areas, major sources of VOCs are changing as pollution controls on vehicles increase the relative importance of non-motor-vehicle ROC (Warneke et al., 2012; McDonald et al., 2013, 2018; Coggon et al., 2021); ongoing measurements are required to assess these newly important sources. To gain the clearest picture of sources and chemical processes predominant in a given environment, measurements of ROC across the volatility range from VOCs to SVOCs are needed.

The ROC volatility range spans over 15 orders of magnitude of vapor pressure (Jimenez et al., 2009; Donahue et al., 2011). This enormous range of volatility combined with the varied functionality afforded by the chemical complexity contained therein represents an important research challenge for state-of-the-art detection methodology. Over the past few decades, substantial progress has been made in atmospheric instrumentation to characterize this complexity. Sample collection on adsorbent beds (for VOCs) or filters (for PM) followed by offline analysis by thermal desorption into a gas chromatograph (GC) coupled to a mass spectrometer (MS) affords high chemical specificity but usually low temporal resolution limited by sample extraction techniques that demand large sample sizes. Automated in situ field-deployable GC-MS instruments increase the time resolution to timescales more relevant for atmospheric processes (i.e. hourly measurement or faster) (Gentner et al., 2012; Goldstein et al., 1995; Goldan et al., 2004; Hopkins et al., 2003; Lamanna and Goldstein, 1999; Lerner et al., 2017; Millet et al., 2005; Williams et al., 2006). Particle-phase measurements have been extended to include first low-polarity gas-phase IVOCs and SVOCs (Zhao et al., 2013) and later more polar species via implementation of online derivatization (Isaacman et al., 2014). With these advancements, speciated measurements of ROC across the full volatility range are collected by collocating multiple instruments at a single site.

1.2 Overview of this work

This work explores speciated ROC to infer and describe their sources in different environments and expands the instrumentation arsenal used to detect them. Chapter 2 focuses on a suite of SVOCs that are known markers of fresh biomass burning (BB) emissions. Using measurements from a Semivolatile Thermal desorption Aerosol Gas chromatograph (SV-TAG), mean concentrations and partitioning of 16 BB markers are presented from a rural field site in

Amazonia, Brazil during both the dry and wet seasons. Fresh BB accounts for approximately the same fraction of OA in both the dry and wet seasons, despite greatly increased BB activity and BB marker concentrations in the dry season. The particle phase fraction of the quantified BB markers correlates strongly with and accounts for most of the mass of BB-related portions of OA as determined by an independent analysis of coincident aerosol mass spectrometer measurements. No significant differences were found between marker profiles of time periods experiencing elevated fresh emissions versus suspected periods that have undergone atmospheric aging, but the reported markers nonetheless represent a relatively complete chemical profile of fresh BB in the Amazon for modeling purposes. 4-Hydroxybenzoic acid is inferred to have an additional major source, suggesting its use as a marker of BB may be inaccurate in some environments.

Achieving the goal of comprehensive measurements of ROC across the relevant volatility range, Chapter 3 presents the Comprehensive Thermal desorption Aerosol Gas chromatograph (cTAG), a new field-deployable instrument that provides consistent quantification of VOCs, IVOCs and SVOCs at hourly time resolution and gas-particle partitioning of SVOCs every other hour. cTAG employs two separate collection, thermal desorption and GC analysis channels joined to a single high-resolution time of flight MS. One channel (the “I/VOC channel”) collects C₅ through C₁₆ alkane-equivalent volatility VOCs and IVOCs on a layered bed of adsorbents while the other channel (the “SVOC channel”) collects C₁₄ through C₃₂ IVOCs and SVOCs on a reusable high-surface area metal mesh filter cell, based on SV-TAG. I/VOC channel collector optimization design details are presented, and calibration curves generated using a newly developed custom liquid evaporation system for the I/VOC channel are found to agree within 5% of those produced using a gas cylinder. The addition of an ozone removal filter upstream of the I/VOC collector improves recovery of highly ozone reactive sesquiterpenes without incurring losses of other compounds. A quantification comparison for a compound detected on both channels shows agreement within 11% on average. Finally, a brief analysis of field data from Livermore, California demonstrates some of the analytical capabilities of this instrument.

Chapter 4 applies the advancements described in Chapter 3 to more completely characterize sources of pollution in a suburban setting. Measurements of 123 VOCs, IVOCs and SVOCs from cTAG in springtime in Livermore, California are source-separated using positive matrix factorization, a mathematical technique that apportions measured compound mass into source profiles based on temporal covariance. The 13 factor solution best resolves the pollution sources, with major source categories including gasoline exhaust, consumer product emissions, biomass burning, secondary oxidation and emissions from evaporative sources. Monoterpenoid compounds were most strongly associated with consumer product emissions rather than biogenic sources, consistent with recent findings that emissions of monoterpenes from fragrances in consumer products far exceed those from biogenic sources in urban contexts (Coggon et al., 2021). Several factors contained mass from compounds spanning cTAG’s measured volatility range. For example, the consumer products factor, which predominantly contains VOCs, also had major contributions from the IVOCs methyl salicylate (from wintergreen oil) and α -isomethyl ionone (floral compound used in cosmetics and personal care products) measured on the SVOC channel of cTAG, demonstrating the enhanced source characterization possible with cTAG.

Finally, future research opportunities are described in Chapter 5, ranging from expanding the body of literature that supports and aids interpretation of speciated ROC measurements to specific applications of and analysis techniques for cTAG.

2 Diel and seasonal variability of semivolatile biomass burning markers in the dry and wet seasons in Amazonia

Abstract

Biomass burning (BB) from deforestation and other human activities in the Amazon basin impacts precipitation patterns and human air pollution exposure on a regional scale. The BB process emits semivolatile organic compounds that act as unique source markers and comprise a significant fraction of the organic mass emitted from fires. As part of the Green Ocean Amazon (GoAmazon 2014/5) field campaign, we deployed a Semivolatile Thermal desorption Aerosol Gas Chromatograph (SV-TAG) instrument at the rural T3 site west of Manaus, Brazil in both the dry and wet seasons to measure hourly concentrations of semivolatile organic compounds in the gas and particle phases. We quantified 16 markers of BB with mean concentrations between 0.1 and 400 ng m⁻³. The total concentration of these markers is 13 times greater in the dry season than the wet season. When comparing with positive matrix factorization of the organic aerosol mass spectra from an aerosol mass spectrometer, we found that the particle phase fraction of the measured markers explains 86% of the variability in the BB factors related to fresh emissions. In the dry season, the markers also accounted for 96% of the mass of fresh BB emissions. Diurnal variability of BB markers is pronounced, with mean concentrations up to 10 times larger at night than during the day. Relative ratios of these markers varied significantly between periods of high BB influence as well as during periods identified as having more aged emissions, but the averaged composition provides a representation of primary biomass burning markers that may be useful for modeling of Amazonian fire emissions. We explore the factors contributing to the seasonal and diurnal changes observed. This work enhances our understanding of semivolatile BB marker contributions to the Amazonian regional burden of particulate matter pollution.

2.1 Introduction

Globally, human activities have complex effects on the amount and composition of particulate matter (PM) in the atmosphere. Better understanding of the sources, transformation and fate of PM is needed to improve predictions of the effects of PM on climate change through changes in radiative forcing (Shrivastava et al., 2017; Myhre et al., 2013; Kanakidou et al., 2005) and the negative impacts of PM on human health (Brunekreef and Holgate, 2002; Donaldson and Tran, 2002; Nel, 2005; Lippmann and Chen, 2009; Anderson et al., 2012; Kim et al., 2015). Biomass burning (BB) is a major direct source of PM, especially submicron PM (PM₁), a large fraction of which is organic (Bond et al., 2004; De Gouw and Jimenez, 2009). Additionally, BB can contribute to PM indirectly through emission of gas phase organic compounds that can react to form secondary organic aerosol (SOA) (Donahue et al., 2009; Akherati et al., 2020), a major subcategory of PM₁ (Murphy et al., 2006; Zhang et al., 2007; Jimenez et al., 2009).

In the Amazon basin, BB is predominantly a result of human activities, in particular, land clearing for agricultural uses and the burning of wood for fuel (Davidson et al., 2012; van Marle et al., 2017). Aerosol emissions from these activities impact cloud formation and precipitation regionally (Andreae et al., 2004; Koren et al., 2008). The burning is most frequent in the dry season (August through October) (Artaxo et al., 2013; Martin et al., 2016) which is characterized

by greatly reduced precipitation ($\approx 75\%$ lower) (INMET, 2022; Carneiro and Fisch, 2020) and on average 2°C warmer temperatures (Alves et al., 2016; INMET, 2022). Between the wet and dry seasons a ≈ 10 -fold increase in PM_{10} concentration is typically observed and has been commonly ascribed to the impact of BB (Artaxo et al., 1994, 2002, 2013; Holben et al., 1996).

To enable better predictions of and mitigation strategies for the impact of BB on particulates, it is necessary to (1) distinguish BB emissions from other pollution sources and (2) understand their composition. In addition to the emissions of primary combustion products carbon dioxide and carbon monoxide, BB emits thousands of distinct gas- and particle-phase organic compounds from incompletely combusted fuels. Smoldering conditions in particular, which are characterized by a greater fraction of incomplete combustion, produce larger quantities of semivolatile organics compared to flaming conditions during which more complete combustion occurs (Akagi et al., 2011; Hosseini et al., 2013; Jen et al., 2019). Among the organic compounds emitted, many molecular marker species have been identified that are specific to biomass combustion but which have differing volatility and chemical reactivity under atmospheric conditions (Rogge et al., 1998; Andreae and Merlet, 2001; Nolte et al., 2001a; Schauer et al., 2001; Simoneit, 2002; Iinuma et al., 2007; Akagi et al., 2011; Hatch et al., 2015; Bertrand et al., 2018; Jen et al., 2019). These compounds serve as useful indicators of BB influence and some are emitted in large enough quantities to affect local and regional PM mass concentrations.

In this work we characterize a subset of the semivolatile organic carbon emissions from Amazonian biomass burning over a ≈ 1.5 -month period in each of the dry and wet seasons. We report concentrations and gas-particle partitioning of 16 distinct sugar, methoxyphenol, nitrophenol and carboxylic acid markers of BB on an hourly time basis. The seasonal and diurnal variability is explored in the context of local meteorology and land use practices, the specific chemical characteristics of the included markers, and the total organic aerosol (OA) mass concentration. The total concentration of the markers is compared to the total biomass burning organic aerosol (BBOA) fraction as determined by positive matrix factorization analysis. Finally, specific periods of elevated BB influence are compared with possible periods of more aged BB influence. This work provides a detailed look at the abundance and behavior of the main semivolatile BB markers measured in a tropical rainforest context in both the dry and wet seasons.

2.2 Experimental methods

2.2.1 Green Ocean Amazon (GoAmazon 2014/5) field campaign: T3 site description

Measurements were conducted as part of the Green Ocean Amazon (GoAmazon 2014/5) Experiment at the T3 site, described in detail in Martin et al. (2016). The T3 site (-3.2133° , -60.5987°) is 70 km downwind (west) of Manaus, a city of over 2 million people centrally located in the Amazon rainforest. The forest extends over 1000 km in every direction uninterrupted by other major urban areas. Locally, T3 is surrounded by 1 km of pasture in all directions, is 2 km north of a minor highway (AM-070), and is 10 km upwind (northeast) of Manacapuru, a city of between 85,000 and 100,000 people at the time measurements were taken (IBGE, 2022). Measurements were conducted during two Intensive Operating Periods (IOPs) in 2014. IOP1,

during the wet season, began February 1st and ended March 31st, 2014, while IOP2, during the dry season, began August 15th and ended October 15th, 2014. The measurements reported herein were taken February 14th – March 25th, 2014 (IOP1) and August 27th – October 15th, 2014 (IOP2).

2.2.2 Deployment of a Semivolatile Thermal desorption Aerosol Gas Chromatograph (SV-TAG)

We deployed a Semivolatile Thermal desorption Aerosol Gas Chromatograph (SV-TAG) at the T3 site. SV-TAG is described elsewhere in detail (Williams et al., 2006; Isaacman et al., 2011; Zhao et al., 2013; Kreisberg et al., 2014; Isaacman et al., 2014); a brief overview in the context of this deployment is provided here. Approximately 5 m above ground level, ambient air was pulled into a duct with an inner diameter (ID) of 15.24 cm at a fast ($\approx 100 \text{ L m}^{-1}$) laminar flow rate to minimize loss of semivolatile compounds to adsorption onto the wall of the duct. 20 L m^{-1} was subsampled for 22 min out of every hour and passed through a sharp-cut cyclone (SCC BGI Inc., Waltham, MA; Kenny et al., 2000) removing particles greater than $1 \mu\text{m}$ in diameter (PM_{10}). The air was then split into two 10 L m^{-1} flows, each of which is optionally passed through a multichannel carbon denuder (MAST Carbon) to remove gas-phase organics before passing through a stainless-steel filter collection cell held at 32°C that traps the semivolatile organics remaining in the air stream. The collection cell quantitatively traps gas- and particle-phase organic compounds including a range of volatility from *n*-tetradecane (C_{14}) to *n*-dotriacontane (C_{32}). In normal operation, one cell collects gas- and particle-phase semivolatile organics while the other cell collects either the particle phase only or both gas and particle phases, the latter choice serving to compare and correct for response differences between cells.

After collection, the internal volume around the cell is purged with helium and the cell is heated to 320°C to release the collected compounds. The delivered helium is saturated with the derivatization agent *N*-methyl-*N*-(trimethylsilyl) trifluoroacetamide (MSTFA, Sigma-Aldrich, > 98% purity, synthesis grade), which replaces hydroxyl groups with trimethylsilyl groups, making polar compounds amenable to elution on a nonpolar gas chromatography (GC) column (Isaacman et al., 2014). The desorbed and derivatized sample is reconcentrated onto 1 m of a metal, thick-phase gas chromatography column (MXT-5, 0.53 mm ID, $5 \mu\text{m}$ phase thickness; Restek) held at 30°C while excess MSTFA, which is too volatile to be retained on the column, is discarded. The reconcentrated sample is subsequently transferred onto another gas chromatography column (Rtx-5Sil MS; 20 m, 0.18 mm ID, $0.18 \mu\text{m}$ phase thickness; Restek) via a valveless injector (Kreisberg et al., 2014). The Agilent 7890A GC oven containing this column is programmed with a constant helium flow of $1 \text{ standard mL min}^{-1}$ and a temperature ramp from 50°C to 330°C ($23.6^\circ\text{C min}^{-1}$), with a hold at 330°C for 2.2 min while the helium flow ramps to $3 \text{ standard mL min}^{-1}$. Eluted compounds are detected by an Agilent 5975 quadrupole mass spectrometer.

2.2.2.1 Compound identification and quantification

All compounds reported in this work are identified and quantified using authentic standards. To ensure a clean signal and mitigate coelutions with other compounds, a single mass-to-charge ratio is chosen as the quantification ion in lieu of using the total ion chromatogram peak. The integrated area of the chromatographic peak associated with the chosen quantification ion is the raw response of the target compound.

Calibration of the raw response is a multi-step process. Best practices are explained in greater detail in Isaacman et al. (2014) and are summarized here in the context of the GoAmazon deployment. In every sample throughout the field campaign, a suite of isotopically labeled compounds was automatically injected (Isaacman et al., 2011) onto the collection cell immediately after the conclusion of sampling and before desorption and purging with MSTFA-saturated helium. These compounds were analyzed along with the ambient sample and, because the same mass is injected on every sample, serve to track variations in instrument performance such as detector response, transfer efficiency during the desorption process and derivatization efficiency. Their isotopic labels give them unique mass spectra and retention indices compared to isotopologues found in the ambient atmosphere. They are identified and their raw response is determined in the same manner as an ambient compound. Ambient compound raw response is then normalized by the raw response of the isotopically labeled standard compound that most closely matches it in volatility and functionality.

Approximately every 6-7 h, in lieu of ambient sampling, a standard mixture of compounds was injected onto the collection cell and analyzed at one of six mass levels, creating a full six-point calibration curve approximately every 40 h. Additionally, calibration curves using another standard mixture containing more BB-related compounds were made after the end of the field deployment. The isotopically labeled compound mixture was also injected, and the raw response of the calibration compounds is normalized in the same manner as ambient compounds. The normalized response is plotted against injected mass and the slope and intercept of the linear calibration curve are determined via least squares regression. The normalized response of ambient compounds is converted to concentration using the linear fit of the calibration curve of its corresponding authentic standard.

Normalization and calibration are applied separately for measurements on each of the two collection cells. While ideally simultaneous ambient measurements on the two cells would yield identical normalized (and therefore calibrated) responses, in practice there is a small difference. Since neither cell is known to be more accurate than the other, their mean is the final reported value. More specifically, a linear regression is applied to all calibrated samples where both cells measured both gas and particle phases (approximately every 2-3 h during the field campaign), with the intercept forced through 0. An equalization factor is applied to each data point such that the best fit slope of the equalized simultaneous gas and particle measurements is 1.

2.2.2.2 Calculation of F_p

The fraction of a compound in the particle phase, F_p , is the normalized response from a particle phase only measurement divided by the normalized response from the simultaneous gas plus particle phase measurement, after applying the correction for response differences between cells. It is not necessary to use fully calibrated data to calculate F_p , as F_p is a ratio and the correction for response differences between cells can be determined using normalized signals instead of calibrated signals. Due to the uncertainty arising from the independent measurements involved in the calculation of F_p , it is possible for F_p to be greater than 1, though in practice it is within uncertainty of 1. If either measurement involved in the F_p calculation is below the detection limit, F_p is not calculated.

2.2.3 Supporting measurements

Total non-refractory PM₁ (NR-PM₁) mass concentration and composition (organic, sulfate, nitrate, ammonium, and chloride) were measured by a High Resolution Aerosol Mass Spectrometer (AMS; Aerodyne, Inc., Billerica, Massachusetts, USA), whose operational details are described in the literature (DeCarlo et al., 2006; Canagaratna et al., 2007; Aiken et al., 2008; Canagaratna et al., 2015). Operational and analysis procedures specific to deployment at GoAmazon are presented in de Sá et al. (2017).

2.3 Results and discussion

2.3.1 Biomass burning markers measured and quantified with SV-TAG

The BB markers quantified with SV-TAG during GoAmazon IOP1 and IOP2 are presented in Table 2.1. Levoglucosan, mannosan and galactosan are products of pyrolysis (thermal degradation above 300°C) of cellulose (levoglucosan) and hemicellulose (mannosan and galactosan) (Simoneit, 2002; Bhattarai et al., 2019). As such, they represent generic markers of burning from any type of vegetation. Levoglucosan alone accounts for approximately half of the mean loading from the measured BB markers in both the wet and dry seasons, consistent with its higher measured emission rates compared to other semivolatile markers, particularly from angiosperms (Simoneit et al., 1999), and consistent with other observational studies (e.g. Graham et al., 2002; Schkolnik et al., 2005; Hoffer et al., 2006; Fuzzi et al., 2007; Claeys et al., 2010).

Vanillin, vanillic acid, guaiacol, 4-hydroxybenzoic acid, syringol, syringic acid, syringaldehyde and sinapaldehyde are pyrolysis products of lignin, a biopolymer of woody tissue (Simoneit, 2002). While none of these compounds represent unique tracers of a specific vegetation type, vanillin and vanillic acid are generally found in greater quantities in smoke from conifers, syringol, syringic acid, syringaldehyde and sinapaldehyde are more prominent in flowering plant burns, and 4-hydroxybenzoic acid is predominantly formed from burning of grasses (Simoneit, 2002; Schauer et al., 2001; Simoneit et al., 1993; Li et al., 2021).

The n-alkanoic acids eicosanoic, docosanoic, tricosanoic and tetracosanoic acid are found in plant waxes (Rogge et al., 1993b; Simoneit, 2002) and may be emitted directly from plants, in addition to contributing substantially to burning emissions from plants. They are found in all plant types and thus represent a generic BB marker (Oros and Simoneit, 2001a, b; Oros et al., 2006).

4-Nitrocatechol is a secondary compound produced from the reaction of catechol, another lignin pyrolysis product (Simoneit, 1999), with nitrate radical in burning plumes. In this data set, the temporal variability of 4-nitrocatechol tracks that of the primary markers closely ($r > 0.5$ when paired with any other BB marker, and typically > 0.7). This is consistent with the finding in the literature that the formation reaction is rapid, with most formation occurring within the first 1–2 h of burning (Finewax et al., 2018; Bertrand et al., 2018; Lin et al., 2016b).

Table 2.1. Mean concentration and partitioning data for biomass burning markers measured by SV-TAG as well as NR-PM₁ and OA as measured by de Sá et al. (2018, 2019). 4-HBA = 4-hydroxybenzoic acid. F_p = fraction in the particle phase, which ideally varies between 0 and 1 but in practice can exceed 1 as it is the ratio of two independent measurements. F_p is blank when fewer than 3 F_p measurements were obtained. Other values are reported in ng m⁻³ unless otherwise indicated. Values with a single asterisk (*) indicate that fewer than 50% and more than 10% of measurements during that season were above the detection limit for that compound. Values with a double asterisk (**) indicate that fewer than 10% of measurements were above the detection limit. For reported minimum values, <DL = below detection limit.

Compound Name	CAS #	Molecular Formula	Wet Season			Dry Season			
			Gas + Particle Mean ± S. Dev	Min – Max	F _p ± S. Dev	Particle Only Mean ± S. Dev	Gas + Particle Mean ± S. Dev	Min – Max	F _p ± S. Dev
NR-PM ₁ (µg m ⁻³)	--	--	--	0.1 – 13.1	--	1.7 ± 1.1	0.8 – 46.3	--	10.2 ± 4.7
OA (µg m ⁻³)	--	--	--	0.1 – 12.1	--	1.3 ± 0.9	0.6 – 42.9	--	8.4 ± 4.1
All BB markers	--	--	65.8 ± 103.6	<DL – 4510	--	53.8 ± 94.8	10.61 – 23690	--	750 ± 773
Cellulose & Hemicellulose									
Levogluconan	498-07-7	C ₆ H ₁₀ O ₅	30.2 ± 64.8	<DL – 983	0.96 ± 0.18	29.7 ± 62.2	6.12 – 7030	1.08 ± 0.22	408 ± 724
Mannosan	14168-65-1	C ₆ H ₁₀ O ₅	2.21 ± 12.83 *	<DL – 235	0.82 ± 0.36	1.78 ± 10.35 *	0.25 – 1700	0.97 ± 0.24	67.8 ± 140.3
Galactosan	644-76-8	C ₆ H ₁₀ O ₅	0.821 ± 9.973 **	<DL – 221	0.76 ± 0.39	0.688 ± 8.960 **	<DL – 962	0.67 ± 0.32	26.2 ± 71.6
Lignin									
Guaiacol	90-05-1	C ₇ H ₈ O ₂	0.134 ± 1.149 **	<DL – 18.5	--	0.0132 ± 0.2498 **	<DL – 127	0.44 ± 0.42	0.834 ± 3.114 *
4-HBA	99-96-7	C ₇ H ₆ O ₃	13.5 ± 27.4	<DL – 616	0.51 ± 0.20	7.76 ± 20.27	4.24 – 228	0.72 ± 0.19	34.6 ± 18.3
Vanillin	121-33-5	C ₈ H ₈ O ₃	1.10 ± 4.33 *	<DL – 68.3	0.05 ± 0.05	0.0167 ± 0.2949 **	<DL – 543	0.15 ± 0.15	1.72 ± 3.69 *
Syringol	91-10-1	C ₈ H ₁₀ O ₃	0.142 ± 1.855 **	<DL – 36.4	--	0 ± 0 **	<DL – 522	0.02 ± 0.02	0.0339 ± 0.2773 **
Vanillic Acid	121-34-6	C ₈ H ₈ O ₄	0.138 ± 1.026 **	<DL – 17.5	0.56 ± 0.27	0.0460 ± 0.5186 **	<DL – 435	0.61 ± 0.31	15.7 ± 30.7
Syringaldehyde	134-96-3	C ₉ H ₁₀ O ₄	2.59 ± 6.37	<DL – 114	0.43 ± 0.11	0.743 ± 1.979	<DL – 969	0.44 ± 0.16	10.2 ± 18.8
Syringic Acid	530-57-4	C ₉ H ₁₀ O ₅	0.201 ± 2.323 **	<DL – 44.4	1.04 ± 0.16	0.163 ± 2.000 **	<DL – 1160	0.92 ± 0.36	40.3 ± 115.7
Sinapaldehyde	4206-58-0	C ₁₁ H ₁₂ O ₄	0.276 ± 5.301 **	<DL – 128	--	0.213 ± 4.040 **	<DL – 517	0.81 ± 0.30	2.29 ± 21.46 **
Secondary									
4-Nitrocatechol	3316-09-04	C ₆ H ₅ NO ₄	1.71 ± 6.27 *	<DL – 134	0.67 ± 0.30	0.465 ± 3.290 **	<DL – 1780	0.78 ± 0.23	26.5 ± 112.5 *
Plant Wax									
C ₂₀ Alkanoic Acid	506-30-9	C ₂₀ H ₄₀ O ₂	6.49 ± 5.16	<DL – 102	1.12 ± 0.32	6.95 ± 4.75	<DL – 386	1.03 ± 0.27	22.3 ± 36.4
C ₂₂ Alkanoic Acid	112-85-6	C ₂₂ H ₄₄ O ₂	0.346 ± 3.222 **	<DL – 68.8	0.71 ± 0.41	0.285 ± 3.113 **	<DL – 361	0.88 ± 0.26	11.9 ± 30.4 *
C ₂₃ Alkanoic Acid	2433-96-7	C ₂₃ H ₄₆ O ₂	0.411 ± 5.970 **	<DL – 129	0.79 ± 0.31	0.365 ± 5.643 **	<DL – 326	0.93 ± 0.32	9.55 ± 28.8 *
C ₂₄ Alkanoic Acid	557-59-5	C ₂₄ H ₄₈ O ₂	4.17 ± 73.42 **	<DL – 1600	0.86 ± 0.31	4.00 ± 67.33 **	<DL – 1430	0.95 ± 0.29	40.1 ± 116.4 *

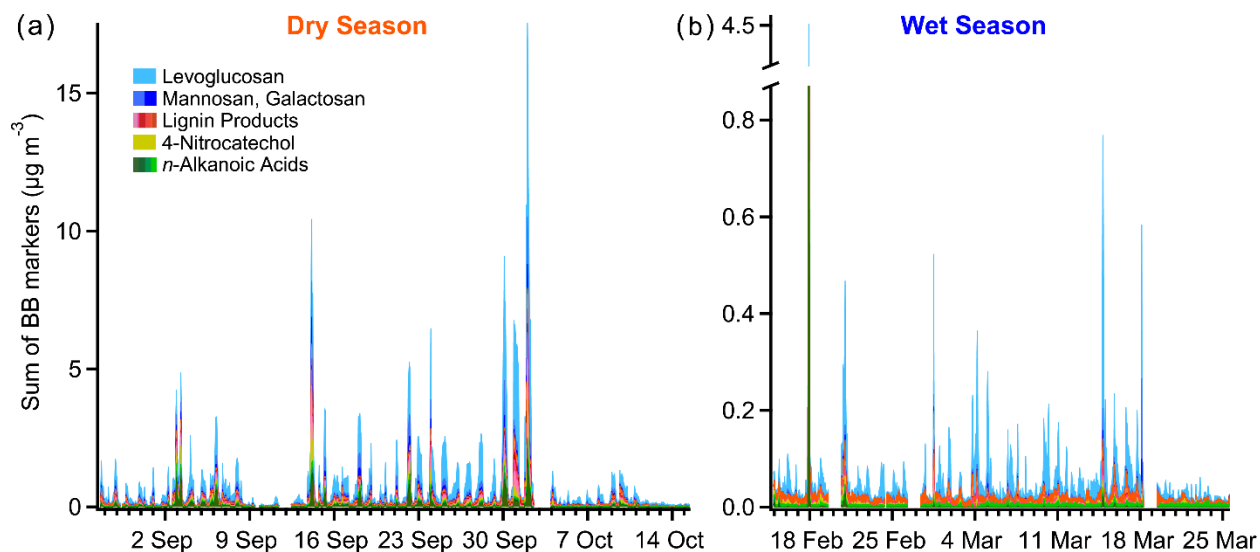


Figure 2.1. Stacked timeline of (a) dry and (b) wet season gas + particle measurements of the 16 reported biomass burning markers measured by SV-TAG. The greater overall mass in the dry season is evident, as is the dominance of levoglucosan by mass. The strong diurnal variability is also apparent, particularly in the dry season, with nighttime peaks and daytime valleys in concentration.

2.3.2 Seasonality

The concentrations of BB markers in the dry season are much higher than during the wet season (Table 2.1 and Figure 2.1). This is commonly observed in the Amazon region (Holben et al., 1996; Artaxo et al., 2013; Brito et al., 2014; de Oliveira Alves et al., 2015) due to the practice of burning cleared forest or crops in preparation for agricultural use, which is easier in the dry season when precipitation rates are relatively low (Hoeve et al., 2012; Artaxo et al., 2013). The sum of the measured markers is approximately 13 times larger in the dry season. However the median fractional contribution of the BB markers to organic NR-PM₁ (hereafter organic aerosol or OA) is 3.3% in the wet season and 4.5% in the dry season (Figure 2.2), an increase of only 1.4 times. Thus while BB contributes a greater fraction of OA, it is not the only source of the increased particle loading in the dry season. OA from other sources (e.g. biogenic, urban, secondary production) also increased in concentration between the wet and dry seasons (de Sá et al., 2019; Yee et al., 2020), leading to an overall increase of 6.5 times between measurement periods (Table 2.1). Possible reasons for the increased OA loading are discussed in de Sá et al. (2019) and include reduced convection, increased SOA formation potential due to less frequent wet deposition, and increased oxidant levels leading to more oxidized, lower vapor pressure products and thus more PM₁ mass, which extends lifetimes against dry deposition (Knote et al., 2015).

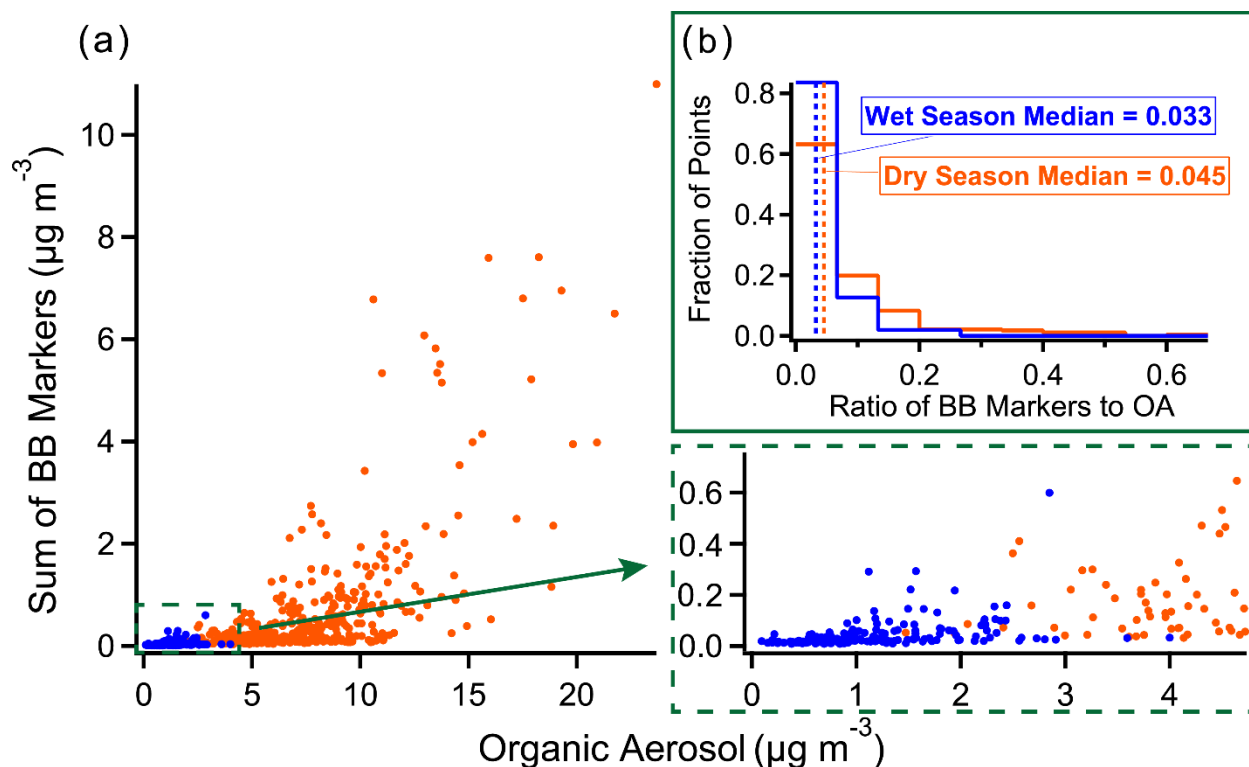


Figure 2.2. (a) The particle phase only sum of the BB markers plotted against total OA measured by the AMS in the dry season (orange) and wet season (blue). OA was reported by de Sá et al. (2018, 2019). (b) The histogram of fractional contributions of the BB markers to total OA. While in absolute terms the concentration of BB markers is much greater in the dry season, the total OA increased by roughly the same ratio. The median contribution of the BB markers to total OA is slightly greater in the dry season, but fresh BB emissions alone cannot account for the larger total OA loading in the dry season vs the wet season.

2.3.3 Strong agreement with AMS PMF BBOA factors

de Sá et al. (2018, 2019) used Positive Matrix Factorization (PMF) to source-separate OA measured by the AMS based on the time series of organic mass spectra in each IOP. They found 6 factors in each IOP, with a single Biomass Burning Organic Aerosol (BBOA) factor in the wet season and two BB-related factors in IOP2: Less Oxidized BBOA (LO-BBOA) and More Oxidized BBOA (MO-BBOA). They interpret the LO-BBOA factor as representing fresh, relatively low oxygen-to-carbon (O:C) ratio BB emissions and the MO-BBOA factor as including higher O:C fresh emissions and slightly aged secondary compounds from fresh BB precursors.

The correlation of the sum of the particle-phase measured markers included in this analysis with the BB-related AMS PMF factors is shown in Figure 2.3. As these are known markers of fresh emissions, the much stronger correlation with the LO-BBOA factor vs the MO-BBOA factor in the dry season is expected. The BB markers explain 86% of the variability of the LO-BBOA factor and nearly all of its mass as indicated by the near unity slope, suggesting the measured markers comprise the great majority of the mass of fresh BB emissions during the dry season. In

the wet season, the BB markers explain 86% of the variability but only about half of the mass of the BBOA factor. The AMS PMF analysis did not separate less oxidized versus more oxidized BBOA contributions in the wet season, so the BBOA factor represents the total mass attributed to BB. Thus, the difference in the mass of measured tracers vs the BBOA factor likely consists mainly of secondary chemicals which we did not quantify, or possibly non-BB related organic mass with similar variability and an imperfect separation of PMF source categories.

2.3.4 Diurnal variability

The BB markers exhibit strong diurnal variability, with maximum concentrations in the nighttime hours for all compounds except 4-hydroxybenzoic acid (Figure 2.2). This general pattern has been observed in previous studies (Schkolnik et al., 2005; Hoffer et al., 2006; Decesari et al., 2006; Claeys et al., 2010). Multiple processes likely contribute to the observed variability. First, because fires in Amazonia in the dry season are purposefully set by humans for agricultural land clearing, they are started in the daytime. Initially, flaming conditions dominate but by nightfall smoldering takes over, increasing the emissions of the BB markers included in this analysis (Schkolnik et al., 2005; Decesari et al., 2006; Fuzzi et al., 2007; Claeys et al., 2012). Second, concentrations are modulated by the height of the planetary boundary layer (PBL), which is shallow at night, allowing for buildup of emitted pollutants, and ≈ 5 times higher and more well-mixed during the daytime, diluting the measured compounds (Fisch et al., 2004; Rissler et al., 2006; Decesari et al., 2006; Fuzzi et al., 2007; Claeys et al., 2010; Fuentes et al., 2016; Carneiro and Fisch, 2020). Third, photochemical reactions deplete the concentrations of some of the markers during the daytime hours. Levoglucosan can react with OH radical ($[OH] = 10^6 \text{ molec cm}^{-3}$ for all lifetime estimates) as a gas and in particles with a lifetime of 1 to 4 days (Hoffmann et al., 2010; Hennigan et al., 2010; Lai et al., 2014). Gas-phase guaiacol and syringol react with OH in 3

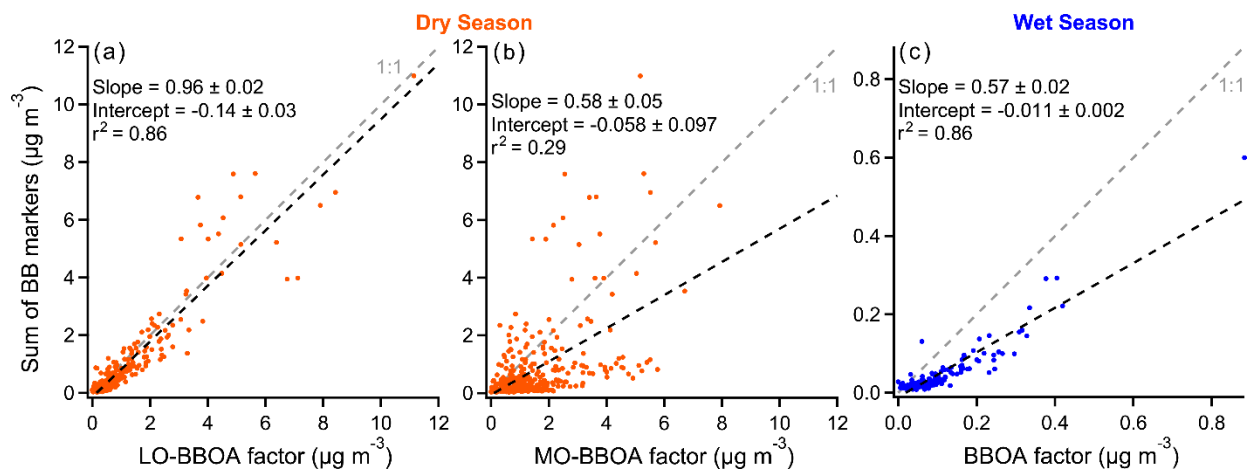


Figure 2.3. The particle phase only sum of the BB markers vs (a) the AMS LO-BBOA PMF factor from the dry season, (b) the AMS MO-BBOA PMF factor from the dry season and (c) the AMS BBOA PMF factor from the wet season. The marker sum correlates very strongly with the dry season LO-BBOA factor and the wet season BBOA factor, indicating that nearly all the variability of these factors is explained by fresh BB emissions. The BB marker variability does not match that of the MO-BBOA factor, which is interpreted by de Sá et al. (2019) to represent more oxidized fresh emissions as well as early secondary BB products.

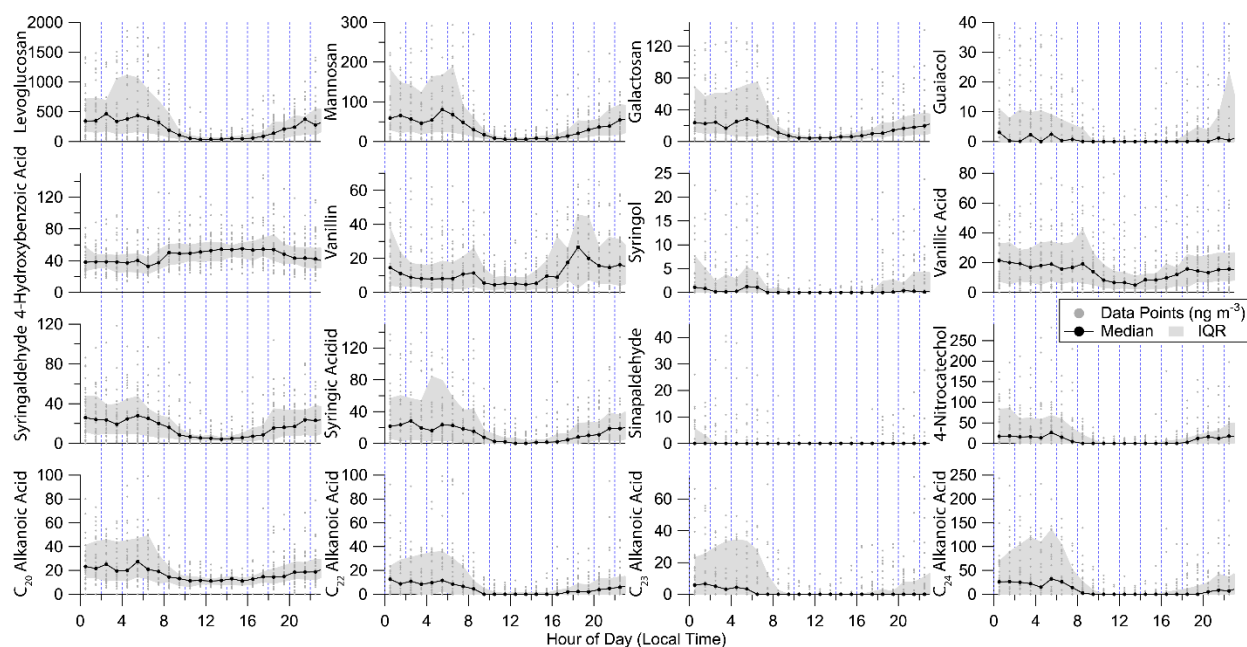


Figure 2.4. Diel plots of gas + particle concentrations in ng m^{-3} of the 16 BB markers in the dry season. IQR = interquartile range. In order to show detail around the median and IQR, the highest values are excluded. Because of much lower concentrations and much more sporadic BB activity, the wet season diel data are not shown. All compounds show nighttime enhancements except 4-hydroxybenzoic acid. The nighttime enhancements can be explained by a combination of a shallow nighttime boundary layer, increased emissions at night as flaming fires started in the daytime transition to smoldering, and daytime photochemistry.

to 4 h under similar conditions (Coeur-Tourneur et al., 2010; Lauraguais et al., 2012) while vanillin and vanillic acid have estimated OH lifetimes of approximately 2 days (Sun et al., 2022). Little information is available for the photochemical oxidation of the other cellulose, hemicellulose and lignin pyrolysis products reported in this study, but given their structural similarity to the more well-studied markers, it is likely photochemical reactions play a role in daytime depletion of these compounds. However photochemistry is unlikely to be an important sink for the n-alkanoic acids due to their low volatility and thus low gas-phase concentrations as well as their lack of reactive functional groups (Chebbi and Carlier, 1996). 4-Nitrocatechol is also relatively stable with respect to OH radical, with a lifetime of 9 days (Roman et al., 2022).

Curiously, 4-hydroxybenzoic acid is not elevated at night like the other compounds reported here, but instead has a very mild enhancement in the daytime hours. Hoffer et al. (2006) do not observe a daytime enhancement of 4-hydroxybenzoic acid but do observe a weaker nighttime enhancement compared to the anhydrosugars and vanillic and syringic acids. They attribute the reduced diurnal variability to less reactivity compared to vanillic and syringic acid, whose methoxy groups contribute a radical stabilizing effect that lowers the energy required for formation of phenoxy radicals (Kjällstrand and Petersson, 2001a, b). While this could explain the lack of a decrease in concentration of 4-hydroxybenzoic acid during the daytime, it cannot explain

the observed increase. Our observations clearly imply the existence of another significant, non-BB source of 4-hydroxybenzoic acid. Secondary production via photooxidation could be responsible for the daytime increase, e.g. from benzoic acid (Zhang et al., 2019), a widely prevalent pollutant from primary vehicle exhaust (Kawamura et al., 1985, 2000; Rogge et al., 1993a) and secondary oxidation of toluene (Suh et al., 2003).

2.3.5 Variability in composition during BB events

We hypothesized that, due to the differing chemical lifetimes of the BB markers (Sect. 2.3.4), a characteristic compositional profile for fresh BB emissions could be gleaned from the data and contrasted with an analogous profile for periods dominated by slightly more aged and oxidized emissions, as identified by the MO-BBOA PMF factor. Based on the diurnal profiles of the BB markers (Figure 2.4), typically concentrations begin to rise around 7 PM local time and by 9 AM are no longer substantially elevated. Therefore nights with an average 7 PM to 9 AM LO-BBOA PMF factor concentration above $2 \mu\text{g m}^{-3}$ were considered to be heavily impacted by fresh emissions for the purposes of this analysis. Aged emissions were identified by 8 h or longer periods of elevated MO-BBOA factor concentration ($> 2 \mu\text{g m}^{-3}$) and low LO-BBOA factor concentration ($< 1 \mu\text{g m}^{-3}$), where at least 2/3rds of data points in the 8 h period must meet the concentration criteria and only those points were included in this analysis. 4-Hydroxybenzoic acid was excluded from the analysis due to its apparent additional daytime source (Sect. 2.3.4).

There were 7 fresh emission nights and 4 aged emission time periods identified (Figure 2.5). All 11 periods had highly variable composition. The mean fresh and aged profiles are contrasted in Figure 2.5 (a). While the generally observed reduction in the mean concentration of guaiacol and syringol between the fresh and aged profiles and lack of a reduction for vanillin and vanillic acid is consistent with the reported atmospheric lifetimes of these compounds (Sect. 2.3.4), because of the large variability in individual data points this observation is not statistically significant. In fact no significant difference between the two mean profiles was found for any of the 15 considered compounds. We conclude that the variability in emission of traditional BB markers between different BB plumes is too great to clearly differentiate fresh and aged BB composition profiles at this site.

BB marker emissions are known to depend on the fuel composition and burning conditions and remain highly variable even when these factors are controlled for (Iinuma et al., 2007; Jen et al., 2019), which they were not for this analysis. Variability in atmospheric conditions, particularly photochemistry, likely contributed to differences between the aged profiles. An expanded analysis including more oxidized compounds and secondary BB markers might nonetheless yield significant differences in a comparison of mean fresh and aged profiles. Despite the variability, the averaged composition across all BB events provides a representation of primary BB markers that may be useful for modeling Amazonian fire emissions.

2.4 Conclusion

In this work, hourly concentrations and gas-particle partitioning were reported for 16 semivolatile BB marker compounds for representative periods of the dry and wet seasons in central Amazonia. Their diurnal and seasonal profiles were described and compared to the total OA measured at the site as well as the PMF-derived BBOA factor concentrations previously

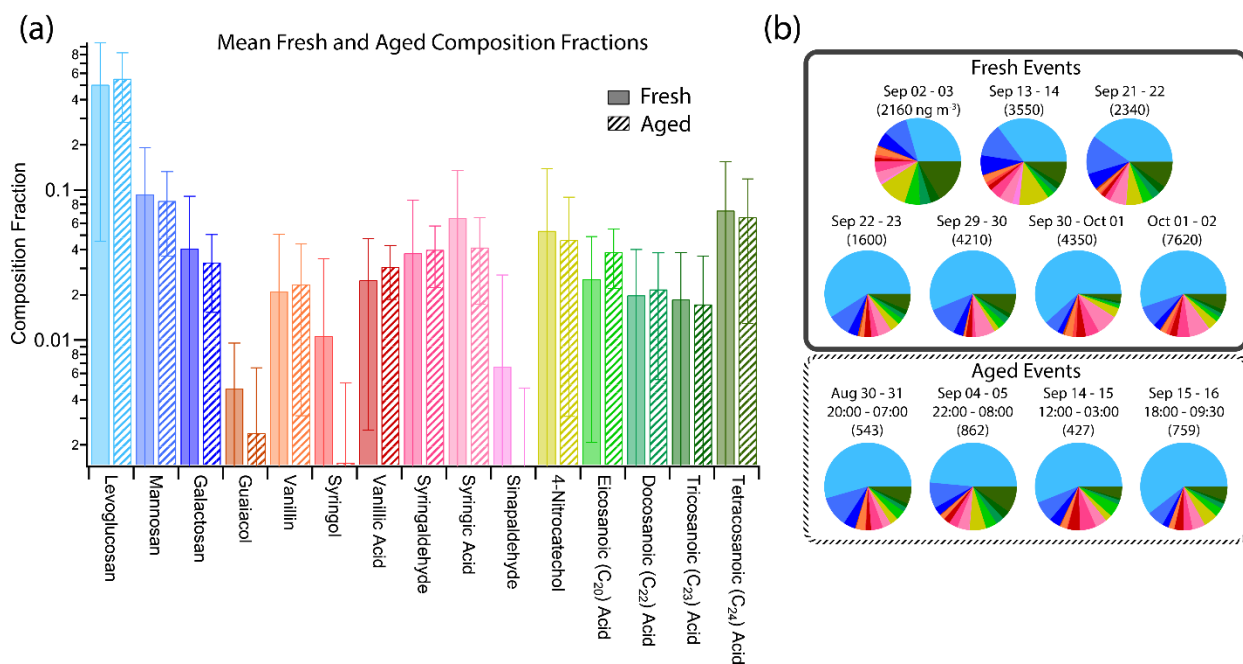


Figure 2.5. (a) Mean composition of the 7 periods of fresh emissions vs that of the 4 periods of slightly aged and/or more oxidized BB emissions. (b) Composition of individual periods of fresh and aged emissions. The periods of fresh burning are always from 19:00 to 09:00 the next day. The concentration in parentheses is the sum of the mean of the 15 included BB markers during each period in ng m^{-3} (4-hydroxybenzoic acid is excluded). Significant variability exists between fresh and aged emissions as well as between the individual periods of fresh emissions and of aged emissions, but the mean composition across all these events provides a representative mix of biomass burning tracers observed.

reported for both seasons. Consistent with previous studies, we observed much higher concentrations of BB markers in the dry season than the wet season. However we find that increased burning is not the only factor leading to elevated PM_{10} in the dry season, as has previously been assumed. Our results agree with those of de Sá et al. (2019) in demonstrating that relative to total OA, fresh BB emissions account for only a slightly larger fraction in the dry season than the wet season, and thus that other sources must be contributing substantially to the increased OA loading in the dry season. Comparisons with PMF results of the AMS OA mass spectra indicate that the 16 BB marker compounds comprise nearly all of the fresh BB emissions (LO-BBOA) in the dry season and likely also in the wet season when the factor analysis only resolved a single BBOA factor. We conclude that the 16 reported markers thus represent a relatively complete chemical profile of fresh BB in the Amazon in terms of total mass for modeling purposes.

The fresh BB markers presented here exhibit strong diurnal variability, with up to 10 times higher concentrations at night versus during the day on average. We note that 4-hydroxybenzoic acid, which is commonly assumed to be a specific BB marker, apparently has an additional source in our dataset leading to slightly higher concentrations in the daytime. Oxidation studies of many of the observed markers are recommended to obtain currently lacking information on their

reaction kinetics with common atmospheric oxidants to better constrain the impact of atmospheric chemistry on their concentration and their potential role in SOA formation.

2.5 Acknowledgments

The SV-TAG deployment for the GoAmazon 2014/15 field campaign was supported by NSF ACP grant no. 1332998. Further analysis of the dataset was supported by DOE ASR grant no. DE-SC0014040. SV-TAG was developed through support from U.S. Department of Energy (DOE) SBIR grant DE-SC0004698. Institutional support was provided by the Central Office of the Large Scale Biosphere Atmosphere Experiment in Amazonia (LBA), the Instituto Nacional de Pesquisas da Amazonia (INPA), the Universidade do Estado do Amazonia (UEA), and the local foundation FAPEAM. The work was conducted under 001030/2012-4 of the Brazilian National Council for Scientific and Technological Development (CNPq). We acknowledge logistical support from the Atmospheric Radiation Measurement (ARM) Climate Research Facility, a U.S. Department of Energy Office of Science user facility sponsored by the Office of Biological and Environmental Research. Rebecca A. Wernis was supported by the US Environmental Protection Agency (EPA) Science To Achieve Results (STAR) fellowship assistance agreement no. FP-91778401-0. The author would like to thank collaborators and organizers of the GoAmazon field campaign, including S. T. Martin, J. L. Jimenez, P. Artaxo, A. Manzi, J. Viegas and R. de Souza. SV-TAG data collection occurred with the assistance of L. D. Yee, G. Isaacman-VanWertz, N. M. Kreisberg, S. V. Hering and A. H. Goldstein. AMS data was collected by W. Hu, P. Campuzano-Jost, B. B. Palm, D. A. Day, S. S. de Sá, and M. L. Alexander.

Disclaimer: This work has not been formally reviewed by EPA. The views expressed in this work are solely those of the authors, and EPA does not endorse any products or commercial services mentioned in this work.

3 Development of an in situ dual-channel thermal desorption gas chromatography instrument for consistent quantification of volatile, intermediate-volatility and semivolatile organic compounds

Adapted from:

Wernis, R. A., Kreisberg, N. M., Weber, R. J., Liang, Y., Jayne, J., Hering, S., and Goldstein, A. H.: Development of an in situ dual-channel thermal desorption gas chromatography instrument for consistent quantification of volatile, intermediate-volatility and semivolatile organic compounds, *Atmos. Meas. Tech.*, 14, 6533–6550, <https://doi.org/10.5194/amt-14-6533-2021>, 2021.

Abstract

Aerosols are a source of great uncertainty in radiative forcing predictions and have poorly understood health impacts. Most aerosol mass is formed in the atmosphere from reactive gas phase organic precursors, forming secondary organic aerosol (SOA). Semivolatile organic compounds (SVOCs) (effective saturation concentration, C^* , of 10^{-1} – 10^3 $\mu\text{g m}^{-3}$) comprise a large fraction of organic aerosol, while intermediate volatility organic compounds (IVOCs) (C^* of 10^3 – 10^6 $\mu\text{g m}^{-3}$) and volatile organic compounds (VOCs) ($C^* \geq 10^6$ $\mu\text{g m}^{-3}$) are gas phase precursors to SOA and ozone.

The Comprehensive Thermal Desorption Aerosol Gas Chromatograph (cTAG) is the first single instrument simultaneously quantitative for a broad range of compound-specific VOCs, IVOCs and SVOCs. cTAG is a two-channel instrument which measures concentrations of C_5 – C_{16} alkane equivalent volatility VOCs and IVOCs on one channel and C_{14} – C_{32} SVOCs on the other coupled to a single High Resolution Time of Flight Mass Spectrometer, achieving consistent quantification across 15 orders of magnitude of vapor pressure. cTAG obtains concentrations hourly and gas–particle partitioning for SVOCs every other hour, enabling observation of the evolution of these species through oxidation and partitioning into the particle phase. Online derivatization for the SVOC channel enables detection of more polar and oxidized species.

In this work we present design details and data evaluating key parameters of instrument performance such as I/VOC collector design optimization, linearity and reproducibility of calibration curves obtained using a custom liquid evaporation system for I/VOCs and the effect of an ozone removal filter on instrument performance. Example timelines of precursors with secondary products are shown and analysis of a subset of compounds detectable by cTAG demonstrates some of the analytical possibilities with this instrument.

3.1 Introduction

In recent years, understanding of organic aerosol (OA) sources has changed substantially. Globally, the burden of secondary organic constituents, i.e. those formed via atmospheric transformation processes, is much larger than that of directly emitted primary organic particulate matter. This is observed in both rural and urban areas (Docherty et al., 2008; Jimenez et al., 2009; Williams et al., 2010; Zhang et al., 2007). Volatile organic compounds (VOCs) are critical precursors to OA. VOC oxidation controls the cycling of hydroxyl and nitrogen oxide radicals and

the formation of tropospheric ozone (Atkinson and Arey, 2003). The oxidation of VOCs produces lower vapor pressure compounds that form secondary organic aerosol (SOA) through condensation onto preexisting particles, through new particle formation and growth (Seinfeld and Pankow, 2003) and through aqueous oxidation processes in aerosol or cloud water (Ervens et al., 2011). The fate of approximately half the VOC emissions entering the atmosphere cannot be observationally accounted for, and this discrepancy is likely at least partially due to a lack of comprehensive measurements of speciated organic constituents in a variety of atmospherically distinct environments (Goldstein and Galbally, 2007; Hallquist et al., 2009; Heald and Kroll, 2020).

Recent work has demonstrated that a large fraction of organic aerosol (OA) is semivolatile (Robinson et al., 2007a). Intermediate volatility organic compounds (IVOCs, defined as having an effective saturation concentration C^* of 10^3 to $10^6 \mu\text{g m}^{-3}$) and semivolatile organic compounds (SVOCs, C^* of 10^{-1} to $10^3 \mu\text{g m}^{-3}$) have been proposed as a substantial unaccounted for source of SOA in urban areas (Robinson et al., 2007a; Weitkamp et al., 2007) but are notoriously hard to measure (Goldstein and Galbally, 2007; Hunter et al., 2017; Isaacman-VanWertz et al., 2018). This hypothesis is supported by estimates of intermediate volatility and semivolatile organic compound (I/SVOC) abundances in the atmosphere that are an order of magnitude larger than primary organic aerosol (Robinson et al., 2007a), and direct evidence that oxidation of compounds in the IVOC range efficiently produces SOA (Chan et al., 2009a; de Gouw et al., 2011; Lim and Ziemann, 2009; Presto et al., 2010).

There is a need for simultaneous measurement of VOCs, IVOCs and gas- and particle-phase SVOCs with sufficient temporal resolution to track the rapidly changing chemical composition and atmospheric conditions that directly affect SOA formation reactions. Owing to the enormous range of volatility encompassed by VOCs and I/SVOCs, this has typically been achieved through collocation of at least two separate instruments – one to measure VOCs ($C^* \geq 10^6 \mu\text{g m}^{-3}$) and IVOCs and another to measure SVOCs. VOCs have traditionally been measured using one of two methods. One way is to collect onto a bed of adsorbent materials and desorb and analyze into a gas chromatograph (GC) coupled to a flame ionization detector (FID) or a quadrupole mass spectrometer (MS) (e.g. Gentner et al., 2012; Goldan et al., 2004; Goldstein et al., 1995; Hopkins et al., 2003; Lamanna and Goldstein, 1999; Lerner et al., 2017; Millet et al., 2005). This method offers excellent chemical specificity as isomers are detected separately and low detection limits as samples are usually collected for many minutes before analysis. However due to the GC temperature ramp and sample collection time GC-based methods have a temporal resolution of 20 min to 1 h. Additionally, typically primary pollutants such as alkanes and aromatics and early generation secondary products such as carbonyls and alcohols are measurable but multifunctional or fully aged species are too thermally unstable or polar to measure by GC-MS. For example, Chung et al. (2003) were able to speciate 55-85% of total VOCs in urban sites in the Los Angeles Basin, with the lower end of the range corresponding to greater photochemical processing and more of the VOC mass present in oxidized species. Another widespread method is chemical ionization mass spectrometry (CIMS), e.g. the Proton Transfer Reaction Mass Spectrometer (Ionicon Analytik) and related technologies, which compared to GC-based methods offers far greater temporal resolution but less specificity as isomers cannot be

separated, and detection is limited to compounds for which the ionization reaction with the chosen reagent is energetically favorable.

Particle-phase SVOCs and lower volatility organics have traditionally been collected on disposable filters and analyzed offline via GCMS (Turpin et al., 2000). Field measurement techniques for gas- and particle-phase SVOCs have been developed relatively more recently. The FIGAERO-CIMS utilizes automated quartz filter collection for aerosol particles and controlled thermal desorption into a CIMS instrument (Lopez-Hilfiker et al., 2014), offering similar advantages and tradeoffs of CIMS applied to gas-phase measurements. The Volatility And Polarity Separator (VAPS) sacrifices detailed speciation in order to functionally characterize a larger fraction of the organic aerosol mass (Martinez et al., 2016). The Thermal desorption Aerosol Gas chromatograph (TAG) family of instruments, consisting of a reusable filter-based collection cell or impactor cell coupled to a GCMS, maximizes chemical speciation of gas and particle SVOCs, including separation of isomers, at hourly time resolution. The first TAG was developed by Williams et al. (2006) with the impactor cell, sensitive to particle-phase SVOCs only. Later versions incorporated an automatic liquid injection system for calibrations (Isaacman et al., 2011), a filter cell and denuder for measurement of gas-phase SVOCs and gas-particle partitioning of SVOCs (the SV-TAG; Zhao et al., 2013), a valveless injector for transferring the sample onto the GC column with minimal losses (Kreisberg et al., 2014) and online derivatization to enable detection of polar SVOCs including alkanolic acids, polyols, diacids, sugars and other multifunctional compounds in addition to nonpolar ones (Isaacman et al., 2014). A version of TAG using the impactor cell, valveless injector and online derivatization is commercially available from Aerodyne Research, Inc. Recently, automated quartz filter collection with thermal desorption and GCMS for chemical speciation of particle-phase SVOCs has also been developed (Cropper et al., 2017; Ren et al., 2019). Using TAG with an impactor cell, Williams et al. (2010) were able to quantify an estimated 20% of fine (PM₁) organic aerosol mass as measured by an aerosol mass spectrometer at an urban site. While this statistic has not been estimated directly for the SV-TAG and likely varies with the measurement location and conditions, the use of online derivatization on that instrument would increase the analyzable fraction of OA mass.

In recent years both I/VOC instruments and SVOC instruments have benefitted from field-deployable High Resolution Time of Flight Mass Spectrometry (HRToFMS, e.g. TOFWERK and IONICON Analytik). This technology affords two main advantages over quadrupole mass spectrometers. First, the high resolution ($m/\Delta m \approx 4000$ or more) allows for identification of chemical formulas of ions detected due to the unique mass defects of the different elements. Second, whereas the quadrupole MS scans over a user-specified range of atomic mass units, presenting an implicit tradeoff between sensitivity and the range of possible ions detected (because a smaller range or set of discreet masses to detect allows for increased dwell times), the HRToFMS has no such limitation and allows the user to detect the entire useful range of ion masses with no compromise in sensitivity and indeed overall enhanced sensitivity.

The Comprehensive Thermal desorption Aerosol Gas chromatograph (cTAG) combines an I/VOC collector based upon the design of Gentner et al. (2012) and one channel of the SV-TAG joined together before a HRToFMS to access a broader volatility range of speciated organic compounds in a single instrument than previously achieved. Nonpolar and some polar VOCs and

IVOCs as well as nonpolar and derivatization amenable polar SVOCs are quantitatively collected, including many primary and secondary organics that lend insight into important sources and oxidation processes in atmospheric chemistry.

3.2 Description of instrument

Utilizing reusable adsorbent and stainless steel filter collection, thermal desorption, online derivatization, GC and HRTofMS in a dual-channel setup the cTAG measures concentrations of speciated organic compounds from C₅ through C₃₂ alkane equivalent volatility. The instrument operates in an automated fashion with hourly time resolution for concentrations and gas-particle partitioning measurements of SVOCs every other hour. Derivatization of SVOCs allows for detection and analysis of polar compounds with hydroxyl groups in addition to nonpolar species. In this section, we describe the key components of the system, the sample collection, separation and detection pathways, calibration methods, timing, and data processing procedures.

Figure 3.1 shows a schematic of the instrument.

3.2.1 Inlet and I/VOC channel

Ambient air enters the instrument through either a sharp cut PM_{2.5} cyclone or a sharp cut PM₁ cyclone depending on application-specific criteria (SCC BGI Inc., Waltham, MA) (Kenny et al., 2000). The flow is then split to collect I/VOCs and SVOCs in parallel.

On the I/VOC channel, 50 sccm of ambient air is pulled from downstream of the cyclone through a stack of three quarter-inch diameter punches of sodium thiosulfate (Na₂S₂O₃) impregnated glass fiber filters to remove ozone, followed by a six-port valve (6PV, Valco Instruments Co. Inc.) and the I/VOC collector for I/VOC pre-concentration. The I/VOC collector consists of a layered bed of adsorbents based on the design of Gentner et al. (2012) whose types and quantities were chosen in order to efficiently collect I/VOCs with volatilities between those of n-pentane and n-hexadecane in a 1 L total sample volume when the collector is held at 30 °C. Adsorbents are layered from least to most adsorptive strength, with the IVOCs adsorbing on the least adsorptive material and the most volatile VOCs passing through and adsorbing onto the most adsorptive material. Figure 3.2 is a diagram of the collector. In order along the sample flow path are 60 mg glass beads (Alltech, 60/80 mesh, DCMS-treated), 10 mg Tenax TA (Supelco, 60/80 mesh), 10 mg glass beads, 20 mg Carbopack B (Supelco, 60/80 mesh), 10 mg glass beads, 20 mg Carbopack X (Supelco, 60/80 mesh) and 10 mg glass beads. The glass beads do not efficiently trap VOCs or IVOCs and serve solely as separators for the adsorbents. Once assembled and before installation on the instrument, the collector is conditioned at 325 °C with 50 sccm nitrogen for 3 h. Breakthrough volume measurements described in Sect. 3.3.1 were performed to ensure that this bed composition would fully collect and transfer all VOCs and IVOCs in the range of interest.

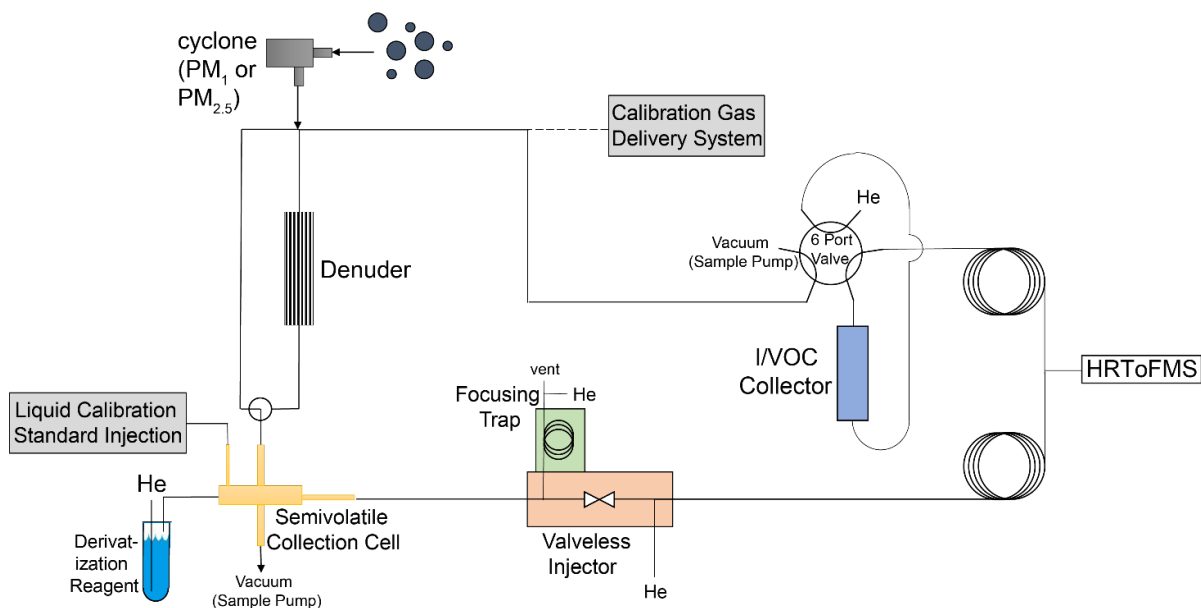


Figure 3.1. Schematic of cTAG. VOCs and IVOCs are collected on the I/VOC collector while SVOCs are collected on the collection and thermal desorption cell. The I/VOC and SVOC channels are independent until the GC column outputs from each channel meet and enter the HRTofMS. Optionally, the SVOC channel can collect only particle-phase SVOCs by first passing sampled air through a denuder that removes all gas-phase compounds. A derivatization agent introduced upon desorption of the SVOCs from the collection cell enables detection of polar SVOCs in addition to nonpolar ones. Sample collection happens in parallel, for 23 min, followed by analysis of the I/VOC collector contents, then analysis of the semivolatiles collection cell contents, for a total turnaround time of 1 h. Calibration is done for VOCs and IVOCs by manually disconnecting the ambient inlet and connecting and sampling the output of the calibration gas delivery system (Figure 3.3) and for SVOCs via liquid standard injections onto the semivolatiles collection cell.

Adsorbents are packed in a custom, pure stainless-steel housing consisting of a 3.18 mm outer diameter (OD) thin-walled (0.13 mm) tube brazed to a 1.59 mm OD, 0.51 mm ID tube (Figure 3.2). A section of the 3.18 mm portion that contains the adsorbents is flattened to 1.59 mm OD to reduce swept volume in the collector and improve heat transfer to enable sharper injections of highly volatile compounds. Brazing to the 1.59 mm tube eliminates the need for a union and the associated internal volume, again aiding the rapid injection of the most volatile species. A stainless steel microfiber mesh screen (Bekaert) installed at the braze point keeps out particles and retains the adsorbents on the upstream sampling end, while a glass wool plug retains the adsorbents on the downstream end. The entire housing is chemically passivated (Inertium[®] treatment, AMCX, PA, USA) to prevent active compounds from reacting with the stainless steel.

During sampling the I/VOC collector is held at a temperature at least several degrees above the dew point to avoid water condensation in the system; this is typically around 30 °C. After sampling the I/VOC collector is briefly purged with helium to reduce the amount of air and

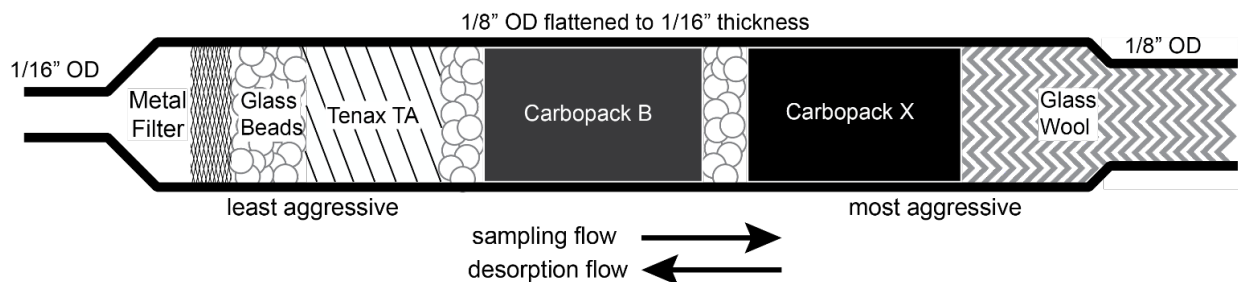


Figure 3.2. Schematic of I/VOC collector. Semivolatile and lower volatility species, including particles, are captured on the metal filter. IVOCs are captured on the Tenax TA, while the most volatile analytes including isoprene are retained by the more aggressive adsorbents. Flow is reversed for desorption so that the less volatile compounds never interact with the more aggressive adsorbents.

water sent to the detector. Then the 6PV actuates and helium flows through the collector in the reverse direction as the collector heats from ambient temperature to 260 °C to desorb the analytes onto the GC column (metal MXT-624, 30 m, 0.32 mm ID, 1.8 μm phase). Two 100 W cartridge heaters mounted in an aluminum block clamped to the collector housing ensure a rapid initial heating time of 35 s, producing sharp chromatography peaks even for the unretained, most volatile species. Total desorption time is 4 min. GC analysis time is 25 min, with an initial hold for 1 min at 40 °C followed by a 10 °C min⁻¹ ramp to 250 °C and a 3 min hold at 250 °C.

3.2.2 SVOC channel

After splitting off from the combined ambient air flow through the cyclone, 10 L min⁻¹ of ambient air passes through a stainless steel filter collection and thermal desorption cell (F-CTD) maintained at 30 °C. The F-CTD quantitatively collects compounds with volatilities as high as n-tetradecane (C₁₄) and as low as n-dotriacontane (C₃₂) in the gas and particle phases.

Directly upstream of the F-CTD, an optional 500-channel activated carbon denuder (MAST Carbon) efficiently removes gas-phase species, allowing for gas-particle partitioning measurements by difference with and without the denuder in line. F-CTD and denuder characteristics are described in further detail in Zhao et al. (2013).

After collection, the F-CTD is heated to 315 °C and flushed with 20–150 sccm helium during a two-stage desorption process as described in Zhao et al. (2013). Upstream of the F-CTD the helium may optionally be bubbled through a liquid reservoir of N-methyl-N-(trimethylsilyl) trifluoroacetamide (MSTFA, Sigma-Aldrich, > 98 % purity, synthesis grade) for online derivatization of species containing hydroxyl groups. Evaluation of online derivatization for TAG is discussed in Isaacman et al. (2014). The sample is re-concentrated onto a focusing trap held at 30 °C made of a 1 m metal, thick phase chromatography column (MXT-5, 0.53 mm ID, 5 μm phase thickness; Restek). This step allows for faster transfer of low volatility species and efficient purging of excess derivatization agent and by-products. Flow is reversed on the trap to about 2 sccm for transfer of the sample onto the GC column (metal MXT-5, 20 m, 0.18 mm ID, 2 μm phase thickness; Restek) via the restrictive section of a valveless interface (VLI), described by Kreisberg

et al. (2014). GC analysis time is 19 min, with an initial hold for 1 min at 50 °C followed by a 20 °C min⁻¹ ramp to 330 °C and a 4 min hold at 330 °C.

3.2.3 Miniature gas chromatographs

cTAG requires two separate GC columns each optimized for the separation of target species on a given channel and whose temperatures are controlled independently. In order to achieve this while preserving the instrument's compactness and time resolution we developed miniature gas chromatographs. Each chromatograph consists of a custom machined aluminum hub around which the metal column is wrapped in a single layer so that it is in thermal contact with the hub along its entire length. On the inside surface of the hub, an expanding split-band 150 W heater heats the hub evenly around its circumference. A thermocouple inserted into a bored hole in the hub body tracks its temperature. Proportional-integral-derivative (PID) heating control allows for programmable, reproducible temperature ramping for GC analysis. When the temperature program completes, a fan blows ambient air onto the hub to bring it back to its initial temperature in time for the next sample injection. As with traditional GC systems, the front of the column may be trimmed (at the expense of one full winding on the aluminum hub) to extend column life. Design schematics, photos and temperature ramp reproducibility data can be found in Appendix A.

The use of miniature gas chromatographs has obvious benefits for instrument compactness and field portability. Additionally, the independent temperature control allows analysis on one channel to start while the column from the other channel is cooling down, increasing the maximum possible time resolution as compared with the traditional approach of using a single oven for dual column GC methods. While commercial miniature GC systems are available, e.g. from Valco Instruments Company Inc. (Column/Fan Modules for Fast GC, 2020), we chose to design our own for greater flexibility and the ability to use off-the-shelf columns.

3.2.4 High resolution time of flight mass spectrometer

The two chromatography columns are joined in a passivated tee connected to an approximately 18 cm passivated stainless steel 794 mm OD, 125 µm ID tube that serves as the mass spectrometer transfer line, held at a constant 275 °C. While one column progresses through its temperature program, the other is held at its initial temperature with constant flow and the analytes and carrier gas are pulled through the transfer line into the vacuum chamber of the mass spectrometer.

Chromatographically separated analytes are detected by a field portable HRTofMS (TOFWERK). The HRTofMS is operated at 70 eV electron impact ionization over a user-selected mass-to-charge ratio range, typically from 15 to 450 on cTAG. This allows for matching to compounds found in mass spectral databases. For compounds not identifiable by database matching or authentic standard calibration, the mass to charge resolution of $m/\Delta m \approx 4000$ enables determination of the molecular formula of the ions, lending insight to molecular structure and ultimately compound identity, a critical capability for studying the complex interactions of organic molecules in the atmosphere.

3.2.5 Calibration

Calibration on both channels relies on injection and analysis of a suite of authentic standards in varying amounts. On the I/VOC channel, a mixture in either liquid or gas form is introduced into a custom dynamic dilution system for fine control of the output concentration. The dynamic dilution system uses a heated platinum catalyst to generate zero air at ambient relative humidity and a series of mass flow controllers (0–20 and 0–1000 sccm MFCs, Bronkhorst EL-FLOW) and valves to choose and dilute the input mixture for sampling (Figure 3.3). Dilution ratios ranging from 50:1 to 1000:1 ensure near ambient relative humidity for diluted mixtures. From the point of mixing to the collector, all plumbing is heated to at least 55 °C. A specialty gas cylinder with multiple components at parts-per-million levels is introduced in one port of the system.

Calibration using custom compressed gas cylinders limits the user to compounds amenable to storage in cylinders over years and does not allow significant flexibility after standard cylinders are produced. We developed a liquid evaporation system modeled after Jardine et al. (2010) to circumvent these limitations by allowing the user to purchase individual pure standards and prepare liquid solutions for evaporation and sampling. The liquid mixture is drawn into a syringe pump (TECAN Cavro Centris Pump, 250 μL glass syringe) and dispensed into another port of the dynamic dilution system at a rate of 1.6 $\mu\text{L min}^{-1}$ into a dedicated evaporation chamber. From one end of the chamber a dedicated MFC flows 1000 sccm zero air over the emerging liquid feed. Most of the resulting evaporated mixture in zero air is exhausted while 0–20 sccm is subsampled for subsequent dilution in the same manner as a gas cylinder. Once diluted, the gas or liquid calibration mixture is collected on the I/VOC collector, then desorbed and analyzed exactly like ambient air samples.

On the SVOC channel, liquid calibration mixtures are held in reservoirs pressurized under helium. A multiport selector (Rheodyne MHP7970-500-4) selects a reservoir to fill a 5 μL sample loop. A 6-port valve (Rheodyne MHP9900-500-1) actuates to allow pressurized helium to push the liquid out of the loop and inject it directly onto the F-CTD via a dedicated port in the cell housing. A detailed description of the SVOC liquid calibration injection system may be found in Isaacman et al. (2011).

Prior to applying calibrations from analysis of authentic standards, ambient data are normalized by an internal standard introduced onto the sampling medium of each channel on every ambient sample. For the I/VOC channel, several ambient long-lived and therefore atmospherically well-mixed anthropogenic compounds with no significant current emission sources serve as suitable internal standards to control for run-to-run variability. Carbon tetrachloride is commonly used for this purpose (Lerner et al., 2017) and CFC-113 and 1,1,1-trichloroethane are also adequate for cTAG on the timescale of a typical field campaign (Engel et al., 2018; Karbiwnyk et al., 2003). The compound with the clearest signal and fewest coelutions among these is generally preferred. On the SVOC channel, a single 5 μL loop of a calibration mixture of isotopically labeled compounds spanning a variety of volatilities and functional groups is injected onto the F-CTD after collection of every ambient sample. These compounds are desorbed and analyzed with the sample and serve to track variability of derivatization efficiency and instrument response.

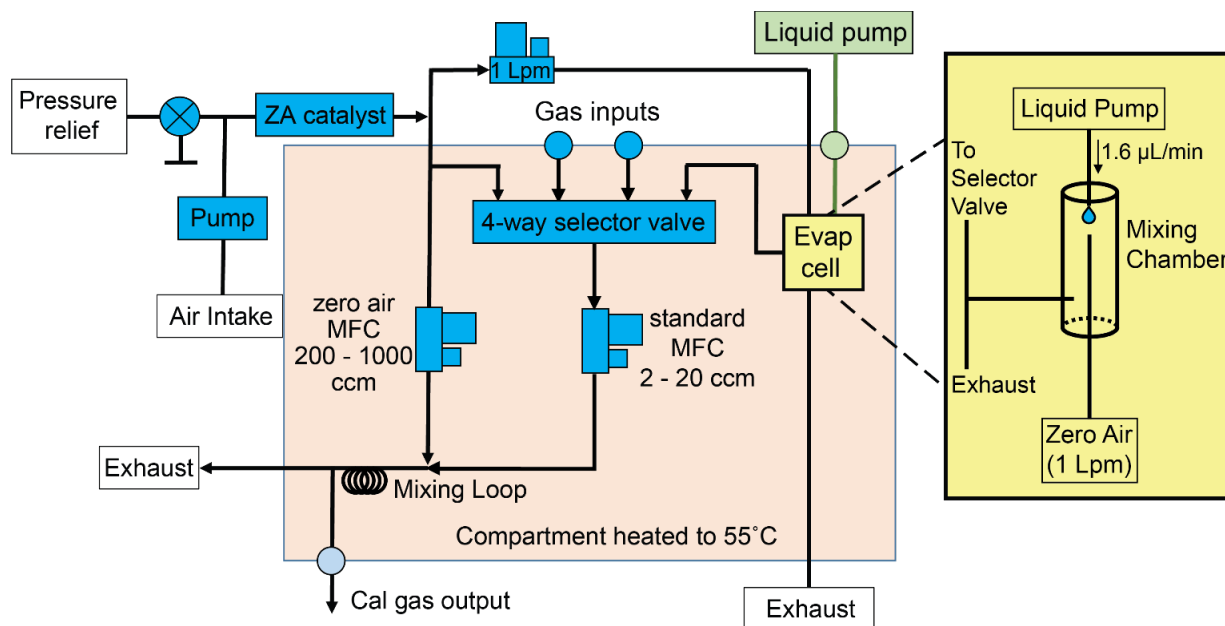


Figure 3.3. Schematic of dynamic dilution system for VOC and IVOC calibration. Gas cylinders or liquid mixtures can be used for calibration. Liquid mixtures are introduced into an evaporation cell using a syringe pump. The liquid is evaporated into 1 L min^{-1} of zero air to reach parts-per-million or lower concentrations. The resulting gaseous mixture (or, by user choice, the output of a calibration gas cylinder) is subsampled with a 2–20 sccm MFC and further diluted up to 500 times with more zero air before being sampled by the I/VOC collector. Zero air for the dilution system is generated by passing ambient air through a heated platinum catalyst.

3.2.6 Instrument operation

cTAG is fully automated. All valves, fans, temperature-regulated zones and electronic pneumatic controllers are controlled by a microprocessor-based control box developed by Aerodyne Research, Inc. for commercially available TAG systems and adapted and upgraded for our system. A Microsoft Visual Basic .NET software program operating on a PC platform interfaces between the user and the control box, using serial communication to send commands and load sequences for unattended field operation and receive, display, plot and record temperature and voltage readings.

Total turnaround time for a single instrument cycle is exactly 1 h. A typical operation sequence begins with 23 min of concurrent sampling on the I/VOC and SVOC channels with the SVOC channel optionally sampling through the denuder to remove gas phase species. During sampling the SVOC chromatographic analysis of the previous hour's sample finishes. Once sampling is completed, the I/VOC collector is purged with helium for 1 min. Then the 6PV actuates, at which point the 25 min I/VOC GC temperature program and HRTofMS data acquisition begin and the I/VOC collector is rapidly heated to $280 \text{ }^\circ\text{C}$ and held at that temperature for 4 min while 1.5 sccm of helium carries the analytes to the head of the GC column.

While the I/VOC sample is being analyzed, the SVOC liquid calibration system injects 5 μL of the internal standard mixture onto the F-CTD. The F-CTD is then heated to 315 °C under 20 sccm of helium. Total helium purge flow is controlled by a mass flow controller (MFC). The flow is split downstream of the MFC, with 80 % bubbling through the reservoir of liquid derivatization agent before rejoining the other 20 % and purging the F-CTD. This flow ratio was determined to be sufficient for complete derivatization of all compound classes of interest in Isaacman et al. (2014). After 8 min, the total flow is increased to 150 sccm for 4 min to aid the transfer of the least volatile compounds. During this process analytes are refocused on the focusing trap, held at 30 °C. Flow is then reversed and the trap heats to 315 °C as the I/VOC GC analysis finishes. Continued purge flow from the MFC raises the pressure in the F-CTD and forces the analytes through the restrictive portion of the VLI and onto the head of the GC column over the course of the 4 min trap desorption period. The SVOC GC analysis begins, followed by sampling for the next cycle.

A typical field campaign day sees round-the-clock sampling and analysis as previously described, alternating sampling with and without the denuder inline on the SVOC channel. Approximately every 2 weeks, calibrations are performed on both channels of the instrument simultaneously lasting 10 to 12 h to generate multiple data points per compound for a range of loadings. The stack of sodium thiosulfate filters is replaced every 2 weeks to avoid ozone breakthrough by a safe margin (Sect. 3.3.4). At least once per field campaign a tank of nitrogen or zero air is plumbed into the inlet and sampled on both channels in order to quantify contaminants in the system.

3.2.7 Data processing

Chromatogram integrations are performed in TERN, software developed in Igor Pro 7 (Wavemetrics) by Isaacman-VanWertz et al. (2017). TERN enables automatic batch integration of single compounds on hundreds of chromatograms at a time for rapid generation of compound concentration timelines. Compounds are organized in templates and the ability to search commercial or custom mass spectral libraries for compound identification is built in.

3.3 System evaluation

The focus of development and system evaluation was on the I/VOC channel, as the SVOC channel is identical to a single channel of the previously developed SV-TAG instrument extensively documented elsewhere (Isaacman et al., 2011, 2014; Kreisberg et al., 2014; Zhao et al., 2013). Development for the cTAG focused on optimizing the design of the I/VOC collector, developing a calibration system for the I/VOC channel capable of using custom liquid mixtures, ensuring removal of ozone for accurate collection of ozone-reactive VOCs and IVOCs, and field deployment in a polluted urban area.

3.3.1 I/VOC collector breakthrough tests

The target collection range for the I/VOC channel was chosen to include isoprene, a key biogenic C_5 hydrocarbon, on the high volatility end. The low volatility end was chosen to overlap with the SVOC channel range (which starts at C_{14}) by several carbon numbers and to include sesquiterpenes, a class of C_{15} compounds also of biogenic origin but with greatly varying

structures and reactivity and which are far less well documented and understood (Bouvier-Brown et al., 2009; Chan et al., 2016; Yee et al., 2018).

In order to decide the final quantities of adsorbents in the I/VOC collector, three different collector compositions were tested for breakthrough of the most volatile species. Briefly, breakthrough volume is defined as the volume of carrier gas required to purge an analyte through the adsorbent bed, dependent on adsorbent quantity, temperature and analyte volatility (Definition of Breakthrough Volumes, 2020). The breakthrough volume must be larger than the volume of air sampled for the most volatile analyte of interest to ensure complete collection of all analytes.

Breakthrough volumes were measured using a real-time VOC instrument, a Proton Transfer Reaction Mass Spectrometer (PTR-MS, IONICON Analytik). The output of a specialty gas cylinder of biogenic VOCs was diluted using the custom dynamic dilution system to deliver ppb-level concentrations of analytes to the collector, held via PID temperature control at 30 °C. The PTR-MS inlet was connected downstream of the prototype collector while sampling from the controlled gas mixture at 100 sccm. For each analyte, the PTR-MS measured zero concentration until the breakthrough volume was reached, after which the downstream measured concentration rapidly rose and plateaued. The beginning of the rapid rise in concentration was taken to be the point of breakthrough.

Breakthrough volume measurement results for isoprene and the sum of methyl vinyl ketone and methacrolein (MVK+MACR) for several collector prototypes are shown in Table 3.1. For compactness and to reduce thermal mass to ensure rapid desorption, we targeted a final design containing the minimum quantity of adsorbents that would safely and robustly meet our requirements for breakthrough volume. Collector #3, which had the lowest quantities of adsorbents of the three different prototype collectors tested, had a breakthrough volume of twice our usual 1 L sample volume for MVK+MACR. We therefore settled on a fourth prototype with quantities intermediate between collectors #2 and #3 of the most aggressive adsorbents to ensure a safe margin. We also reduced the quantity of Tenax TA, as the 10 mg final quantity provides more than sufficient breakthrough volumes for the lower volatility compounds that it collects (Tenax® TA Breakthrough Volume Data, 2020).

3.3.2 Dynamic dilution system testing

The dynamic dilution system for evaporation of liquid I/VOC mixtures and dilution and delivery of liquid and gas calibration mixtures was evaluated for linearity and reproducibility of delivered concentrations. In addition, for compounds present in both gas cylinders and liquid solutions calibration curves were compared for agreement. Calibrant compounds from liquid (prepared in lab) and gas cylinder (Custom mixture prepared by Apel-Riemer Environmental, Inc., 2019) mixtures were introduced at 0, 1, 2, 4, 8 and 12 ppb (10 times lower concentration for β -caryophyllene) with a total volume of air sampled of 280 cm³ with 6 (0, 1, 2, 4, 8 ppb) or 3 (12 ppb) replicates at each level. From a separate gas cylinder, 1 ppm neohexane was simultaneously sampled at a constant flow rate of 1 sccm and used to normalize the responses from the calibrant compounds. This step served to account for variations in sample volume and instrument sensitivity between samples.

Table 3.1. Composition of different I/VOC collectors and corresponding breakthrough volumes for some of the most volatile target compounds. Collector #4 is a compromise between collectors #2 and #3 with reduced Tenax TA.

Collector No:	1	2	3	4
<i>Bed Material (mg of sorbent)</i>				
Glass beads	40	40	40	40
Tenax TA	20	20	20	10
Carbopack B	30	20	10	20
Carbopack X	40	30	15	20
<i>Breakthrough volume at 30 °C (L)</i>				
MVK+MACR	13.2	8.7	2.0	>2
Isoprene	18.3	19.9	3.6	>2

Figure 3.4 shows calibration curves for benzene, o-xylene, α -pinene and β -caryophyllene from both the standard gas cylinder and the custom liquid solution evaporated and delivered via the dynamic dilution system. Normalized detector response on the y-axis is the integrated area of the chromatographic peak divided by that of neohexane on the same chromatogram. Additionally, for benzene all data points had the mean of the 0 ppb values subtracted from them to account for a small persistent benzene contaminant likely due to the presence of Tenax TA in our adsorbent bed (Cao and Hewitt, 1994). Points are mean values of the six individual samples at each level (three samples at the highest level) with error bars representing plus or minus one standard deviation. To evaluate performance against our theoretical model of linear response with zero response at zero concentration, dotted curves are best fit lines forced through the origin.

These compounds show excellent linearity with $R^2 \geq 0.93$. Agreement between gas and liquid is within 5 %, as measured by the difference in the slopes of the best fit lines. The compounds span a range of volatility from that of a C_6 alkane to a C_{15} alkane, demonstrating the dynamic dilution system's suitability for evaporating and diluting IVOCs as well as VOCs.

Isoprene and methyl vinyl ketone were also analyzed and found to be linear, with $R^2 \geq 0.92$. However, we found consistently and significantly lower responses using the liquid mixtures, likely indicating issues during preparation and storage of the liquid solution related to the high volatility and reactivity of these compounds. For C_5 to C_6 alkane-equivalent volatility compounds, we thus plan to continue to rely on gas cylinder standards until and unless our liquid preparation process can be modified to remove this source of error.

Octamethylcyclotetrasiloxane and decamethylcyclopentasiloxane also had excellent linearity ($R^2 \geq 0.91$) but were found to have about 30 % higher responses using the liquid solution than using the gas cylinder. This could suggest depletion of these compounds in the gas cylinder, but we were not able to test this hypothesis.

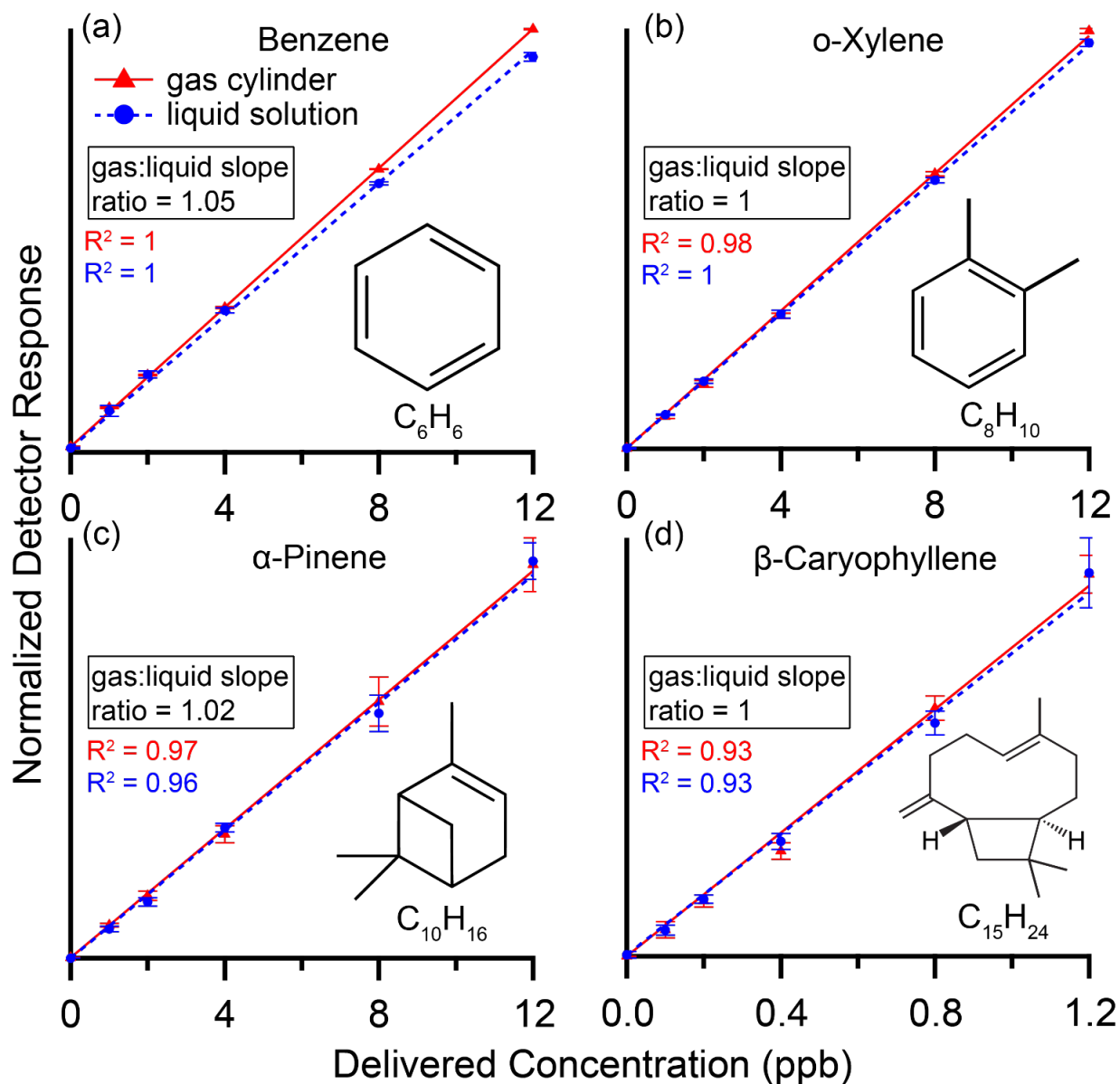


Figure 3.4. Calibration curves with R^2 values for (a) benzene, (b) o-xylene, (c) α -pinene and (d) β -caryophyllene in a gas cylinder (red) and in a custom liquid mixture (blue), delivered by the dynamic dilution system (Figure 3.3). Normalized detector response on the y-axis is the integrated area of the chromatographic peak divided by that of neohexane, our internal standard, on the same chromatogram. Maximum normalized detector response for a given compound ranged from 0.030 (β -caryophyllene, max concentration delivered 1.2 ppb) to 3.0 (o-Xylene, max concentration delivered 12 ppb). Additionally, for benzene all data points had the mean of the 0 ppb values subtracted. Points are mean values of the individual samples at each level with error bars representing plus or minus one standard deviation. Dotted lines are best fit lines forced through the origin, while R^2 values are from best fits not forced through the origin. Compounds show excellent linearity and agreement within 5 % between the gas cylinder and liquid solution.

3.3.3 Limits of detection

Limits of detection (LOD) are species dependent. On the I/VOC channel, limits of detection were estimated using the following formula:

$$\text{LOD} = 3 * \sigma_{\text{blank}} / m \quad (\text{Eq. 3.1})$$

where σ_{blank} is the standard deviation of the integrated area of the chromatographic blank signal (12 replicates) of the quantification ion at the retention time of the analyte in question in units of counts and m is the instrument sensitivity for that analyte, i.e., the slope of the best fit to the calibration curve, in units of counts pptv⁻¹ (Foley and Dorsey, 1984).

Limits of detection were estimated for the 44 compounds present in the Photochemical Assessment Monitoring Stations 57-component commercial standard (Scott-Specialty) that are within the volatility range collected on cTAG's I/VOC channel, including linear, branched and aromatic hydrocarbons (Table 3.2). The LODs range from 0.5 to 8 pptv except for benzene and toluene which have known contamination issues from the Tenax used in the collector (Cao and Hewitt, 1994).

The SVOC channel is equivalent to one channel of the SV-TAG as described in Isaacman et al. (2014). The average limit of detection reported for that instrument is 1 to 2 ng m⁻³ (~0.1 ppt) for a 20 min sample collected at 10 L min⁻¹. We determined that the LOD for the SVOC channel on cTAG determined according to equation (1) is consistent with that reported previously for SV-TAG.

3.3.4 Evaluation of ozone removal on the I/VOC channel

Ozone has been shown to be able to penetrate standard VOC sampling inlets and react with certain analytes collected on adsorbent beds like ours (Calogirou et al., 1996; Helmig, 1997; Pollmann et al., 2005a). A common practice for ozone removal is to pass the sample flow through a sodium thiosulfate impregnated filter upstream of the adsorbent bed (Helmig, 1997). Pollmann et al. (2005) demonstrated that this technique is effective at preventing ozone reaction artifacts for some sesquiterpenes as well as the previously studied monoterpenes and other hydrocarbons. We explored the effects of ozone on the recovery of a suite of compounds of interest known to have short lifetimes with respect to reaction with ozone, including monoterpenes and sesquiterpenes, and tested how placement of sodium thiosulfate (Na₂S₂O₃) impregnated filters upstream of the collector altered the recovery of these compounds. The Na₂S₂O₃ filters were obtained from the Barsanti research group at UC Riverside (Hatch et al., 2017).

To quantify the effects of the presence of ozone in sampled air, we diluted air from the output of an ozone generator (Model 1008-RS, Dasibi Environmental Corp) with humidified zero air to achieve an ozone concentration of 100 ppb ozone. We then verified that the ozone was completely removed by three inline filters by measuring the ozone concentration downstream (Model 202, 2B Technologies). At 1 L min⁻¹ (20 times our ambient sampling rate), ozone breakthrough through a stack of three Na₂S₂O₃ filters occurred after 8 h, indicating a single filter stack can be used without breakthrough for 9,600 min, or about 20 days of continuous operation.

Table 3.2. Limits of detection (LOD) for a selection of linear, branched and aromatic hydrocarbons on the I/VOC channel of cTAG. Compounds are presented in order of volatility from isopentane (5 carbon atoms) to dodecane (12 carbon atoms). *Contamination from the adsorbent materials used in the collector leads to elevated limits of detection for benzene and toluene, consistent with previous reports (Cao and Hewitt, 1994).

Compound	LOD (pptv)	Compound	LOD (pptv)	Compound	LOD (pptv)
Isopentane	2.0	2,3-Methylpentane	3.8	o-Xylene	3.7
1-Pentene	0.5	3-Methylhexane	0.6	Styrene	7.1
Pentane	2.2	Cyclohexane	0.9	Cumene	1.1
<i>trans</i> -2-Pentene	8.0	2,2,4- Trimethylpentane	0.9	n-Propylbenzene	2.5
<i>cis</i> -2-Pentene	1.3	Benzene	90*	Decane	2.7
Isoprene	6.7	Heptane	1.1	m- and p- Ethyltoluene	0.7
2,3-Dimethylbutane	2.3	Methylcyclohexane	1.1	1,3,5- Trimethylbenzene	1.5
2-Methylpentane	7.7	2,3,4- Trimethylpentane	1.3	o-Ethyltoluene	1.1
Cyclopentane	2.4	2-Methylheptane	1.2	1,2,4- Trimethylbenzene	0.6
3-Methylpentane	2.1	3-Methylheptane	0.9	1,2,3- Trimethylbenzene	0.9
1-Hexene	7.2	Octane	3.1	m- Diethylbenzene	0.6
Hexane	1.3	Toluene	60*	Undecane	2.6
2,4- Dimethylpentane	1.1	Nonane	2.8	p-Diethylbenzene	0.6
Methylcyclopentane	0.8	Ethylbenzene	3.9	Dodecane	2.4
2-Methylhexane	1.1	m- and p-Xylene	3.5		

After verifying the efficient removal of ozone by the filter stack, we combined 9 L min⁻¹ of 100 ppb ozone with the 1 L min⁻¹ output from our dynamic dilution calibration system described in Sect. 3.2.5. Using that calibration system, we evaporated a liquid mixture of sesquiterpenes and other compounds to achieve a concentration of 5.60 ppb, which once combined with the 9 L min⁻¹ zero air was reduced to 560 ppt for sampling.

We sampled this liquid mixture onto the I/VOC channel under four different conditions: without ozone and without a Na₂S₂O₃ filter, without ozone and with the filter, with 100 ppb ozone and without the filter, and with 100 ppb ozone with the filter. This allowed us to establish (1) whether an ozone removal method is needed in our instrument for accurate quantification of ozone-reactive species such as some sesquiterpenes and (2) whether the presence of the filter

altered the concentrations of non-ozone-reactive VOCs and IVOCs or of reactive VOCs and IVOCs in the absence of ozone.

Figure 3.5 shows the effects of the Na₂S₂O₃ filter on several analytes of interest with and without ozone. In the absence of ozone, VOC and IVOC concentrations were unperturbed by the presence of the filter except for manageable losses of lower volatility compounds when the filter was present (Figure 3.5 (a)). In the presence of ozone, placement of the Na₂S₂O₃ impregnated filters in the sampling flow upstream of the collector prevented degradation (Figure 3.5 (b)). In general, losses of analytes in the absence of the filter were greater for compounds with lower atmospheric lifetimes with respect to reaction with ozone.

Instrument Response With and Without Na₂S₂O₃ Filter In Presence or Absence of O₃

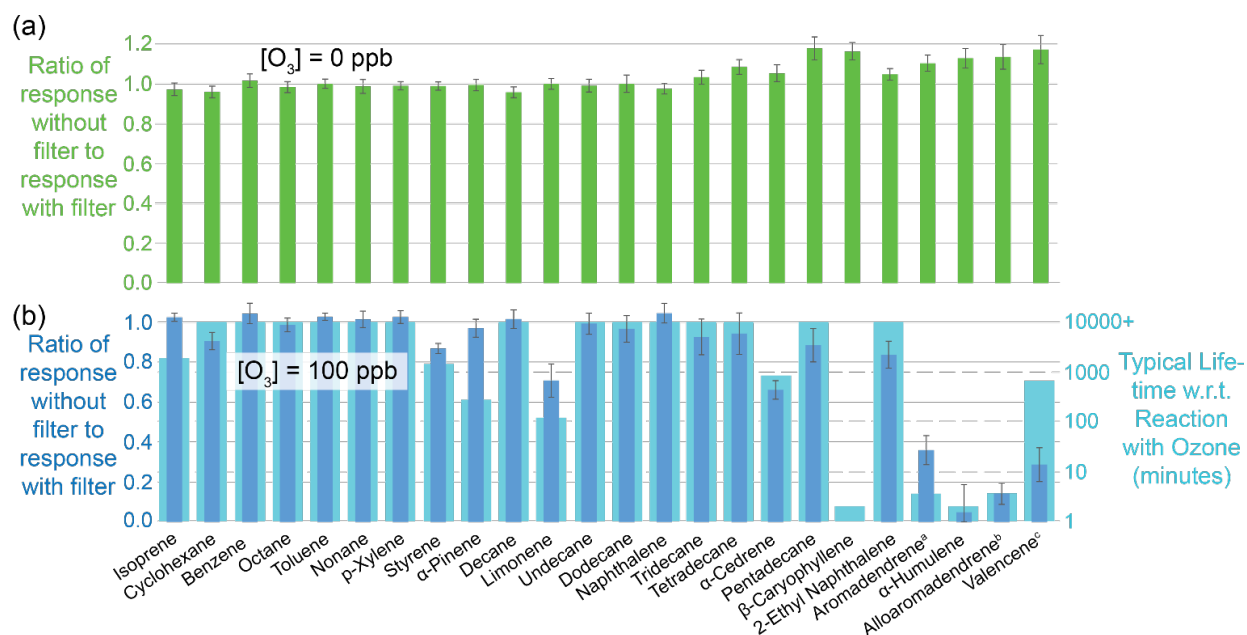


Figure 3.5. Results of evaluation of effectiveness of sodium thiosulfate filter in mitigating the effects of ozone on reactive analytes during collection of VOCs and IVOCs. Error bars represent plus or minus one standard deviation of six replicate measurements. Panel (a) confirms that in the absence of ozone, the filter does not affect the detected quantities of each compound, except for slight (< 15 %) losses of IVOCs with the filter present leading to response ratios greater than 1. Panel (b) demonstrates that the filter prevents substantial losses of reactive species in the presence of ozone, confirming that without preventive measures ozone can significantly deplete certain analytes. Values are compared with published lifetimes with respect to reaction with ozone, with overall qualitative agreement. Published lifetimes are from Atkinson and Arey (2003) unless above 10,000 min or otherwise indicated. ^aPollmann et al., 2005; ^bNo published experimental value; assumed reactivity equal to that of the stereoisomer aromadendrene; ^cHam, 2013.

The results imply having a $\text{Na}_2\text{S}_2\text{O}_3$ impregnated filter inline improves quantification of ozone-reactive species without significant downsides. However, prior literature suggests some very polar compounds, not tested in this experiment, may become trapped on the filter, hindering their measurement (Hatch et al., 2017). Such compounds are unlikely to elute on our GC column, which is optimized for less-polar species. During normal operation of the instrument we thus include a filter inline.

3.3.5 Region of sensitivity overlap

Some of the chemical compounds with alkane equivalent volatility between that of n-tetradecane and n-hexadecane can be detected and quantified on both the I/VOC and the SVOC channels. Comparing quantifications of such compounds between channels can serve as a useful check of instrument performance. However in practice the number of compounds suitable for such an analysis is small, and for any given ambient data set there may be none. One reason for this is the 200 times larger sample volume collected on the SVOC channel, so that some compounds that are easily quantifiable on the SVOC channel are below detection limit on the I/VOC channel. Compounds which are reactive with ozone on timescales of under an hour or so, including many sesquiterpenes (Figure 3.5), must be quantified on the I/VOC channel where ozone is removed at the inlet. Highly polar species may not elute on the I/VOC column; the SVOC channel with its online derivatization is more appropriate in this case. Thus there is usually reason to choose one channel over the other for quantification purposes.

A survey of compounds from the ambient data set from the cTAG deployment in McCall, Idaho for the 2019 Fire Influence on Regional to Global Environments and Air Quality (FIREX-AQ) field campaign was conducted to test cross-channel agreement for compounds in the volatility overlap region. Of the compounds found, all but one, bornyl acetate, was subject to one of the restrictions listed above.

Bornyl acetate ($\text{C}_{12}\text{H}_{20}\text{O}_2$) is found in essential oils from pine trees (Garneau et al., 2012). Though it elutes close to tridecane, which is outside the reliably quantifiable range on the SVOC channel, we were able to quantify it on both the I/VOC and SVOC channels in McCall, Idaho during the 2019 FIREX-AQ field campaign. The concentration ranges from 0.1 to 16.5 ppt as measured on the SVOC channel. The correlation of concurrent sampling points on both channels is shown in Figure 3.6. The I/VOC and SVOC channels agree on average within 11 %, with $R^2 = 0.79$ and 96 % of the data points agreeing within ± 4.8 ppt (3 times the I/VOC channel limit of detection for bornyl acetate). We consider this excellent agreement between the two channels given that the sample sizes differ by more than 2 orders of magnitude, they are calibrated independently, and all data points are within a factor of 10 of the detection limit on the I/VOC channel.

Bornyl Acetate Cross-Channel Comparison

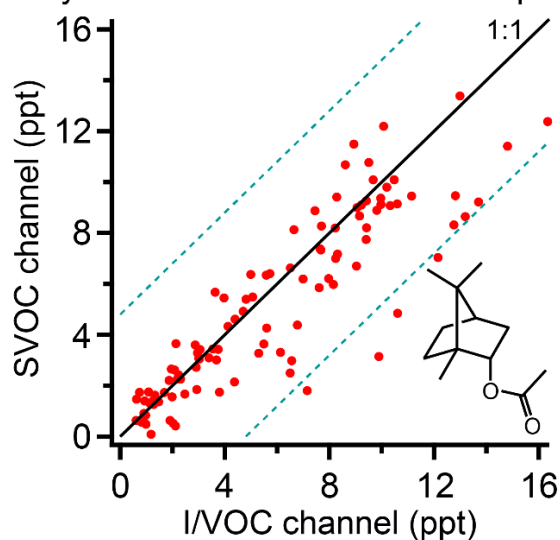


Figure 3.6. Bornyl acetate measured on the I/VOC and SVOC channels of cTAG during FIREX-AQ. Dashed lines represent ± 4.8 ppt (3 times the I/VOC channel limit of detection for bornyl acetate). A total of 96 % of data points fall within the region bounded by the dashed lines. R^2 is 0.79.

3.3.6 Measurements of ambient air

The cTAG was deployed in Livermore, CA in April 2018 for its first field test. This test was undertaken to evaluate the stability of instrument performance during round-the-clock automated operation and demonstrate the capability to measure concentrations of a variety of compound classes from C_5 to C_{32} alkane-equivalent volatility. The instrument was deployed approximately 100 m from a Bay Area Air Quality Management District monitoring site to make use of their air quality measurements for comparison (specifically, ozone and ambient temperature reported here). Livermore is a valley city on the eastern and downwind edge of the San Francisco Bay Area, where pollution outflow from the region combined with optimal conditions for secondary photochemical smog formation frequently leads to the highest ozone levels in the Bay Area (Knoderer et al., 2018). In addition, Livermore has substantial wood burning for heat during winter. An analysis of a subset of VOCs, IVOCs and SVOCs measured in Livermore by cTAG is presented to demonstrate some of the analytical capabilities of this instrument.

cTAG is sensitive to a wide variety of organic compound classes. Figure 3.7 shows some sample chromatograms from Berkeley, California ambient air sampled from outside the lab window, the Livermore 2018 deployment and McCall, Idaho for the 2019 FIREX-AQ field campaign highlighting compounds of interest. The total ion chromatograms and selected ion chromatograms with mass-to-charge ratio of 57, the dominant ion in most alkanes, show the volatility range detected as well as the overlap region of both channels between C_{14} and C_{16} alkane-equivalent volatility. Common air toxics such as benzene, toluene, ethylbenzene, xylene, polycyclic aromatic hydrocarbons and quinones are readily visible, as well as biogenic terpenes and aldehydes, organic acids and polar biomass burning markers. Compounds as polar as glucose (five hydroxy groups) can be detected on the SVOC channel.

cTAG can observe gas-phase chemicals and many of their oxidation products in gas and particle phases. Naphthalene is a gas phase product of incomplete combustion of fossil fuels (Baek et al., 1991) and in urban areas has been observed to primarily originate from vehicle emissions (Howsam and Jones, 1998; Lim et al., 1999). Phthalic anhydride is a major gas-phase photooxidation product of naphthalene and phthalic acid has been found in secondary organic aerosol formed from naphthalene photooxidation (Chan et al., 2009a; Kleindienst et al., 2012; Wang et al., 2007). cTAG is sensitive to naphthalene on the I/VOC channel and the sum of phthalic anhydride and phthalic acid on the SVOC channel. (We have found through laboratory testing of an authentic phthalic acid standard that phthalic acid converts to and is detected as phthalic anhydride in cTAG.) As Figure 3.8 shows, the precursor and products have extremely distinct temporal profiles, with naphthalene concentrations elevated at night and in the early morning hours while the phthalic anhydride plus phthalic acid signal rises in the early to mid-afternoon, consistent with secondary formation and in agreement with observations at other field sites (Williams et al., 2010).

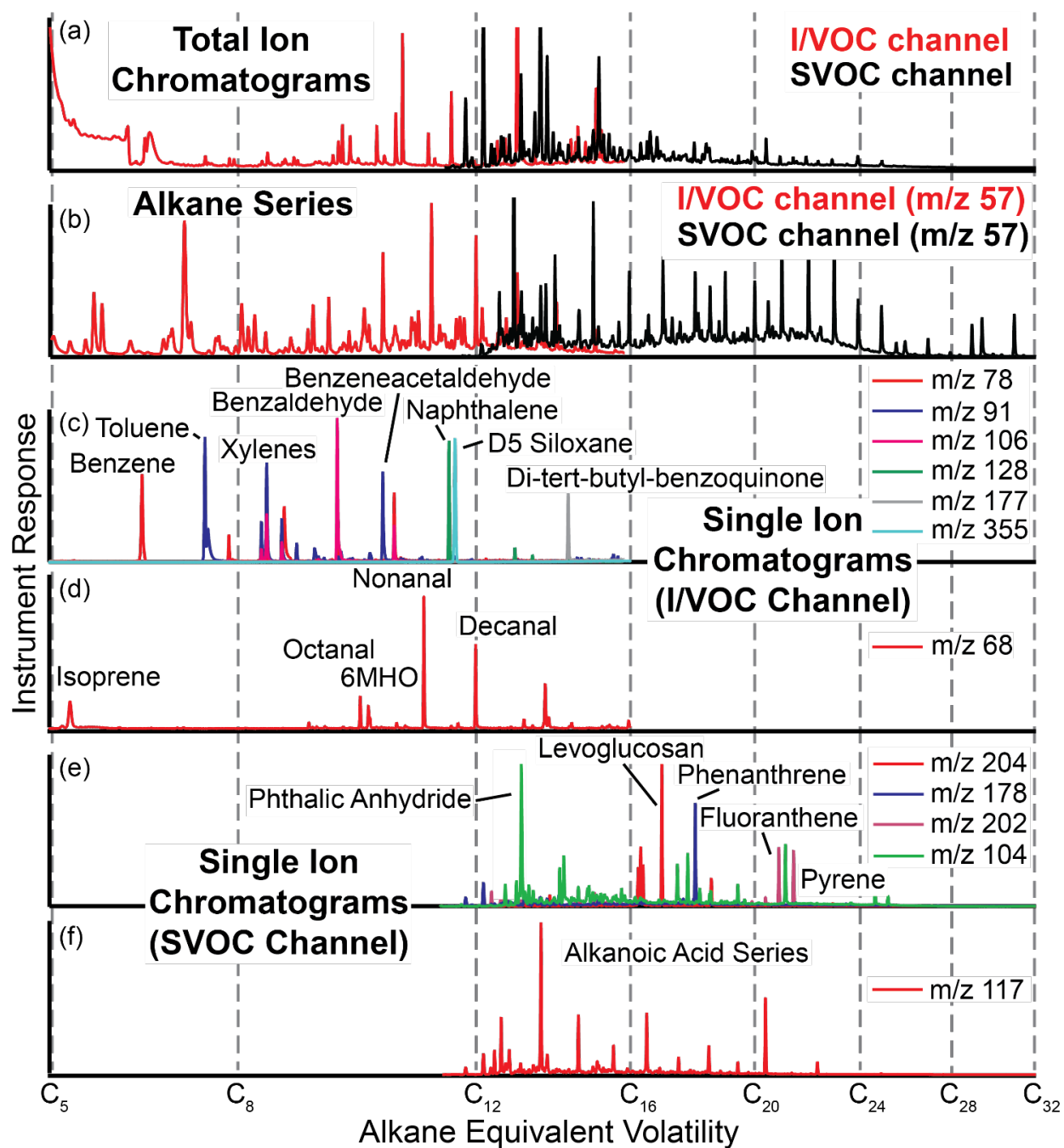


Figure 3.7. Example chromatograms from cTAG. Panels (a) and (b) from FIREX-AQ 2019 in McCall, Idaho demonstrate the range of volatility covered by the two channels, including their overlap region. Single ion chromatograms (panels (c), (d) and (f) from Berkeley, California and (e) from Livermore, California) show examples of the compound classes observable by cTAG, including aromatics, polycyclic aromatic hydrocarbons, organic acids and anhydrosugars.

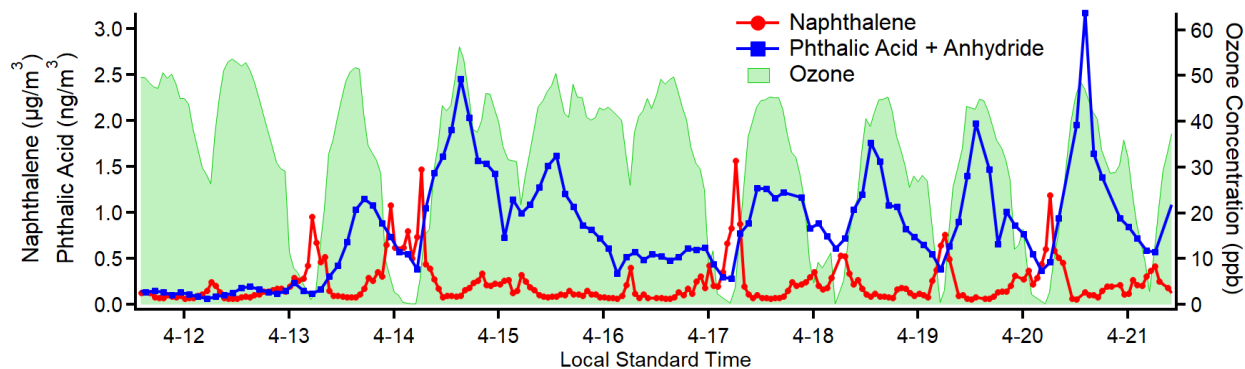


Figure 3.8. Concentration timelines for naphthalene, a primary emission from vehicle exhaust measured on cTAG’s I/VOC channel, and the sum of phthalic anhydride and phthalic acid, secondary photooxidation products of naphthalene detected on cTAG’s SVOC channel. Another secondary compound, ozone, measured at a nearby Bay Area Air Quality Management District monitoring site, provides an independent indication of photochemical activity.

An analysis of straight-chain alkanes along with some aromatics, alkenes and branched alkanes demonstrates cTAG’s volatility range and highlights the different source categories for sub-groups of this set of compounds. The cross-correlation matrix (Figure 3.9) indicates three distinct groupings of compounds. The first group is characteristic of gasoline emissions, spanning a volatility range from below C_5 alkane-equivalent volatility to about C_{11} (Gentner et al., 2013a) and including linear, branched and cyclic alkanes as well as aromatics. It shows short periods of elevated levels in the early morning consistent with a morning rush hour traffic pattern (Figure 3.10). The lack of a similar peak near the end of the day could point to the outsized contribution of cold start emissions to total VOC emissions from gasoline vehicles (Drozd et al., 2016, 2019), as the sampling site was located in a primarily residential area. There is also a well-defined group from C_{20} to C_{26} alkanes with a smooth diurnal variability and daily maximum concentration in the late afternoon (Figure 3.10), consistent with a petroleum-based evaporative source such as asphalt (Khare et al., 2020). The afternoon peaks in concentration result in a clear anti-correlation with the rest of the alkanes in Figure 3.9 (blue and dark red areas). The third group is less pronounced but follows a roughly similar pattern to the high-volatility source category and likely corresponds to diesel fuel emissions, which typically span a volatility range from about C_{10} to C_{22} , with minor contributions from C_{23} – C_{25} alkanes (Drozd et al., 2021; Gentner et al., 2013a; Isaacman et al., 2012b). Our data suggest that overlapping contributions from gasoline and the petroleum-based evaporative sources make this source group less well-defined in the correlation matrix, but semivolatile compounds that have no other major source still correlate well with each other.

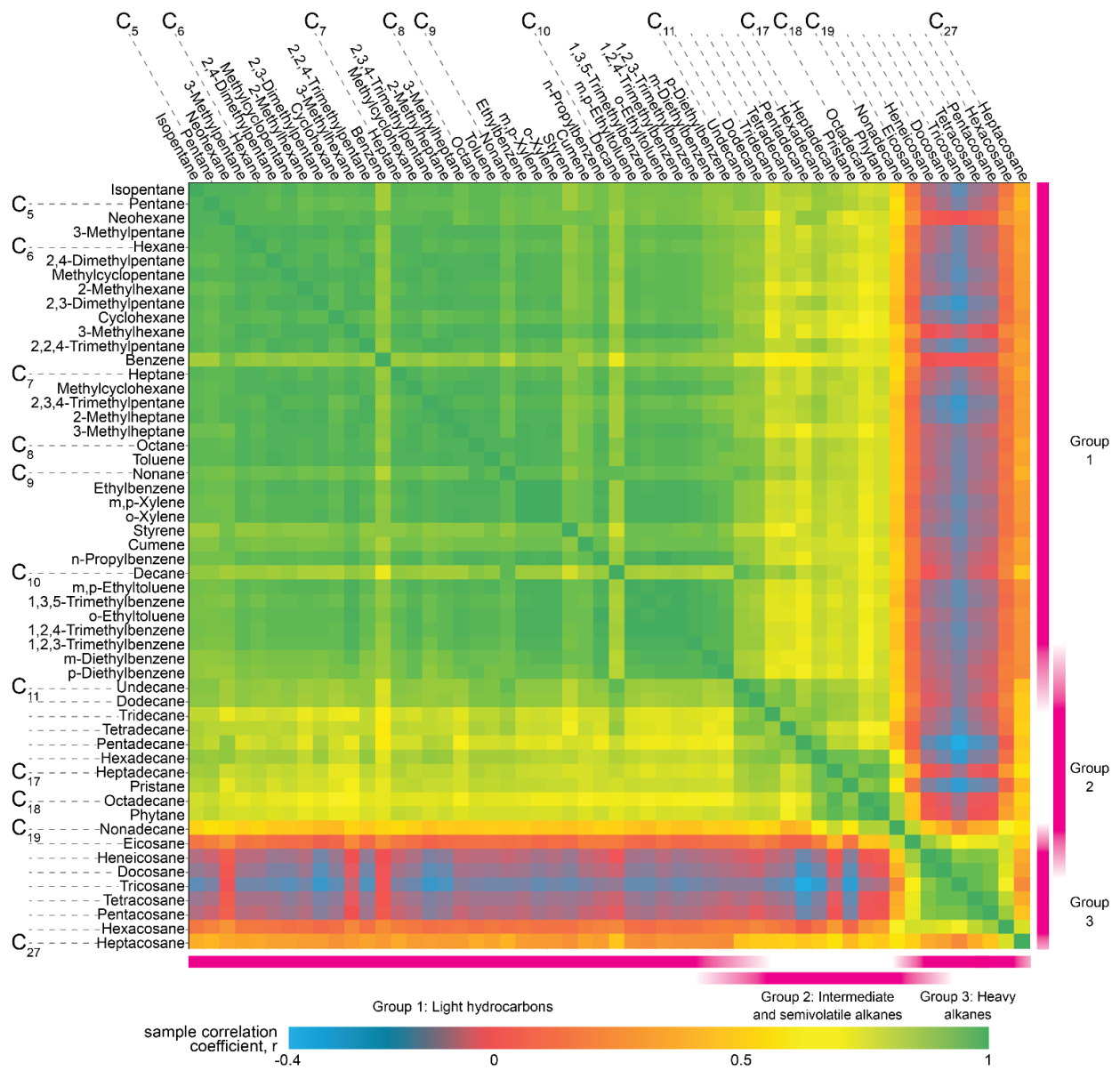


Figure 3.9. Pearson's R correlation matrix for a suite of petroleum-derived compounds observed by cTAG in Livermore, California between 11 April and 21 April 2018, ordered by volatility. Two distinct groupings emerge from C₅ alkane-equivalent volatility to about C₁₁ and C₂₀ to C₂₆, with a third less distinct but still prominent grouping from approximately C₁₁ to C₁₉.

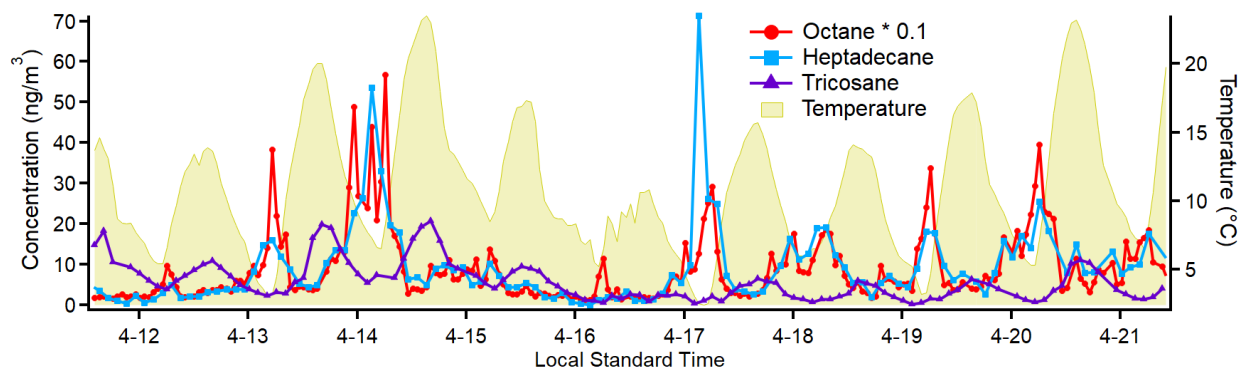


Figure 3.10. Timelines for characteristic species from each of the three main groupings of compounds evident in the correlation matrix (Figure 3.9). The two more volatile groups, represented by octane and heptadecane, tend to peak in the early morning, consistent with morning rush hour cold start emissions. The least volatile group, which includes tricosane, appears to have an evaporative source as it tracks closely, but slightly delayed, with ambient temperature.

3.4 Summary and concluding remarks

The Comprehensive Thermal Desorption Aerosol Gas Chromatograph is a novel instrument capable of measuring nonpolar and some polar organic compounds as well as some more oxidized semivolatile organics from C_5 through C_{32} alkane-equivalent volatility on two separate channels connected to a single HRTofMS. This set of quantifiable compounds encompasses many key VOC pollutants, reactive intermediates, and secondary products, all captured at hourly time resolution. The expanded range of measurable compounds allows for more robust source categorization, with detailed chemical specificity of each identified source category.

Building off development of previous TAG family instruments, development for cTAG focused on the I/VOC channel as well as miniature gas chromatographs to enhance field portability of the instrument. The I/VOC collector is optimized for collection of C_5 through C_{16} alkane-equivalent volatility organics to capture major biogenic VOC and IVOC emissions and ensure overlap with the SVOC channel collection range. The dynamic dilution system with controlled liquid evaporation developed in house is shown to produce stable, linear calibration curves and allows for maximum flexibility in calibration of the I/VOC channel, including quantification of commercially available VOCs and IVOCs not commonly available in calibration gas cylinders or which are difficult or prohibitively expensive to put in such cylinders. Placement of a $Na_2S_2O_3$ impregnated filter in the sampling path for the I/VOC channel is shown to effectively remove ozone without removing appreciable amounts of analytes of interest. Example chromatograms, timelines and correlations for a suite of compounds at a polluted urban field site demonstrate some of the potential for analysis of the data sets produced by this instrument.

Comprehensive, speciated measurements of reactive organic carbon across the full range of volatility are required to fully understand the atmospheric processes that lead to

secondary aerosol formation and dictate the atmospheric lifetimes of key atmospheric oxidants (Heald and Kroll, 2020; Hunter et al., 2017). Moreover, the organic composition and thus the dominant atmospheric processes are likely to vary greatly in different environments (e.g. remote, forested, rural/agricultural, urban), and current science lacks such comprehensive measurements across these different types of sites (Heald and Kroll, 2020). The cTAG is designed for field portability and speciated measurement of a significant fraction of the total reactive organic carbon, making it an ideal choice for helping to close this gap in our current scientific understanding.

3.5 Acknowledgments

Wen Xu and Thorsten Hohaus provided support and customization for the instrument control software. The Livermore Area Recreation and Park District (LARPD) provided the site and infrastructure in Livermore for the Spring 2018 field deployment. The authors would like to especially thank Bruce Aizawa and Steve Sommers of LARPD for enabling us to do measurements at the site. Hourly temperature and ozone measured approximately 100 m away from our site were provided by the Bay Area Air Quality Management District. Christos Stamatis, Dr. Lindsay Hatch and Dr. Kelley Barsanti from the Barsanti research group at University of California Riverside provided sodium thiosulfate impregnated filters and advised and assisted with ozone testing. Instrument development work was supported by the US Department of Energy SBIR/STTR under grant DE-SC0011397. R. Wernis was supported by the US Environmental Protection Agency (EPA) Science To Achieve Results (STAR) Fellowship Assistance Agreement no. FP-91778401-0. FIREX measurements were supported by the National Oceanic and Atmospheric Administration under grant NA16OAR4310107.

Disclaimer: This work has not been formally reviewed by EPA. The views expressed in this work are solely those of the authors, and EPA does not endorse any products or commercial services mentioned in this work.

4 Source apportionment of VOCs, IVOCs and SVOCs by positive matrix factorization in suburban Livermore, California

Abstract

Gas- and particle-phase molecular markers provide highly specific information about the sources and atmospheric processes that contribute to air pollution. In urban areas, major sources of pollution are changing as regulation selectively mitigates some pollution sources and climate change impacts the surrounding environment. In this study, a Comprehensive Thermal Desorption Aerosol Gas Chromatograph (cTAG) was used to measure volatile, intermediate volatility, and semi-volatile molecular markers every other hour over a 10-day period from 11 April to 21 April 2018 in suburban Livermore, California. Source apportionment via Positive Matrix Factorization (PMF) was performed to identify major sources of pollution. The PMF analysis identified 13 components, including emissions from gasoline, consumer products, biomass burning, secondary oxidation, aged regional transport, and several factors associated with single compounds or specific events with unique compositions. The gasoline factor had a distinct morning peak in concentration but lacked a corresponding evening peak, suggesting commute-related traffic emissions are dominated by cold starts in residential areas. More monoterpene and monoterpene mass was assigned to consumer product emissions than biogenic sources, underscoring the increasing importance of volatile chemical products to urban emissions. Daytime isoprene concentrations were controlled by biogenic sunlight- and temperature-dependent processes, mediated by strong midday mixing, but gasoline was found to be the dominant and likely only source of isoprene at night. Biomass burning markers indicated residential wood burning activity remained an important pollution source even in the springtime. This study demonstrates the utility of specific high-time-resolution molecular marker measurements across a wide range of volatility in more comprehensively describing pollution source profiles than a narrower volatility range would allow.

4.1 Introduction

Organic carbon in the atmosphere spans more than 15 orders of magnitude of volatility (Jimenez et al., 2009; Donahue et al., 2011). Some of the organic carbon is emitted directly as primary organic aerosol (POA), but most organic carbon is emitted in the gas phase as thousands of distinct compounds (Goldstein and Galbally, 2007). The most volatile class, volatile organic compounds (VOCs), exist exclusively in the gas phase. Many VOCs are toxic or contribute to respiratory illness (Srivastava et al., 2005; Nurmatov et al., 2013). They play a critical role in urban and regional ozone formation (National Research Council, 1992; Atkinson, 2000) and produce lower vapor pressure compounds via atmospheric oxidation reactions (Seinfeld and Pankow, 2003) which form secondary organic aerosol (SOA). Intermediate volatility organic compounds (IVOCs, defined as having an effective saturation concentration C^* of 10^3 to $10^6 \mu\text{g m}^{-3}$) and semi-volatile organic compounds (SVOCs, C^* of 10^{-1} to $10^3 \mu\text{g m}^{-3}$), can partition between gas and particle phases in the atmosphere and can account for a large fraction of total organic aerosol (OA) (Robinson et al., 2007b; Weitkamp et al., 2007; Chan et al., 2009b; de Gouw et al., 2011; Lim and Ziemann, 2009; Presto et al., 2010). OA is a major source of uncertainty for radiative forcing

predictions (Myhre et al., 2013) and negatively impacts human health (Brunekreef and Holgate, 2002; Nel, 2005; Lippmann and Chen, 2009). In the United States, it comprises 30-80% of annually averaged particulate matter with a diameter of less than 2.5 μm ($\text{PM}_{2.5}$; Hand et al., 2013). $\text{PM}_{2.5}$ is regulated by the U.S. Environmental Protection Agency due to its adverse impacts on human health (Ridley et al., 2018).

Sources of VOCs, IVOCs and SVOCs in urban areas are changing. Historically, vehicle exhaust has been responsible for the bulk of VOC emissions in polluted urban areas such as Los Angeles, but VOC emissions from gasoline vehicles have decreased by almost two orders of magnitude between 1960 and 2010 (Warneke et al., 2012). Diesel emissions have also decreased, though to a lesser extent (McDonald et al., 2013). As a result, sources of non-motor-vehicle organic carbon in urban areas have increased in relative importance. McDonald et al. (2018) recently showed that volatile chemical products, including fragrances, solvents, pesticides, coatings, inks, adhesives and cleaning agents, were responsible for more VOC emissions by mass than vehicle and upstream petrochemical emissions combined in Los Angeles. Coggon et al. (2021) demonstrated the same for New York City and showed that monoterpene emissions from fragrances in Manhattan rivaled those of a comparably sized U.S. forest. Furthermore, global climate change directly affects biogenic emissions of reactive organic carbon (Heald et al., 2008; Lin et al., 2016a) and, in the American West, has led to increased emissions from forest fires (Hurteau et al., 2014; Westerling, 2016); indirectly, climate change may affect pollution patterns related to heating and cooling indoor spaces. Given the changing urban and regional environments, sources of pollution in urban and suburban areas need to be continually reevaluated to improve predictions of ozone and SOA formation and inform policy decision making around emission reductions and mitigation of pollution impacts.

Many organic compounds have more than one source category contributing to their abundance in the atmosphere. Source apportionment models may be used to identify the underlying sources behind the measured concentrations of speciated organics based on the variation of individual concentration timelines. Positive Matrix Factorization (PMF; Paatero and Tapper, 1994; Hopke, 2016) is a technique often used to apportion VOCs (e.g. Brown et al., 2007; Yuan et al., 2009; Yuan et al., 2012) and compositionally resolved particulate matter (e.g. Wang et al., 2019a; Li et al., 2020) into different factors contributing to their measured abundance. PMF does not require pollution source profiles as inputs, making it an attractive approach to analyzing contributions to ambient atmospheric abundances when not all possible sources are known.

In this work PMF was applied to concentration timelines of a suite of VOCs, IVOCs and SVOCs in the gas and particle phases measured every other hour by the Comprehensive Thermal Desorption Aerosol Gas Chromatograph (cTAG) over a 10-day period in Livermore, CA. Our aim was to identify and understand the major sources of pollution in a suburban setting in the context of changing emission controls and dominant sources observed in other urban and suburban areas nationwide. With compounds encompassing such a wide range in volatility and degree of oxidation, we sought to more comprehensively describe the composition of the identified pollution sources. We examine the detailed temporal patterns of the different factors and provide possible explanations for their variability based on likely activity patterns, atmospheric chemistry and the meteorology of the region.

4.2 Methods

4.2.1 Sampling site

Livermore, California is a suburban city located on the eastern edge of the San Francisco Bay Area in the Livermore Valley. It is subject to prevailing winds from the larger Bay Area region to the west, bringing primary pollutants that, combined with optimal conditions in the city itself for photochemical smog formation, often lead to the highest ozone levels in the Bay Area (Flagg et al., 2020). Regional transport is also possible from the neighboring San Joaquin Valley to the east. In wintertime, temperature inversions and low wind speeds can lead to elevated particulate matter concentrations.

Speciated VOC, IVOC and SVOC concentration measurements were collected at the May Nissen Swim Center, 685 Rincon Avenue in Livermore (37.687°N, 121.784°W). The Swim Center is approximately 60 m west of Rincon Avenue, the closest road, and 1.4 km south of Interstate 580. An uncovered outdoor swimming pool, closed to public access for the season, was 10 m to the northeast of the sampling site. Approximately 100 m to the north at 793 Rincon Ave, the Livermore Bay Area Air Quality Management District Monitoring Site obtained hourly measurements of ozone, temperature, black carbon and wind direction and speed used in this analysis.

4.2.2 cTAG measurements of VOCs, IVOCs and SVOCs

Hourly VOC, IVOC and SVOC speciated concentration measurements were collected and analyzed by cTAG between 9 April and 11 May 2018. This work analyzes data from a 10-day focus period between 11 April and 21 April when the cTAG instrument was operating optimally. Ambient air from approximately 5 m above ground was pulled through a 25 cm diameter duct to the inlet of cTAG at 1000 Lpm. This high flow rate ensured small residence times for semivolatile analytes of interest in the ducting and thus negligible partitioning to the walls of the duct. cTAG is described in detail in Chapter 3. Briefly, 10.1 Lpm of ambient air is pulled from the duct through a cyclone (PM_{2.5} cut point) and split. To measure gas-particle partitioning, on every other sample 10.0 Lpm is passed through a denuder to remove gas phase compounds, resulting in alternating hourly measurements of total gas plus particle concentration versus particle phase only concentration. This 10.0 Lpm is then pulled through a coated metal mesh filter cell held at 30°C which collects IVOCs and SVOCs between C₁₄ and C₃₂ alkane equivalent volatility. The remaining 100 sccm is pulled through a bed of adsorbent materials also held at 30°C designed to efficiently collect VOCs and IVOCs between C₅ and C₁₆ alkane equivalent volatility. After the 22 minute sampling period, the collected samples are analyzed in series. The I/VOC collector is desorbed in helium onto the I/VOC channel GC column, which is designed for separation of volatile organics (Restek metal MXT-624, 30 m, 0.32 mm inner diameter, 1.8 μm phase). Column effluent enters the high-resolution time-of-flight mass spectrometer (HRTofMS, TOFWERK), operated at 70 eV electron impact ionization energy to generate individual mass spectra for the separated compounds. GC analysis time is 25 min, with an initial hold for 1 min at 40°C followed by a 10°C min⁻¹ ramp to 250°C and a 3 min hold at 250°C.

During GC and HRTofMS analysis of the I/VOC sample, desorption begins for the SVOC sample in helium saturated with the derivatization agent *N*-methyl-*N*-(trimethylsilyl)

trifluoroacetamide (MSTFA). The MSTFA reacts with OH groups on polar SVOCs to make them less polar and thus more amenable to measurement on the SVOC channel GC column, which is optimized for nonpolar organics. After a reconcentration step which removes excess MSTFA and allows for faster transfer of low volatility species from the collection filter cell, the sample is transferred to the GC column (Restek metal MXT-5, 20 m, 0.18 mm inner diameter, 2 μm phase) for separation and detection by the HRTofMS. GC analysis time is 19 min, with an initial hold for 1 min at 50°C followed by a 20°C min^{-1} ramp to 330°C and a 4 min hold at 330°C.

4.2.2.1 Compound identification

Two chromatograms with mass spectral information are generated every hour – one for I/VOCs and one for SVOCs. Typical total ion chromatograms (TICs) can contain hundreds to thousands of compounds, often leading to overlapping peaks. Single ion chromatograms (SICs) have far fewer overlaps; thus integrated peaks on the SIC corresponding to a prominent mass-to-charge ratio in the target compound's mass spectrum are used as the basis for quantification. Background subtraction isolates the mass spectral fingerprint of the target compound for better matching with searches against the 2020 National Institute of Standards and Technology (NIST) mass spectral library (NIST Standard Reference Database 1A, 2022) and authentic standards analyzed on cTAG or similar instruments. The retention index (RI) describes the relative location of a compound in a chromatogram to a series of reference compounds. The n -alkane retention index for a compound i is defined as:

$$\text{RI} = 100 \times \left[n + \frac{t_i - t_n}{t_{n+1} - t_n} \right] \quad (\text{Eq. 4.1})$$

where n is the number of carbon atoms of the n -alkane that elutes immediately prior to compound i and t is the retention time. N -alkane RI comparisons between the target compound and candidate matches aid in conclusively identifying the target compound.

4.2.2.2 Compound quantification

The integrated peak area calculated for a given compound on a given chromatogram depends on a number of variable factors including but not limited to drift in the response of the detector, ion source cleanliness, transfer efficiency between the collectors and the GC columns and derivatization efficiency (SVOC channel only). Furthermore, these variables can affect the integrated peak area in a compound-dependent way. To account for these variables, compound quantification involves a multistep process. On the SVOC channel:

- (1) A constant quantity of a suite of isotopically labeled compounds with a variety of volatilities and functional groups comprising an internal standard mixture was automatically injected (Isaacman et al., 2011) onto the filter cell after every sample collection and before thermal desorption. These compounds were analyzed along with the ambient sample. Variations in integrated peak area for these compounds capture the instrument response variability described above, improving measurement precision. Ambient compound peak areas are normalized by the SIC peak area of the internal standard that most closely matches it in volatility and functionality.
- (2) In the laboratory after the field campaign, an external standard mixture consisting of 218 compounds was injected onto the filter cell in varying concentrations to obtain a 6-point

calibration curve for those compounds. The same internal standard mixture used during ambient sampling was injected during calibration runs, and peak-integrated ion signals of the calibrant compounds were normalized by the most suitable internal standard.

- (3) External standard calibration curves are fit with a least-squares regression. Ambient compounds with exact matches in the external standard mixture have the slope b and y -intercept a from this fit applied directly to convert peak area S_A to mass M_A . For ambient compounds without exact external standard matches the final mass M_A is adjusted by the ratio of the fraction of signal represented by each SIC in each TIC:

$$M_A = \left(\frac{S_A - a}{b} \right) \left(\frac{f_C}{f_A} \right) \quad (\text{Eq. 4.2})$$

$$f = s_{\text{SIC}} / \sum_{i=4}^{400} s_i \quad (\text{Eq. 4.3})$$

where f is the fraction of TIC signal represented by the signal at the SIC used for quantification (f_A is for the analyte and f_C is for the external standard calibration compound), s_{SIC} is the quantification SIC signal, and the denominator is the sum of all SIC signals (i.e. the TIC signal). i is a mass to charge ratio, which ranges from 4 to 400 for this campaign and analysis.

- (4) The final mass M_A is divided by the sample volume to get the concentration of each compound at each time, which is input into the PMF model.

I/VOC channel calibration is functionally equivalent to SVOC channel calibration with a couple important differences. (1) A single gas-phase internal standard, neohexane, was introduced at the inlet at a constant 100 parts-per-trillion throughout every sampling period for run-to-run normalization. All analytes are normalized by neohexane. (2) External standard compounds originated from a Photochemical Assessment Monitoring Stations 57-component commercial standard gas cylinder (Scott-Specialty), a gas cylinder with a custom mixture (Apel-Riemer Environmental, Inc., 2019), and two custom liquid mixtures. Standards were delivered with the dynamic dilution system developed for cTAG (Section 3.3.2), generating 6-point calibrations. Neohexane could not be sampled during calibrations, so was sampled before and after each set of calibration runs and the average was used to normalize all calibration points.

4.2.2.3 Uncertainty in reported concentration

There are two distinct types of uncertainty affecting reported concentrations for compounds measured by cTAG. The first, uncertainty around accuracy, arises from calibration, which affects all ambient data points of a given compound identically. Uncertainty on the least squares fit of the calibration data and uncertainty arising from the lack of an authentic external standard are uncertainties of this type. The second, uncertainty of precision, arises from run-to-run variability (Section 4.2.2.2), which we assume to be independent between samples. Internal standard normalization greatly mitigates this source of uncertainty but does not eliminate it. The uncertainty that remains depends on the choice of internal standard. The total uncertainty in the reported concentration of a given compound is all of these sources of uncertainty added together in quadrature.

4.2.2.3.1 Accuracy uncertainty

Accuracy uncertainty from the least squares fit is generally limited to the uncertainty of the slope, Δ_b , as the y-intercept is kept fixed at 0 for compounds without background contamination, which is the great majority of them. The percent uncertainty from calibration fit UC_b is thus:

$$UC_b = 100 \times \left(\frac{\Delta_b}{b} \right) \quad (\text{Eq. 4.4})$$

In practice, this adds less than 5% uncertainty to the total for a given compound.

Compounds without an authentic external standard have an additional source of accuracy uncertainty arising from the use of a surrogate standard. This source is much greater than that from the calibration fit, and impossible to quantify individually for each compound in the absence of an authentic standard to serve as the control. Jaoui et al. (2005) report approximately 30% error from this step; we conservatively estimate 50% uncertainty for surrogate standard use.

4.2.2.3.2 Precision uncertainty

Precision uncertainty is based on choice of internal standard. To estimate this source of uncertainty, all possible pairs of internal standards were ratioed for all ambient data points and each distribution of ratios analyzed, a technique used with previous TAG instruments (Isaacman et al., 2014). Ideally, all internal standards would vary proportionally and the ratio between two standards would remain constant, implying no error from internal standard choice. In practice the ratio varies between samples and the relative standard deviation (RSD, standard deviation divided by mean) of the ratios provides an estimate of the precision uncertainty.

Figure B.1 shows the relative standard deviations of the internal standard ratios for all internal standards used for normalization in this analysis and Figure B.2 shows examples of the distributions of ratios. Overall, hydrocarbons paired with hydrocarbons have the lowest RSDs, especially for compounds with similar RIs. An exception is made for compounds with a RI below 1400, where occasional losses during the refocusing step due to high ambient temperature increase the variability. Ambient compounds in this category are normalized by deuterated n-tetradecane. Oxygenated internal standards exhibit the greatest RSD values whether they are paired with hydrocarbons or other oxygenates. Ambient oxygenated compounds are thus assigned the highest uncertainty and are normalized by the nearest deuterated oxygenate if their RIs are within 200 and the nearest hydrocarbon otherwise. Table B.1 summarizes the categories of precision uncertainty assigned to ambient compounds for this analysis.

4.2.3 Positive matrix factorization

Positive matrix factorization is a mathematical source apportionment technique that groups measured ambient compounds based on their covariance in time, taking into account their measurement uncertainty (Paatero and Tapper, 1994). PMF is a receptor-only model that requires no a priori information about pollution sources, instead inferring source composition from the compound groupings in the solution. The solution is constrained to non-negative values and assumes source profiles do not vary with time. It takes the form of three matrices **G**, **F** and **E** such that

$$x_{ij} = \sum_{k=1}^p g_{ik}f_{kj} + e_{ij} \quad (\text{Eq. 4.5})$$

where x_{ij} is an element of the $m \times n$ matrix \mathbf{X} of input data. As applied to this cTAG dataset, the m rows of \mathbf{X} are the individual compounds and the n columns of \mathbf{X} are the sample times. Element g_{ik} of \mathbf{G} represents the source contribution of the i^{th} compound to the k^{th} factor, and element f_{kj} of \mathbf{F} represents the k^{th} factor at sample j . \mathbf{E} is the $m \times n$ matrix of residual values. Crucially, the total number of factors p is an input to the model, requiring the model user to use PMF solution diagnostics and outside information to determine the most meaningful number of factors. The solution is determined by minimizing the sum of squares of error-weighted residuals, known as the quality of fit parameter Q , given by

$$Q = \sum_{i=1}^m \sum_{j=1}^n \left(\frac{e_{ij}}{\sigma_{ij}} \right)^2 \quad (\text{Eq. 4.6})$$

where σ_{ij} is the uncertainty in concentration units for compound i at sample j and e_{ij} is the corresponding element of matrix \mathbf{E} .

This analysis is performed on 2 hour time resolution data aligning with the gas plus particle phase concentration measurements on the SVOC channel. For the PMF, I/VOC channel data that coincides with particle only measurements on the SVOC channel are not used, though the full hourly resolution I/VOC data are used for other data analysis (e.g., correlations) and in figures. Similarly, particle only data on the SVOC channel are not used in the PMF analysis but partitioning information does inform some of the interpretation of factor results.

In this analysis the precision uncertainty (Section 4.2.2.3.2) is the only uncertainty assigned to each compound for use in the PMF model, since the model assumes uncertainty between samples is independent, which is not true of the accuracy uncertainties described above (section 4.2.2.3.1). In the final PMF solution, accuracy uncertainty increases the uncertainty of the factor timelines (while preserving ratios between individual data points) but not the source contributions. PMF modelling was carried out with the United States Environmental Protection Agency PMF 5.0 program (Norris et al., 2014). The program automatically handles uncertainty for concentrations near the detection limit by applying a smooth function to the uncertainty between the input percent uncertainty (applies to concentrations \gg the detection limit) and a large fixed fraction of the detection limit (applies to concentrations at or below the detection limit). We use the “robust” mode of the PMF algorithm, which limits the weight of outliers ($|e_{ij}/\sigma_{ij}| > 4$) by increasing the uncertainty of those outliers. We also explore the stability of the most plausible solutions by varying FPEAK, a parameter which applies rotations by adding \mathbf{G} columns to each other and subtracting \mathbf{F} rows from each other or vice versa (Paatero and Hopke, 2009).

4.3 Results and discussion

Of 163 ambient compounds processed in the dataset, 123 were used in the PMF analysis. The remaining 40 were excluded for one of the following reasons: the compound’s concentration was below the detection limit more than 90% of the time (27 compounds), the compound was

determined to have too much instrument contamination to be quantifiable (7 compounds), the compound could not be definitively identified (3 compounds), the compound's transfer losses were not well characterized due to being outside cTAG's designed optimal volatility range (2 compounds), or the compound is nonreactive in the atmosphere (1 compound).

Of the 123 compounds used in the PMF analysis, 58 compounds were measured on the I/VOC channel and the remaining 65 were measured on the SVOC channel. Table 4.1 shows the compounds included in the PMF analysis. Major compound categories represented include branched and linear alkanes and aromatics important for photochemical smog formation, monoterpenes and other biogenic compounds, polycyclic aromatic hydrocarbons, biomass burning markers, alkanolic acids, chlorobenzenes, and plasticizers and other industrial chemicals.

4.3.1 Positive matrix factorization solution

We find the 13 factor PMF solution to best resolve the pollution sources in Livermore in Spring 2018. Solutions between 3 and 16 factors were considered and are contrasted in Section B.2. In summary, solutions with additional factors have less uniqueness between factors and the source profiles of the additional factors are either not physically meaningful or are too similar to factors present in the 13 factor solution. Solutions with fewer factors fail to separate factors with meaningful physical interpretations and do not incorporate one of the largest reductions in Q/Q_{exp} .

The 13 factor solution has a Q/Q_{exp} value of 0.79, which is close to 1, implying the data are neither overfitted nor underfitted (Ulbrich et al., 2009). Positive FPEAK rotations increase factor cross correlations and Q/Q_{exp} and were therefore not considered (Figure B.4 and Figure B.5). Negative FPEAK rotations slightly decrease factor cross correlations but increase Q/Q_{exp} . We chose to proceed with the unrotated solution because the improvement in factor cross correlations for negative FPEAK rotations was minor and because the unrotated solution minimizes Q/Q_{exp} .

Table 4.1. Compounds measured by cTAG and included in the PMF analysis. The compound index is used in Figure 4.2 and throughout the text for ease of reference. PAH = Polycyclic Aromatic Hydrocarbons; Ox. = Oxidation; Alk. Acids = Alkanolic Acids; HCs = Hydrocarbons; BB = Biomass Burning; THM = Trihalomethanes; DCB = Dichlorobenzenes; DEHA = Bis(2-ethylhexyl) adipate; DEHP = Bis(2-ethylhexyl) phthalate; D4 = Octamethylcyclotetrasiloxane; D5 = Decamethylcyclopentasiloxane; PCBTF = Parachlorobenzotrifluoride.

Compound Class	Compound Index and Name	CAS #	Meas. Channel	Mean \pm S. Deviation (ng m ⁻³)	Mean \pm S. Deviation (ppt)	Highest Mass Fraction & Factor
Saturated HCs	(1) Methylcyclopentane	96-37-7	I/VOC	290 \pm 320	85 \pm 93	0.33 3
Saturated HCs	(2) 2-Methylhexane	591-76-4	I/VOC	140 \pm 170	33 \pm 40	0.45 3
Saturated HCs	(3) 3-Methylhexane	589-34-4	I/VOC	360 \pm 190	87 \pm 47	0.19 1
Saturated HCs	(4) 2,3-Dimethylpentane	565-59-3	I/VOC	130 \pm 180	33 \pm 44	0.31 3

Compound Class	Compound Index and Name	CAS #	Meas. Channel	Mean ± S. Deviation (ng m ⁻³)	Mean ± S. Deviation (ppt)	Highest Mass Fraction & Factor	
Saturated HCs	(5) Cyclohexane	110-82-7	I/VOC	120 ± 140	35 ± 42	0.44	3
Saturated HCs	(6) 2,2,4-Trimethylpentane	540-84-1	I/VOC	400 ± 503	86 ± 108	0.29	3
Saturated HCs	(7) Benzene	71-43-2	I/VOC	610 ± 310	190 ± 100	0.23	3
Saturated HCs	(8) Heptane (C ₇)	142-82-5	I/VOC	170 ± 180	42 ± 43	0.31	3
Saturated HCs	(9) Methylcyclohexane	108-87-2	I/VOC	120 ± 140	30 ± 34	0.35	3
Saturated HCs	(10) 2,3,4-Trimethylpentane	565-75-3	I/VOC	140 ± 190	29 ± 40	0.29	3
Saturated HCs	(11) 2-Methylheptane	592-27-8	I/VOC	370 ± 470	79 ± 102	0.32	3
Saturated HCs	(12) 3-Methylheptane	589-81-1	I/VOC	84 ± 100	18 ± 21	0.36	3
Saturated HCs	(13) Octane (C ₈)	111-65-9	I/VOC	86 ± 88	18 ± 19	0.26	3
Saturated HCs	(14) Toluene	108-88-3	I/VOC	930 ± 960	250 ± 250	0.30	3
Saturated HCs	(15) Nonane (C ₉)	111-84-2	I/VOC	64 ± 68	12 ± 13	0.20	3
Saturated HCs	(16) Ethylbenzene	100-41-4	I/VOC	190 ± 220	43 ± 51	0.36	3
Saturated HCs	(17) m-Xylene + p-Xylene	108-38-3, 106-42-3	I/VOC	670 ± 840	150 ± 190	0.36	3
Saturated HCs	(18) o-xylene	95-47-6	I/VOC	290 ± 360	66 ± 83	0.37	3
Saturated HCs	(19) Styrene	100-42-5	I/VOC	52 ± 61	12 ± 14	0.36	3
Saturated HCs	(20) Cumene	98-82-8	I/VOC	10 ± 12	2.1 ± 2.4	0.23	3
Saturated HCs	(21) n-Propylbenzene	103-65-1	I/VOC	39 ± 47	8.0 ± 9.6	0.36	3
Saturated HCs	(22) Decane (C ₁₀)	124-18-5	I/VOC	63 ± 72	11 ± 12	0.18	5
Saturated HCs	(23) m-Ethyltoluene	620-14-4	I/VOC	110 ± 150	23 ± 31	0.41	3
Saturated HCs	(24) 1,3,5-Trimethylbenzene	108-67-8	I/VOC	68 ± 99	14 ± 20	0.44	3
Saturated HCs	(25) o-Ethyltoluene	611-14-3	I/VOC	55 ± 73	11 ± 15	0.41	3
Saturated HCs	(26) 1,2,4-Trimethylbenzene	95-63-6	I/VOC	290 ± 410	60 ± 84	0.41	3
Saturated HCs	(27) 1,2,3-Trimethylbenzene	526-73-8	I/VOC	55 ± 78	11 ± 16	0.42	3
Saturated HCs	(28) m-Diethylbenzene	141-93-5	I/VOC	9.4 ± 14.3	1.7 ± 2.6	0.43	3
Saturated HCs	(29) p-Diethylbenzene	105-05-5	I/VOC	63 ± 98	12 ± 18	0.41	3
Saturated HCs	(30) Undecane (C ₁₁)	1120-21-4	I/VOC	53 ± 92	8.3 ± 14.4	0.18	5
Saturated HCs	(31) Dodecane (C ₁₂)	112-40-3	I/VOC	31 ± 67	4.5 ± 9.6	0.22	11
Saturated HCs	(32) Tridecane (C ₁₃)	629-50-5	I/VOC	56 ± 123	7.4 ± 16.4	0.25	11
Saturated HCs	(33) Tetradecane (C ₁₄)	629-59-4	I/VOC	49 ± 71	6.1 ± 8.8	0.32	5

Compound Class	Compound Index and Name	CAS #	Meas. Channel	Mean \pm S. Deviation (ng m ⁻³)	Mean \pm S. Deviation (ppt)	Highest Mass Fraction & Factor	
Saturated HCs	(34) Pentadecane (C ₁₅)	629-62-9	SVOC	15 \pm 11	1.7 \pm 1.3	0.26	5
Saturated HCs	(35) Hexadecane (C ₁₆)	544-76-3	SVOC	10 \pm 10	1.1 \pm 1.1	0.22	11
Saturated HCs	(36) Heptadecane (C ₁₇)	629-78-7	SVOC	11 \pm 10	1.1 \pm 1.0	0.21	6
Saturated HCs	(37) Pristane	1921-70-6	SVOC	5.3 \pm 4.7	0.48 \pm 0.43	0.24	11
Saturated HCs	(38) Octadecane (C ₁₈)	593-45-3	SVOC	6.8 \pm 6.1	0.66 \pm 0.59	0.26	6
Saturated HCs	(39) Phytane	638-36-8	SVOC	2.8 \pm 2.3	0.24 \pm 0.20	0.24	6
Saturated HCs	(40) Nonadecane (C ₁₉)	629-92-5	SVOC	3.90 \pm 2.2	0.36 \pm 0.20	0.22	10
Saturated HCs	(41) Eicosane (C ₂₀)	112-95-8	SVOC	4.0 \pm 1.9	0.34 \pm 0.17	0.26	4
Saturated HCs	(42) Heneicosane (C ₂₁)	629-94-7	SVOC	8.50 \pm 4.9	0.70 \pm 0.41	0.31	4
Saturated HCs	(43) Docosane (C ₂₂)	629-97-0	SVOC	9.0 \pm 6.5	0.71 \pm 0.51	0.37	2
Saturated HCs	(44) Tricosane (C ₂₃)	638-67-5	SVOC	6.3 \pm 5.40	0.47 \pm 0.41	0.49	2
Saturated HCs	(45) Tetracosane (C ₂₄)	646-31-1	SVOC	2.3 \pm 2.0	0.16 \pm 0.14	0.54	4
Saturated HCs	(46) Pentacosane (C ₂₅)	629-99-2	SVOC	4.0 \pm 2.8	0.28 \pm 0.19	0.43	4
Saturated HCs	(47) Hexacosane (C ₂₆)	630-01-3	SVOC	2.1 \pm 1.7	0.14 \pm 0.11	0.50	4
Saturated HCs	(48) Heptacosane (C ₂₇)	593-49-7	SVOC	1.5 \pm 1.2	0.09 \pm 0.08	0.31	4
Alk. Acids	(49) Octanoic (C ₈) Acid	124-07-2	SVOC	11 \pm 5	1.9 \pm 0.8	0.20	4
Alk. Acids	(50) Nonanoic (C ₉) Acid	112-05-0	SVOC	41 \pm 16	6.3 \pm 2.5	0.22	4
Alk. Acids	(51) Decanoic (C ₁₀) Acid	334-48-5	SVOC	17 \pm 7	2.4 \pm 1.0	0.24	4
Alk. Acids	(52) Undecanoic (C ₁₁) Acid	112-37-8	SVOC	7.8 \pm 3.7	1.0 \pm 0.5	0.32	4
Alk. Acids	(53) Dodecanoic (C ₁₂) Acid	143-07-7	SVOC	12 \pm 6	1.5 \pm 0.7	0.29	4
Alk. Acids	(54) Tridecanoic (C ₁₃) Acid	638-53-9	SVOC	5.8 \pm 3.3	0.66 \pm 0.38	0.40	4
Alk. Acids	(55) Tetradecanoic (C ₁₄) Acid	544-63-8	SVOC	15 \pm 8	1.6 \pm 0.9	0.31	4
Alk. Acids	(56) Pentadecanoic (C ₁₅) Acid	1002-84-2	SVOC	9.5 \pm 6.7	0.96 \pm 0.68	0.46	4
Alk. Acids	(57) Palmitic (C ₁₆) Acid	57-10-3	SVOC	66 \pm 63	6.4 \pm 6.1	0.26	4
Alk. Acids	(58) Heptadecanoic (C ₁₇) Acid	506-12-7	SVOC	24 \pm 27	2.1 \pm 2.5	0.42	4
Alk. Acids	(59) Stearic (C ₁₈) Acid	57-11-4	SVOC	1100 \pm 1300	93 \pm 116	0.31	4
Alk. Acids	(60) Azelaic (C ₉) Acid	123-99-9	SVOC	96 \pm 115	12 \pm 15	0.33	4
Other	(61) C ₁₆ acid methyl ester	112-39-0	SVOC	20 \pm 14	1.8 \pm 1.3	0.20	10
Other	(62) Nonanal	124-19-6	I/VOC	890 \pm 1260	150 \pm 220	0.25	11
Terpenoid	(63) Isoprene	78-79-5	I/VOC	190 \pm 220	68 \pm 79	0.73	12

Compound Class	Compound Index and Name	CAS #	Meas. Channel	Mean \pm S. Deviation (ng m ⁻³)	Mean \pm S. Deviation (ppt)	Highest Mass Fraction & Factor	
Terpenoid	(64) Camphene	79-92-5	I/VOC	19 \pm 22	3.5 \pm 3.9	0.29	6
Terpenoid	(65) Camphor	76-22-2	I/VOC	74 \pm 60	12 \pm 10	0.29	8
Terpenoid	(66) alpha-Pinene	80-56-8	I/VOC	480 \pm 1370	87 \pm 246	0.35	5
Terpenoid	(67) beta-Pinene	127-91-3	I/VOC	49 \pm 54	8.8 \pm 9.7	0.25	6
Terpenoid	(68) Limonene	138-86-3	I/VOC	160 \pm 300	28 \pm 53	0.66	5
Terpenoid	(69) 3-Carene	13466-78-9	I/VOC	18 \pm 25	3.3 \pm 4.4	0.35	5
Terpenoid	(70) Eucalyptol	470-82-6	I/VOC	310 \pm 250	49 \pm 40	0.28	8
Terpenoid	(71) Aromadendrene	109119-91-7	SVOC	0.9 \pm 0.6	0.10 \pm 0.08	0.37	4
Terpene Ox.	(72) Pinic Acid	473-73-4	SVOC	2.5 \pm 1.7	0.32 \pm 0.22	0.37	8
Terpene Ox.	(73) Pinonic Acid	473-72-3	SVOC	21 \pm 15	2.8 \pm 1.9	0.52	8
Other	(74) Methyl Salicylate	119-36-8	SVOC	3.3 \pm 1.8	0.52 \pm 0.29	0.22	8
Other	(75) alpha-Isomethyl ionone	127-51-5	SVOC	0.70 \pm 0.99	0.08 \pm 0.12	0.45	5
Other	(76) Dibenzofuran	132-64-9	SVOC	1.6 \pm 0.9	0.23 \pm 0.13	0.21	8
Other	(77) Benzophenone	119-61-9	SVOC	2.9 \pm 1.8	0.38 \pm 0.24	0.24	8
Other	(78) Phthalic Anhydride	85-44-9	SVOC	0.72 \pm 0.53	0.12 \pm 0.09	0.42	4
Plasticizer	(79) Dibutyl Phthalate	84-74-2	SVOC	1.2 \pm 0.8	0.11 \pm 0.07	0.26	4
Plasticizer	(80) Diethyl Phthalate	84-66-2	SVOC	3.7 \pm 2.0	0.41 \pm 0.22	0.20	10
Plasticizer	(81) Dimethyl Phthalate	131-11-3	SVOC	0.61 \pm 0.31	0.08 \pm 0.04	0.23	8
Plasticizer	(82) Benzyl butyl phthalate	85-68-7	SVOC	2.6 \pm 1.5	0.20 \pm 0.12	0.28	10
Plasticizer	(83) DEHA	103-23-1	SVOC	500 \pm 600	33 \pm 40	0.62	4
Plasticizer	(84) DEHP	117-81-7	SVOC	10 \pm 10	0.7 \pm 0.6	0.46	4
BB	(85) Furfural	98-01-1	I/VOC	160 \pm 130	41 \pm 33	0.29	9
BB	(86) Levoglucosan	498-07-7	SVOC	18 \pm 27	2.7 \pm 4.1	0.67	9
BB	(87) Galactosan	644-76-8	SVOC	0.6 \pm 1.1	0.09 \pm 0.17	0.68	9
BB	(88) Mannosan	14168-65-1	SVOC	5.3 \pm 8.5	0.81 \pm 1.3	0.62	9
BB	(89) Catechol	120-80-9	SVOC	0.7 \pm 0.3	0.16 \pm 0.07	0.22	4
BB	(90) p-Anisic Acid	100-09-4	SVOC	2.5 \pm 1.2	0.41 \pm 0.20	0.26	10
BB	(91) 4-Hydroxybenzoic Acid	99-96-7	SVOC	3.1 \pm 1.2	0.56 \pm 0.21	0.35	1
BB	(92) Vanillin	121-33-5	SVOC	8.2 \pm 6.7	1.3 \pm 1.1	0.21	9
BB	(93) Vanillic Acid	121-34-6	SVOC	1.0 \pm 1.0	0.14 \pm 0.14	0.46	9

Compound Class	Compound Index and Name	CAS #	Meas. Channel	Mean \pm S. Deviation (ng m ⁻³)	Mean \pm S. Deviation (ppt)	Highest Mass Fraction & Factor	
BB	(94) Syringaldehyde	134-96-3	SVOC	0.9 \pm 1.8	0.13 \pm 0.24	0.66	9
BB	(95) Syringic Acid	530-57-4	SVOC	0.8 \pm 1.0	0.10 \pm 0.13	0.59	9
BB	(96) 4-Nitrocatechol	3316-09-4	SVOC	1.7 \pm 2.3	0.27 \pm 0.37	0.41	9
Other	(97) 2-Nitrophenol	88-75-5	SVOC	1.3 \pm 1.2	0.23 \pm 0.22	0.25	8
Other	(98) 4-Nitrophenol	100-02-7	SVOC	3.1 \pm 2.6	0.54 \pm 0.45	0.38	4
Other	(99) Palmitoleic Acid	373-49-9	SVOC	2.8 \pm 10.6	0.24 \pm 0.93	0.50	3
Other	(100) Phthalimide	85-41-6	SVOC	7.1 \pm 2.5	1.2 \pm 0.42	0.37	1
Other	(101) 1-Octadecanol	112-92-5	SVOC	6.3 \pm 4.3	0.57 \pm 0.39	0.31	2
Other	(102) 1-Tridecene	2437-56-1	SVOC	0.6 \pm 0.6	0.08 \pm 0.08	0.27	11
Other	(103) 2-Tridecanone	593-08-8	SVOC	2.0 \pm 1.2	0.25 \pm 0.15	0.20	5
Other	(104) Acetone	67-64-1	I/VOC	430 \pm 190	180 \pm 80	0.23	10
Other	(105) 2-Cyclopenten-1-one	930-30-3	I/VOC	71 \pm 22	21 \pm 7	0.32	1
Other	(106) Methyl Ethyl Ketone	78-93-3	I/VOC	1700 \pm 700	580 \pm 250	0.26	4
PAH	(107) Naphthalene	91-20-3	I/VOC	130 \pm 130	25 \pm 25	0.32	3
PAH	(108) 1-Methylnaphthalene	90-12-0	I/VOC	25 \pm 22	4.3 \pm 3.8	0.25	3
PAH	(109) 2-Methylnaphthalene	91-57-6	I/VOC	39 \pm 44	6.8 \pm 7.6	0.30	3
PAH	(110) 2-Methoxynaphthalene	93-04-9	SVOC	1.0 \pm 0.9	0.16 \pm 0.13	0.33	1
PAH	(111) Acenaphthylene	208-96-8	SVOC	0.7 \pm 1.7	0.11 \pm 0.27	0.61	3
PAH	(112) Fluorene	86-73-7	SVOC	1.6 \pm 1.3	0.24 \pm 0.18	0.21	8
PAH	(113) Phenanthrene	85-01-8	SVOC	2.4 \pm 2.1	0.33 \pm 0.29	0.17	1
PAH	(114) Pyrene	129-00-0	SVOC	0.7 \pm 0.9	0.09 \pm 0.11	0.32	10
THM	(115) Chloroform	67-66-3	I/VOC	1900 \pm 700	380 \pm 150	0.33	1
THM	(116) Bromoform	75-25-2	I/VOC	9.0 \pm 2.9	0.87 \pm 0.28	0.28	1
THM	(117) Dibromochloromethane	124-48-1	I/VOC	6.3 \pm 7.5	0.74 \pm 0.88	0.45	5
DCB	(118) p-Dichlorobenzene	106-46-7	I/VOC	38 \pm 41	6.3 \pm 6.8	0.27	5
DCB	(119) o-Dichlorobenzene	95-50-1	I/VOC	11 \pm 3.0	1.9 \pm 0.5	0.36	10
Siloxanes	(120) D4	556-57-2	I/VOC	89 \pm 64	7.4 \pm 5.3	0.29	8
Siloxanes	(121) D5	541-02-6	I/VOC	370 \pm 550	24 \pm 36	0.32	8
Solvents	(122) Isophorone	78-59-1	I/VOC	11 \pm 35	2.0 \pm 6.2	0.21	11
Solvents	(123) PCBTF	98-56-6	I/VOC	590 \pm 1490	80 \pm 200	0.68	7

Figure 4.1 shows the timelines for the 13 factor solution and Figure 4.2 shows the corresponding factor profiles. Specific compounds mentioned in the text have the corresponding compound index (CI) used in Table 4.1 and Figure 4.2 included in parentheses for ease of reference. The diurnal profiles of each of the factor timelines are plotted in Figure 4.3, and relevant meteorological data and stacked factor timelines are plotted in Figure 4.4. Rose plots for periods of elevated concentration for each factor are presented in Figure 4.5. The factors are presented in the order that they first appear in the PMF solution for increasing number of factor solutions, e.g., factor 9 in the 13 factor solution is approximately equivalent to the 9th factor in the 9 factor solution. The factors are (1) long-lived and continuously emitted compounds, (2) episodic petrochemical source, (3) gasoline, (4) oxidized urban and temperature-driven emissions, (5) consumer products, (6) primary biogenic and diesel, (7) Parachlorobenzotrifluoride (PCBTF), (8) secondary oxidation and persistent personal care product emissions, (9) biomass burning, (10) industrial and/or agricultural background and continuous combustion source, (11) early morning cooking/diesel event, (12) isoprene, and (13) possible jet fuel event.

Compounds measured on the I/VOC channel dominate by mass, representing 87% of the total mass of the 123 included compounds. No factor had less than 50% of its mass in VOCs and IVOCs (Figure B.6 (a)), reflecting the fact that even a small fractional contribution from a VOC or IVOC is significant compared to large fractional SVOC contributions due to the generally greater concentrations involved. SVOC mass was less evenly distributed between factors than I/VOC

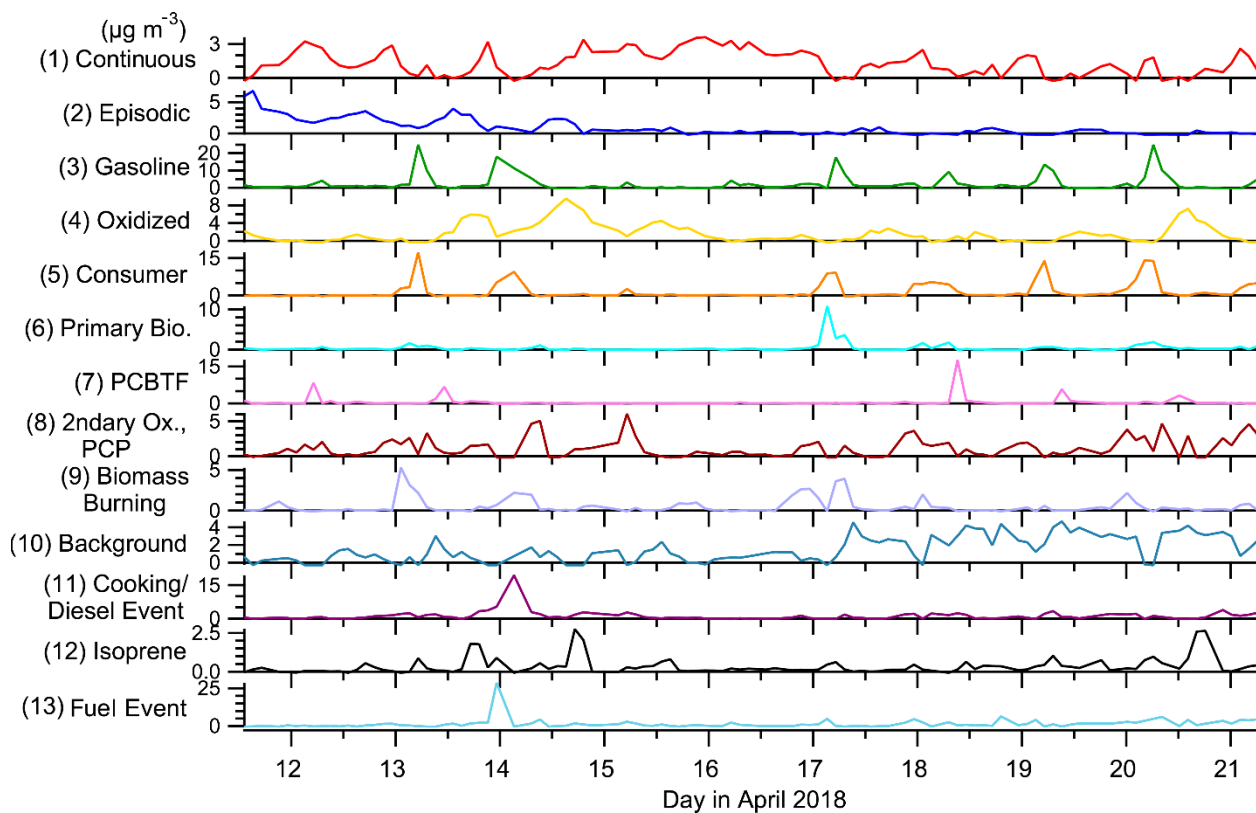


Figure 4.1. 13 factor solution factor timelines. Bio. = Biogenic; PCBTF = Parachlorobenzotrifluoride; 2ndary Ox., PCP = Secondary Oxidation and Personal Care Products. Full factor names are in the main text (Section 4.3.1). Date labels are at midnight.

mass (Figure B.6 (b)), controlled in part by stearic acid (CI 59) and bis(2-ethylhexyl) adipate (hereafter DEHA; CI 83) contributions (Table B.1).

4.3.2 Factor 1: Long-lived and continuously emitted compounds

Factor 1 is mainly long-lived, well-mixed species and species with continuous emissions. Chloroform (CI 115) and bromoform (CI 116) have their highest mass fraction in this factor (33% and 28% respectively). Other well-represented compounds include 4-hydroxybenzoic acid (35%; CI 91), p-anisic acid (26%; CI 90), phthalimide (37%; CI 100), 2-cyclopenten-1-one (32%; CI 105), and 2-methoxynaphthalene (33%; CI 109). This factor is mildly elevated at night, but with high uncertainty, and compounds with a slightly opposite diurnal profile (e.g. 4-hydroxybenzoic acid, phthalimide) can also be found in this factor. When Factor 1 is elevated winds come from all directions, with a mild southwest preference (Figure 4.5). This factor contains high fractional contributions from VOCs, IVOCs and SVOCs, representing a source profile that could not previously be obtained in a single instrument without the expanded volatility range afforded by cTAG.

Both chloroform and bromoform have atmospheric lifetimes of weeks or more (World Meteorological Organization et al., 2019), allowing them to be well-mixed in the troposphere and to therefore have stable concentrations unaffected by meteorological phenomena such as boundary layer height changes. Chloroform accounts for about 40% of the total mass of Factor 1.

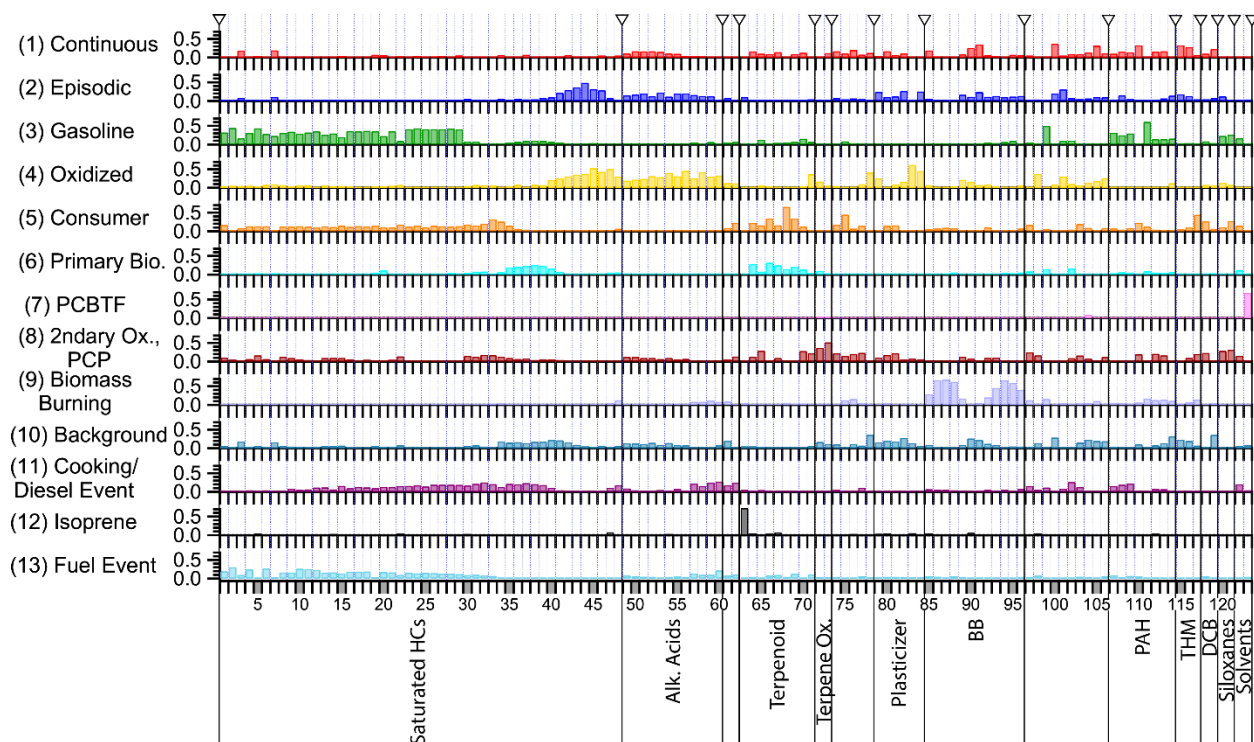


Figure 4.2. 13 factor solution factor profiles. Compounds are ordered as in Table 4.1 using the compound indices assigned. Unlabeled groups are labeled “other” in Table 4.1.

The other compounds present in this factor have the common characteristics of (1) being constantly present and (2) having a weak to nonexistent diurnal variation, but their known sources are distinct and they are much more reactive than chloroform and bromoform. 4-hydroxybenzoic acid and p-anisic acid have been identified as tracers for burning of grasses (Simoneit, 2002) and have an estimated atmospheric lifetime with respect to OH ($[OH] = 2 \times 10^6$ molecules cm^{-3} for this and every atmospheric lifetime estimate hereafter) of about a day (U.S. EPA, 2022). Phthalimide is a fungicide and insecticide degradation product produced in the processing of crops. It may also be formed from phthalic anhydride and primary amino groups in the high temperature desorption process just before chromatographic separation, a possibility that we cannot rule out (Gao et al., 2019). Phthalimide has an estimated OH lifetime of a few hours (U.S. EPA, 2022). Atmospheric studies of 2-cyclopenten-1-one, which is naturally occurring and biologically significant (PubChem, 2022), and of 2-methoxynaphthalene, which has industrial sources and uses (European Chemicals Agency, 2022), are lacking. The latter has an estimated lifetime with respect to reaction with OH of a few hours (U.S. EPA, 2022).

These relatively reactive compounds must have constant emission sources to produce timelines with so little variability. Because Factor 1 is associated with winds from all directions, the sources would need to be either hyper local or ubiquitous in the surrounding area. Agricultural activity may be able to account for 4-hydroxybenzoic acid, p-anisic acid, phthalimide, and 2-cyclopenten-1-one.

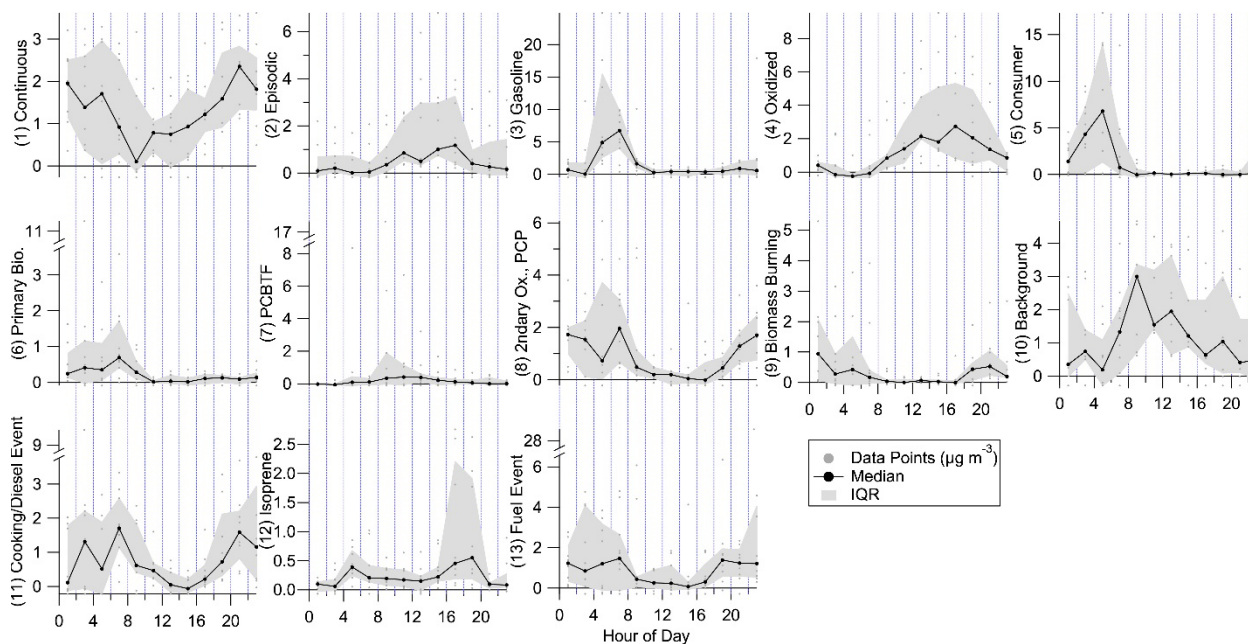


Figure 4.3. Diurnal profiles of the factor timelines in the 13 factor solution. IQR = Interquartile range.

4.3.3 Factor 2: Episodic petrochemical source

Factor 2 is a transient source, elevated during the first few days of the measurement period and nearly nonexistent after that. It contains minor contributions from C_{20} – C_{25} *n*-alkanes (mass fraction 20–50%; CIs 41-46), 1-octadecanol (31%; CI 101) and some semivolatile phthalates (~25% each; CIs 79, 82). Winds tend to originate from the west when this factor is high (Figure 4.5).

The heavy *n*-alkanes are split between Factors 2 and 4 (oxidized urban and temperature-driven emissions), with slightly different distributions; the Factor 2 *n*-alkanes skew slightly lighter, while Factor 4 includes contributions from C_{26} and C_{27} alkanes (CIs 47, 48). C_{20} – C_{27} *n*-alkanes are associated with petroleum-based products (Simoneit, 1999). (Biogenic sources of heavy alkanes exhibit a preference for alkanes with an odd number of carbon atoms over those with an even number (Simoneit, 1989), which is not observed in this dataset, confirming the fossil fuel origin of the *n*-alkanes.) Two possible sources in this study are motor oil (Caravaggio et al., 2007; Mao et al., 2009; Isaacman et al., 2012a) and asphalt (Rogge et al., 1997; Khare et al., 2020), both of which exhibit temperature-dependent evaporation of alkanes in this carbon number range. Since the alkane distribution is different between the two factors, it is reasonable to assume the elevated levels of some of these alkanes at the beginning of the campaign represent a different source than the regular afternoon maxima characteristic of Factor 4. The center of the *n*-alkane mass distribution in motor oil is typically at C_{25} or greater, though Isaacman et al. (2012) observed a peak at C_{24} for motor oil aerosol particles due to preferential evaporation of lighter alkanes at low temperatures. Maximum fresh asphalt alkane emissions occur at C_{14} , though after 2 to 3 days emission is approximately constant across C_{14} – C_{32} alkanes (Khare et al., 2020). Since the alkane distribution of asphalt emissions skews lighter, one possibility is that the elevated concentration of Factor 2 in the first few days is in part due to fresh paving nearby. However, the composition of motor oil is highly variable (Mao et al., 2009); the sources of alkanes in Factors 2 and 4 could be two different motor oils, for example, or could represent fresh vs older asphalt.

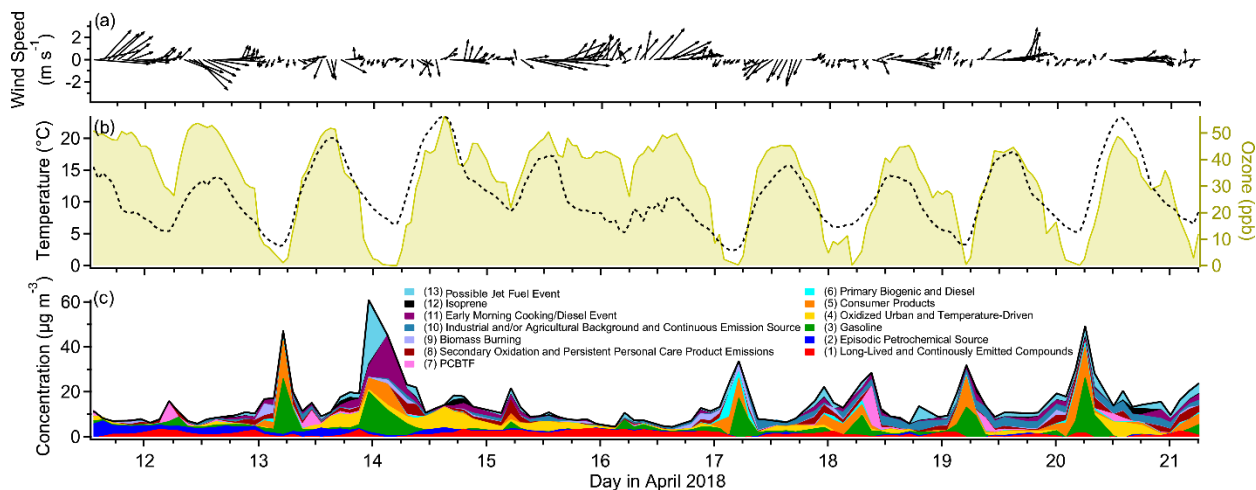


Figure 4.4. (a) Time series of wind speed and direction, (b) time series of temperature (left axis) and ozone (right axis) measured at the Bay Area Air Quality Management District monitoring site, and (c) all factor timelines stacked. Date labels are at midnight.

The semivolatile phthalates in this factor, dibutyl phthalate (CI 79) and benzyl butyl phthalate (CI 82), are plasticizers used as coatings in manufactured goods and in building materials (Zota et al., 2014). Their emission exhibits temperature dependence (Fujii et al., 2003). In this study, their concentrations are moderately correlated with temperature ($r = 0.59$ for dibutyl phthalate and $r = 0.42$ for benzyl butyl phthalate), unlike the less volatile plasticizers bis(2-ethylhexyl) adipate (CI 83) and bis(2-ethylhexyl) phthalate (CI 84), which correlate very strongly with temperature and mostly show up in Factor 4, and the more volatile phthalates associated with personal care products (see discussion for Factor 5). Again we may speculate a unique and temporary source for these two compounds at the beginning of this field campaign, plausibly related to construction activity that could also be responsible for *n*-alkane emissions from fresh asphalt.

1-octadecanol has vegetation/microbial (Nolte et al., 2002; Simoneit, 2006), biomass burning (Nolte et al., 2001b), and anthropogenic (as detergent; Mudge et al., 2012) origins. 1-octadecanol does not appear in Factor 9 (biomass burning), though two short elevated concentration periods on the evening of 16 April and the early morning of 17 April coincide with one of the biomass burning episodes. Given the non-persistent nature of Factor 2 and 1-octadecanol, an intermittent anthropogenic detergent source seems more likely than a biogenic source, which would likely emit continuously or at least regularly throughout the sampling period.

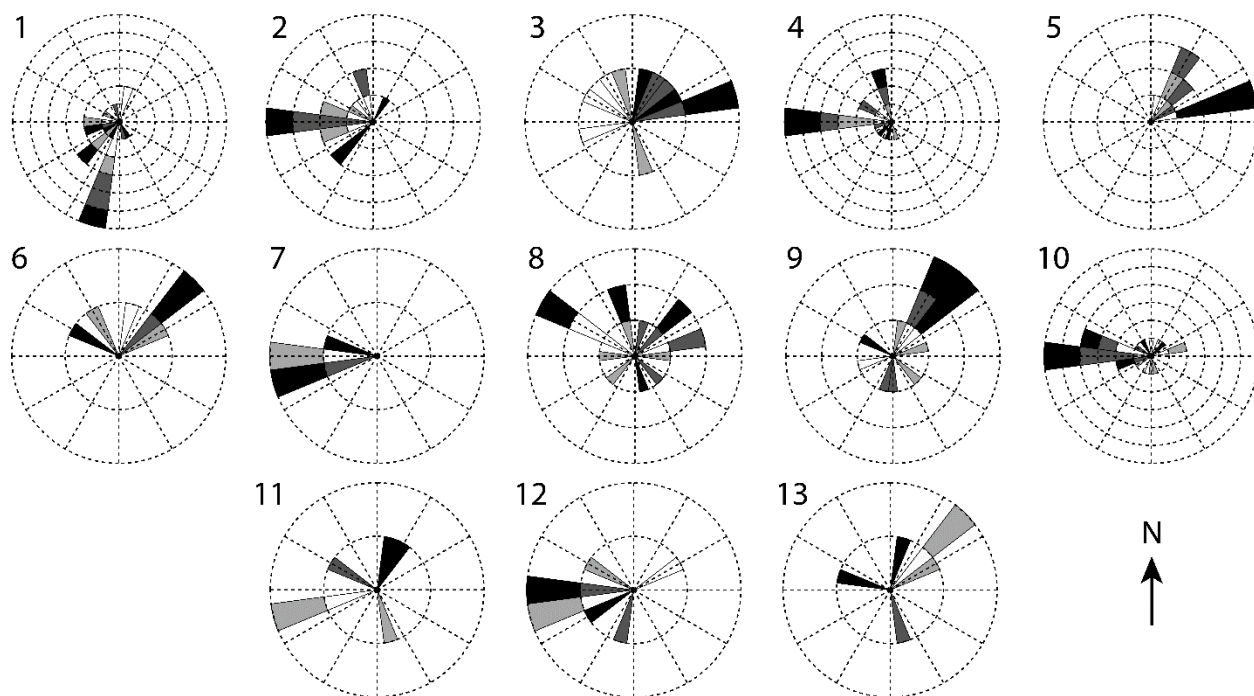


Figure 4.5. Rose plots, showing the correlation of emissions and wind direction, of each factor using only data points where the concentration was elevated, defined as > 1 standard deviation above the mean factor concentration. Frequency of observations are represented by the length of each wedge, where each ring corresponds to one observation. Shading corresponds to quartiles of factor concentration (darker = greater concentration).

4.3.4 Factor 3: Gasoline

Factor 3 is designated as primary gasoline exhaust. Compounds with the highest mass fraction in this factor include linear, branched and aromatic hydrocarbons with 6 to 10 carbon atoms (CIs 1-29) and polycyclic aromatic hydrocarbons (PAHs), especially naphthalene and methylnaphthalenes (CIs 107-109). These are the main organic components of gasoline exhaust (Schauer et al., 2002b; Gentner et al., 2013b). Palmitoleic acid (CI 99) also has a high mass fraction contribution, and octamethylcyclotetrasiloxane (D4; CI 120) and decamethylcyclopentasiloxane (D5; CI 121) are present. In periods of high concentration for this factor, wind speeds were low (about 1 m s^{-1} or lower) and wind directions were variable, with a slight preference for northeastern origin (Figure 4.5).

This factor exhibits a strong diurnal pattern with sharp peaks in concentration in the early morning (between 5 and 7AM local standard time) and near zero loading at other times of day. This factor strongly correlates with NO_x (Pearson's $r = 0.88$) and anti-correlates with ozone ($r = -0.66$). With over 80% of Livermore workers commuting by private vehicle or carpool (United States Census Data, 2022), the early morning elevated concentration is likely commute-related. Our hypothesis for the exhibited diurnal profile is as follows. First, emissions of both hydrocarbons and NO_x from automobile tailpipes are low overnight but increase in the early morning hours as morning commutes begin with cold engine starts. Drozd et al. (2016) found that emissions from cold starts dominate non-methane organic gas emissions from light duty vehicles, with over 45 km of driving required to match the initial cold start emissions for over 97% of light duty vehicles in use in the United States today. The morning peaks are correlated with, and enhanced by, cooler temperatures and generally slower wind speeds (Figure 4.4). The shallow planetary boundary layer overnight and absence of sunlight allow NO_x and hydrocarbons to build up, raising measured concentrations. As the day progresses, the boundary layer rises and wind speeds increase, diluting species near ground level, and photochemistry begins, reacting away hydrocarbons and NO_x and producing ozone. Late afternoon and evening return commutes have greatly reduced emissions because vehicle catalytic converters are already hot by the time drivers return to the predominantly residential area surrounding the sampling site. Higher ambient temperatures in the afternoon also contribute to reduced cold start emissions and greater wind speeds and more rapid oxidative loss prevent what emissions are still produced from building up. In the late evening and night, emissions remain low and thus concentrations also remain low despite the low boundary layer and lack of photochemistry.

Factors 5 and 6 and many marker compounds share this general pattern of elevated concentrations exclusively in the early morning hours. They are governed by the same large-scale atmospheric processes. Thus while differences exist which allow them to be separated by the PMF model, which will be discussed in the descriptions for those factors, their overarching similarity means the sources are not separated perfectly. For example, palmitoleic acid is primarily a tracer of cooking (Rogge et al., 1996; Robinson et al., 2006), yet has its highest mass fraction in this factor, while other cooking tracers appear in other factors. Together with the overall similarity in variability between gasoline and cooking markers, palmitoleic acid's low and noisy signal may have caused it to be placed in this factor primarily by the model, even though it does not originate from the same pollution source.

D4 and D5 siloxanes have substantial fractions of their mass in this factor (23% and 27% respectively). D5 has been established as a tracer compound for personal care product emissions (Horii and Kannan, 2008; Wang et al., 2009; Coggon et al., 2018). It is also prominent (mass fraction of 28%) in Factors 5 and 8, which both contain fragrance compounds commonly found in consumer products, including personal care products. The fact that D5 is present in Factors 3, 5 and 8 while the fragrance compounds are only present in Factors 5 and 8 could be reflective of different emission rates from those products. D5 is found in the greatest concentrations in antiperspirants (Wang et al., 2009); once applied, while emissions are highest immediately after application, it evaporates over the course of several hours (Montemayor et al., 2013) and has even been directly measured in an engineering classroom in the afternoon (Tang et al., 2015) and outside an automobile in cabin fan exhaust from human occupants who had applied D5-containing personal care products earlier that day (Coggon et al., 2018). Evaporation of monoterpenes and monoterpenoids, which comprise the vast majority of the mass of fragrance compounds measured in this study, is likely to happen much faster due to their greater volatility (Hazardous Substances Data Bank, 2022). A study of evaporation of 300 μL of essential oils indoors found that most VOC mass, including most monoterpene mass, was emitted during the first 30 minutes (Su et al., 2007).

D4 is mainly indicative of adhesive and pesticide use (Gkatzelis et al., 2021) but is also found in consumer products (Horii and Kannan, 2008; Wang et al., 2009), though it is not present in Factor 5, the consumer product factor. If the D4 measured in Livermore is from consumer products, it is not clear why the peak concentration coincides with the gasoline markers, later in the day than the peak of the other consumer product compounds.

It is likely that some mass from the diesel emission source is in this factor. Black carbon, which originates almost entirely from diesel emissions (Gentner et al., 2013b), correlates best with this factor ($r = 0.84$), suggesting some of the variability in this factor is driven by diesel exhaust emissions of compounds found in both gasoline and diesel exhaust.

4.3.5 Factor 4: Oxidized urban and temperature-driven emissions

Factor 4 represents aged urban emissions and temperature-driven emissions. This factor includes heavy *n*-alkanes ($\text{C}_{20}\text{--}\text{C}_{27}$; CIs 41-48) as well as the *n*-alkanoic acid series ($\text{C}_8\text{--}\text{C}_{18}$; CIs 49-59), with approximately 30–50% of the mass of each compound in these two classes included in this factor. Several other compounds are also present, including DEHA (62%; CI 83), bis(2-ethylhexyl) phthalate (hereafter DEHP; 46%; CI 84), phthalic anhydride (42%; 78), 4-nitrophenol (38%; CI 98), aromadendrene (37%; CI 71) and azelaic acid (33%; CI 60). This factor contains the largest fraction of semivolatile mass of any of the factors (Figure B.6 (a)), largely due to the presence of DEHA and the fatty acid series. Factor 4 correlates strongly with temperature (Pearson's $r = 0.82$), peaking in the mid to late afternoon. Winds are moderately strong and from the west when this factor is elevated (Figure 4.5). The smooth variation in concentration of Factor 4 suggests a regional source rather than a local one, which would likely display greater inter-hourly variability in concentration and greater sensitivity to small changes in wind direction.

DEHA and DEHP are both semivolatile plasticizers found in polyvinyl chloride, commonly found in building materials (Liu and Little, 2012; Shi et al., 2018; Bui et al., 2016). Like Factor 4,

these two compounds correlate strongly with temperature ($r = 0.83$ for DEHA and $r = 0.73$ for DEHP), consistent with temperature-dependent emission which has been observed in controlled studies (Clausen et al., 2012; Fujii et al., 2003; Liang and Xu, 2014). The heavy alkanes are discussed in detail in the Factor 2 (episodic petrochemical source) section. They are known to originate from evaporative, temperature-dependent sources such as motor oil and asphalt, consistent with the temporal profile of Factor 4.

The remaining compounds represented in this factor are not likely to originate from evaporative sources, but given the consistent winds from the west could represent oxidized emissions transported from the east and south Bay Area. Phthalic anhydride is a secondary product of the photooxidation of naphthalene and phthalic acid has been found in secondary organic aerosol formed from naphthalene photooxidation (Chan et al., 2009b; Kleindienst et al., 2012; Wang et al., 2007). During the study period, conditions for optimal photooxidation (i.e., high solar flux) coincided with periods of high temperature, causing these distinct source categories to appear in the same PMF factor.

In urban and suburban areas, the n-alkanoic acid homologous series is most often ascribed to cooking emissions (Schauer et al., 2002a; Robinson et al., 2006; Allan et al., 2010; Mohr et al., 2012; Yao et al., 2021), but biomass burning, motor vehicle exhaust and road dust can all contribute (Schauer et al., 1996; Rogge et al., 1996). The fatty acids also originate from terrestrial microbial activity (Simoneit and Mazurek, 1982) and marine phytoplankton (Kawamura et al., 2003), sources that tend to dominate in remote areas (Kawamura et al., 2003; Cahill et al., 2006; Fu et al., 2014; Boreddy et al., 2018). Alkanoic acids from cooking exhibit a distinct diurnal profile, with elevated concentrations around dinner time and occasionally another similar peak around lunchtime (Allan et al., 2010; Mohr et al., 2012; Dall'Osto et al., 2015; Yao et al., 2021). In this study, palmitic (C_{16} ; CI 57) and stearic (C_{18} ; CI 59) acids, which are emitted from meat cooking (Rogge et al., 1991), do show occasional evening elevated concentrations (not captured in the Factor 4 profile), but the other alkanoic acids do not. The defining feature that likely caused the fatty acids to be grouped in this factor is the period of sustained elevated concentrations between the evenings of 13 April and 15 April, with almost no diurnal sensitivity (Figure 4.6). This temporal profile is inconsistent with local emissions from the sources mentioned above, but an elevated regional background transported from urban areas to the west could explain the variability. Azelaic acid, the C_9 dicarboxylic acid, has similar sources to the n-alkanoic acids (Kawamura and Bikkina, 2016) and a similar temporal profile to palmitic and stearic acids, including brief evening spikes in concentration likely from cooking and the two-day period of elevated concentration.

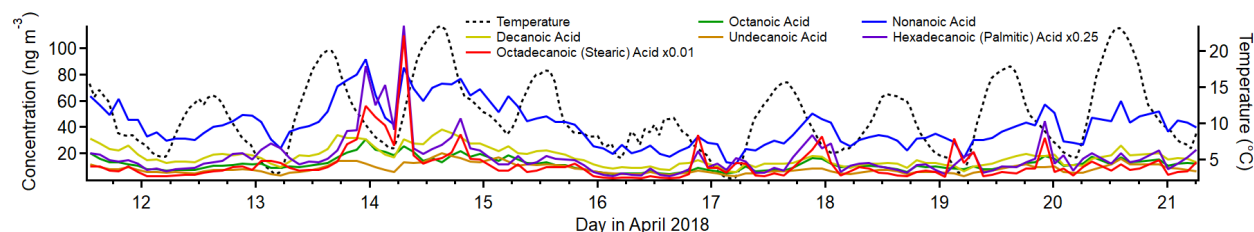


Figure 4.6. Timelines of select alkanoic acids (left axis) and temperature (right axis) for the study period.

The timeline of the sesquiterpene aromadendrene exhibits the same period of sustained elevated concentration as the alkanolic acids and azelaic acid. Sesquiterpene emissions from plants are temperature dependent (Duhl et al., 2008; Bouvier-Brown et al., 2009). Emission outpaces loss on some days despite aromadendrene's very high reactivity with ozone (Pollmann et al., 2005b) and the hydroxyl radical (Ng et al., 2007).

4-nitrophenol is strongly represented in this factor (38% mass fraction), while its isomer 2-nitrophenol (CI 97) does not contribute at all. Both nitrophenols are emitted during motor vehicle combustion (Nojima et al., 1983; Tremp et al., 1993) and in some industrial manufacturing (Harrison et al., 2005b). Biomass burning also leads to production of 4-nitrophenol and possibly 2-nitrophenol (see Factor 9 discussion). Secondary formation of nitrophenols occurs from photooxidation of aromatic hydrocarbons such as benzene, toluene, phenol and cresol (Harrison et al., 2005b). Primary emissions from vehicles and secondary formation are thought to be the most important sources of nitrophenols in polluted urban environments (Inomata et al., 2013; Lu et al., 2019).

4-nitrophenol is observed in greater concentrations than 2-nitrophenol in this study both on average and at each data point except for about 10 nighttime samples (Figure 4.7), even in the gas phase. This is in contrast to other studies (Lüttke et al., 1999; Cecinato et al., 2005), though most modern studies did not distinguish between the two isomers (Yuan et al., 2016; Cheng et al., 2021; Wang et al., 2020; Salvador et al., 2021) or did not quantify 2-nitrophenol (Kitanovski et al., 2012; Wang et al., 2017, 2018, 2019b). Nitrophenols from vehicle exhaust show a mild preference for the ortho isomer (Nojima et al., 1983; Tremp et al., 1993), and gas-phase secondary formation favors 2-nitrophenol as well (Harrison et al., 2005a). Liquid-phase secondary formation is likely to be an important production mechanism for nitrophenols, but the ratio of isomer production for this process is unknown (Harrison et al., 2005a). Observations of particle-phase nitrophenol show a strong preference for the para isomer (Lüttke et al., 1999; Harrison et al., 2005b), likely due to its much lower vapor pressure and much higher Henry's law constant (Sander, 2015; U.S. EPA, 2022), but 4-nitrophenol is observed predominantly in the gas phase in this study, consistent with other studies (Yuan et al., 2016; Cheng et al., 2021). There are several loss processes of gas-phase nitrophenol, with photolysis thought to be the most important (Vione et al., 2009; Yuan et al., 2016), though comparison of gas-phase photolysis between 2NP and 4NP is not currently feasible (Chen et al., 2011; Sangwan and Zhu, 2018).

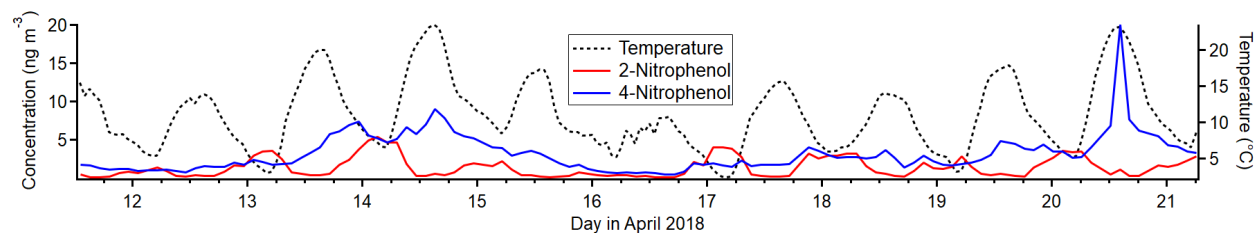


Figure 4.7. Timelines of nitrophenol isomers (left axis) and temperature (right axis) for the study period.

Our data suggest 2-nitrophenol is emitted and concentrated in the nighttime hours and lost in the daytime, while 4-nitrophenol is either not lost during the daytime or has an additional daytime source that 2-nitrophenol lacks, such as regional transport from the Bay Area to the west. The state of the existing literature leaves both possibilities open, and without more information it is not possible to determine what is causing the difference in profiles between these two isomers.

4.3.6 Factor 5: Consumer products

Factor 5 is designated as consumer product emissions. It consists of limonene (CI 68) and other biogenic compounds, D5 siloxane (CI 121), brominated and chlorinated hydrocarbons and small contributions from volatile diesel markers. Of the biogenic compounds present, monoterpenes (CIs 64, 66-69), methyl salicylate (CI 74) and α -isomethyl ionone (CI 75) are well represented while isoprene (CI 63), the monoterpenoids camphor (CI 65) and eucalyptol (CI 70), the sesquiterpene aromadendrene (CI 71), and α -pinene oxidation products pinic and pinonic acid (CIs 72, 73) are not. When the concentration of this factor is high, winds come exclusively from the northeast, though wind speeds are low ($< 1 \text{ m s}^{-1}$) (Figure 4.5). The diurnal profile of this factor qualitatively resembles that of Factor 3 (gasoline), with strongly elevated concentrations in the early morning hours exclusively. Peak consumer products emissions occur slightly earlier than gasoline emissions on average, from about 04:00 to 06:00 LT (Figure 4.3).

As a monoterpene, limonene is often considered to originate from biogenic sources, but limonene is also used ubiquitously in personal care products and cleaning products as a fragrance (Logue et al., 2011; Steinemann et al., 2011). Coggon et al. (2021) showed that fragranced products are the dominant source of limonene in some urban areas. While limonene is the monoterpene typically found in the highest concentrations in fragranced consumer products, the other monoterpenes included in this PMF analysis (α -pinene, β -pinene, camphene and 3-carene) are also common components of consumer products (Steinemann et al., 2011; Steinemann, 2015). The early morning spikes in concentration just before gasoline markers become elevated is consistent with consumer product use by individuals preparing for their day before starting their cars to drive to work. In contrast, studies reporting monoterpene concentrations in rural or remote locations, where biogenic emissions likely dominate, show sustained elevated concentrations throughout the night (Bouvier-Brown et al., 2009), not just early morning.

D5 is also prominent in this factor and, as stated in the discussion of Factor 3, is a tracer for personal care product emissions. Methyl salicylate, as the primary component of wintergreen oil, is also used as a fragrance compound (Lapczynski et al., 2007). α -isomethyl ionone is naturally found in Brewer's yeast and emitted during fermentation (Loscos et al., 2007), but is also commonly produced synthetically and found in cosmetics and personal care products (del Nogal Sánchez et al., 2010). There are three breweries about 1.1 km to the southeast of the sampling site and one about 3.5 km to the northeast; given their distance, the low northeastern winds and the presence of other personal care product fragrance compounds in this factor it is most likely α -isomethyl ionone measured at the sampling site also originates from personal care products. Methyl salicylate and α -isomethyl ionone are low-volatility IVOCs, measured on the SVOC channel of cTAG. Their presence in this factor contributes to a more comprehensive source

profile for consumer product emissions than could be obtained with a VOC-only measurement focus.

p-Dichlorobenzene (CI 118) is an industrial chemical used as a deodorant and insect repellent, especially in mothballs (ATSDR, 2011), that persists for weeks in the atmosphere (Atkinson and Arey, 1993). It is widely available as a consumer product and is typically placed in enclosed spaces with clothes vulnerable to moth damage (Chin et al., 2013). Its inclusion in this factor and Factor 8 could be explained by morning occupant activity that disturbs and ventilates spaces where *p*-dichlorobenzene is placed, temporarily increasing their emission to the rest of the indoor environment and, in turn, outdoors. It is also possible that general household activity correlates with VOC exchange from indoor residences to outdoors, independent of whether occupants are interacting with *p*-dichlorobenzene-containing substances. Further highly time resolved studies are needed to assess time-of-day exposure and transport to the outdoors.

Dibromochloromethane (CI 117) is a disinfection byproduct found in chlorinated tap water (Krasner et al., 1989). It is also produced from marine macroalgae (Manley et al., 1992; Sturges et al., 1992; Carpenter and Liss, 2000), the more important source globally (World Meteorological Organization et al., 2019), and is well-mixed in the troposphere, with a lifetime of 70 days (World Meteorological Organization et al., 2019). One likely source of this compound above the regional background is the outdoor swimming pool 10 m to the northeast, which was closed to the public for the season but was nonetheless kept filled. Trihalomethane emissions from commercial pools have been extensively documented (Fantuzzi et al., 2001; Zwiener et al., 2007; Richardson et al., 2010; Righi et al., 2014; Westerlund et al., 2019). While pool emissions may be responsible for elevated concentrations throughout the nighttime when dilution is low, the spikes in concentration in the early morning hours are more likely related to human activity. Residential showering has been shown to increase the concentration of dibromochloromethane in the bathroom air by 10 $\mu\text{g m}^{-3}$ or more, depending on its initial concentration in the tap water (Kerger et al., 2000). Once ventilated outside, it is plausible that with enough temporally coincident showers in nearby residences the concentration measured at the sampling site would increase by the observed 5–10 ng m^{-3} in the early morning hours.

The C_{10} – C_{16} *n*-alkanes (CIs 22, 30–35) contribute between 15 and 32% of their mass to this factor. These compounds come chiefly from gasoline and diesel exhaust or fuel evaporation (Schauer et al., 1999b, 2002b; Gentner et al., 2013b; Drozd et al., 2021), but use of petroleum distillates in some consumer products is another contributor (McDonald et al., 2018). A consumer product source would be the most consistent with the temporal variability and composition of this factor.

4.3.7 Factor 6: Primary biogenic and diesel

Factor 6 is designated primary biogenic and diesel. Three out of the five monoterpenes measured are shared between this factor and the consumer products factor (camphene, mass fraction 29%, CI 64, α -pinene, 32%, CI 66, and β -pinene, 25%, CI 67). The only other major constituents of Factor 6 are a narrow range of semivolatile *n*-alkanes (C_{16} – C_{19}) and pristane and phytane (CIs 35–40), contributing about 20 to 30% of their mass. Like Factors 3 (gasoline) and 5 (consumer products), Factor 6 is elevated exclusively in the early morning hours. However unlike

those two factors, the majority of the signal from Factor 6 is confined to one event in the early morning hours of 17 April. Winds were calm ($<1 \text{ m s}^{-1}$) and from the northeast during this event (Figure 4.5).

While most of the measured monoterpene mass is likely due to consumer product emissions (see Factor 5 discussion), the personal care product tracer D5 (CI 121) contributes no mass to Factor 6. The peak of the early morning event on 17 April is at 3AM, two hours earlier than the typical diurnal maximum for Factor 5. Therefore this factor is more likely to represent concentrated local biogenic emissions.

The C_{10} – C_{19} alkanes (CIs 22, 30–40) are mainly split between this factor, Factor 5 and Factor 11 (early morning cooking/diesel event). While Factor 11 contains contributions from C_{10} – C_{19} alkanes as well as pristane and phytane, which are expected from diesel exhaust or evaporative emissions (Schauer et al., 1999b; Gentner et al., 2013b), Factor 5 only contains contributions from the lighter alkanes in this range (C_{10} – C_{16}) and Factor 6 from the heavier ones (C_{16} – C_{19} , pristane, phytane). The event on 17 April that defines Factor 6 is relatively enriched in the heavier alkanes within this carbon number range, leading to splitting between factors. The Factor 5 lighter alkane group could come from consumer product use as mentioned in the Factor 5 discussion.

4.3.8 Factor 7: Parachlorobenzotrifluoride (PCBTF)

Factor 7 consists nearly exclusively of *p*-chlorobenzotrifluoride (PCBTF; CI 123), with 68% of that compound's mass present in this factor. No other compound has more than 10% of its mass in this factor. The timeline is extremely episodic, with brief (single data point, or < 3.5 -hour duration) concentration spikes on some days around noon. Winds are exclusively from the west when this factor's concentration is high (Figure 4.5).

PCBTF is a volatile chemical product used exclusively in solvent-based coatings (Stockwell et al., 2021; Gkatzelis et al., 2021). Coatings are defined in emission inventories as paints, varnishes, primers, stains, sealers, lacquers, and any solvents associated with coatings (Stockwell et al., 2021). They tend to be associated with construction projects (McDonald et al., 2018) and Gkatzelis et al. (2021) found that concentrations of PCBTF specifically correlated poorly with population density, which is consistent with industrial rather than individual consumer use.

The specific source of PCBTF in this study is unknown. Though the direction of the source is well-defined, winds originated from the west for the entire morning and afternoon on the days when PCBTF was detected, not just during periods of elevated concentration of PCBTF (Figure 4.4), suggesting the emissions themselves are intermittent rather than being continuous but only sampled intermittently. The lifetime of PCBTF in the atmosphere with respect to reaction with OH is over 20 days (Gkatzelis et al., 2021), so reactive loss is not expected to affect the measured concentration.

4.3.9 Factor 8: Secondary oxidation and persistent personal care product emissions

Factor 8 is designated as secondary oxidation products and semivolatile personal care product emissions. This factor contains moderate ($\approx 25\%$ mass fraction or greater) contributions from 11 different compounds, with 1st generation α - and β -pinene oxidation products pinonic

acid (CI 73) and pinic acid (CI 72) contributing the highest mass fractions (52% and 36% respectively). The factor concentration is elevated throughout the nighttime hours when ozone is present and lower at night when ozone is low as well as midday. Winds come from all directions when this factor's concentration is high, with a slight preference for the northwest and northeast (Figure 4.5), but wind speeds are low ($< 1.8 \text{ m s}^{-1}$ for all but one data point).

Pinic and pinonic acids match the variability of Factor 8 the most closely. Both compounds are both secondary oxidation products and precursors of further oxidized species, with gas phase lifetimes of only a few hours under typical conditions but with low enough volatility to partition into the aerosol phase, which extends and adds uncertainty to their atmospheric lifetimes (Donahue et al., 2012). In general, concentrations are highest at night and mid-morning, and low in the middle to late afternoon. In the afternoon, even though ozone and α - and β -pinene are present, the concentrations of pinic and pinonic acid dip, likely due to the combined effects of continued oxidation and physical dilution. At night, one of two scenarios occurs. When ozone remains high throughout the night (12, 15 and 16 April in this data set), these two acids build up under the shallow boundary layer. When ozone is low at night or early morning, local minima in pinic and pinonic acid concentrations are observed, leading to a bimodal diurnal trend. This trend is noisier and less obvious (though still present) in the Factor 8 timeline due to the contributions of other compounds not driven by the same chemistry.

In addition to pinic and pinonic acids, several compounds used in personal care products are either split between this factor and Factor 5 (consumer products) or are predominantly present in this factor. D5 siloxane's (CI 121) mass is approximately equally split between Factors 3 (gasoline), 5 and 8. Other compounds present in this factor that are used in personal care products include camphor (CI 65) (Drugsite Trust, 2021), eucalyptol (CI 70) (Medcraft and Schnell, 2016), benzophenone (CI 77) (Anderson and Castle, 2003; Downs et al., 2021; U.S. EPA, 2022), dimethyl and diethyl phthalates (CIs 81, 80) (Zota et al., 2014) and methyl salicylate (CI 74) (Lapczynski et al., 2007), with the latter having approximately equal mass in Factors 5 and 8. *p*-Dichlorobenzene (CI 118) and dibromochloromethane (CI 117), which are not from personal care products but are linked to morning indoor residential activity, also share mass between Factors 5 and 8.

When comparing compounds predominantly present in one factor or the other, more volatile, less oxygenated compounds are represented in Factor 5, while oxygen-containing IVOCs and larger, semivolatile compounds, many of them oxygen-containing, are found in Factor 8. Factor 8 species tend to have longer atmospheric lifetimes as well, with camphor (Reissell et al., 2001), eucalyptol (Corchnoy and Atkinson, 1990), methyl salicylate (Ren et al., 2020), benzophenone (U.S. EPA, 2022), dimethyl phthalate (Han et al., 2014), *p*-dichlorobenzene (Atkinson and Arey, 1993), dibromochloromethane (World Meteorological Organization et al., 2019) and D5 siloxane (Navea et al., 2011) all having lifetimes of over 1 day when exposed to typical hydroxyl radical concentrations ($[\text{OH}] = 2 * 10^6 \text{ molecules cm}^{-3}$), and likely even longer lifetimes in practice when the gas-particle partitioning of the semivolatile organics is taken into account (Kroll and Seinfeld, 2008; Cousins and Mackay, 2001). In contrast, the compounds in Factor 5 associated with personal care product emissions that are not also present in this factor (the monoterpenes) have atmospheric lifetimes of a few hours at most (Atkinson and Arey,

2003). This is consistent with the diurnal profiles of the two factors: long-lived personal care product compounds, while they may be emitted in the early morning, are not fully reacted away during the day and get reconcentrated under the boundary layer in the evening, leading to elevated concentrations throughout the night. Short-lived compounds are only observed during and shortly after their morning emission.

D4 siloxane (CI 120) has a somewhat greater mass fraction in Factor 8 (29%) than in Factor 3 (23%). Like the compounds split between factors 5 and 8, D4 has a long atmospheric lifetime (11 days; Navea et al., 2011), likely leading to elevated concentrations outside of typical emission times, unlike the gasoline markers that make up the bulk of the mass of Factor 3.

2-Nitrophenol (CI 97) contributes moderately to Factor 8 (mass fraction 24.8%). Possible sources are discussed in the Factor 4 and Factor 9 descriptions.

4.3.10 Factor 9: Biomass burning

Factor 9 represents primary biomass burning emissions. The top mass fraction contributors, in order, are galactosan (CI 87), levoglucosan (CI 86), syringaldehyde (CI 94), mannosan (CI 88), syringic acid (CI 95), vanillic acid (CI 93), 4-nitrocatechol (CI 96), and furfural (CI 85), all tracers of biomass burning (Simoneit et al., 1999; Simoneit, 2002; Bertrand et al., 2018; Finewax et al., 2018). This factor is consistently elevated exclusively in the nighttime hours. Winds are light ($< 1.5 \text{ m s}^{-1}$ except for one data point) and come from all directions, with a mild northeast preference, when Factor 9 is elevated (Figure 4.5).

Despite a recent local ban on wood burning stoves in new construction and renovations (Bay Area Air Quality Management District, 2022), wood burning in residences for heat or recreation continues to be a significant source of pollution in the Bay Area, with 25% of primary $\text{PM}_{2.5}$ emissions attributed to residential wood burning annually (Kniss et al., 2017). That fraction rises to 33% or more between November and April (Bay Area Air Quality Management District, 2012; Bhattacharyya, 2022). With average evening temperatures (19:00 to 21:00 LT) of 10.4°C during the sampling period, some residential wood burning activity is anticipated. While we expect wood burning to occur only early in the nighttime hours before residents go to sleep, the lower boundary layer throughout the night traps emissions, keeping concentrations elevated.

Some biomass burning markers included in this analysis did not show up in Factor 9. 4-hydroxybenzoic acid (CI 91) and p-anisic acid (CI 90) are tracers for burning of grasses (Simoneit, 2002), an unlikely fuel source for residential fireplaces. 4-nitrophenol (CI 98) has been observed in biomass burning plumes or otherwise attributed to biomass burning (Hoffmann et al., 2007; Mohr et al., 2013; Wang et al., 2017, 2020) and is likely formed secondarily within hours inside the biomass burning plume (Mason et al., 2001). 2-nitrophenol (CI 97), to our knowledge, has either not been detected in biomass burning plumes (Hoffmann et al., 2007), or was simply not measured or not distinguished from the other isomer (Mohr et al., 2013; Wang et al., 2017; Wang et al., 2020). However, biomass burning is thought to be a minor source for 4-nitrophenol in urban areas (Harrison et al., 2005b; Li et al., 2016), where motor vehicle combustion is responsible for primary emissions of nitrophenols as well as precursors to their secondary formation (Trempe et al., 1993; Harrison et al., 2005b), which also plays a major role in their formation (Lüttke et al., 1997, 1999; Harrison et al., 2005b; Yuan et al., 2016; Cheng et al., 2021).

Further discussion on the sources and timelines of the nitrophenol isomers can be found in the Factor 4 description.

4.3.11 Factor 10: Industrial and/or agricultural background and continuous combustion source

Factor 10 is elevated in the latter half of the campaign (17 April late morning onwards) with maximum concentrations in the late morning and early afternoon hours but weak diurnal variability. Its main constituents include *o*-dichlorobenzene (mass fraction 36%; CI 119), phthalic anhydride (36%; CI 78), the PAH pyrene (32%; CI 114), high volatility phthalates (15–30%; CIs 79–82) and grass burning tracers 4-hydroxybenzoic acid (22%; CI 91) and *p*-anisic acid (26%; CI 90), with a small contribution from C₁₅–C₂₁ alkanes, pristane and phytane (14–22%; CIs 34–42). Winds come from all directions when this factor is elevated, but mostly from the west (Figure 4.5). This factor appears to be part of the regional background.

o-Dichlorobenzene is used in the production of herbicides and dyes and as a solvent (Meek et al., 1994; ATSDR, 2006) and lasts for weeks in the atmosphere (ATSDR, 2006). It contributes to Factor 1 (long-lived and continuously emitted compounds) as well; as such, it is likely part of the regional background that could include industrial and/or agricultural sources. It is not found in consumer products like its isomer *p*-dichlorobenzene.

PAHs would be expected to contribute to this combustion-related factor, because they are formed from incomplete combustion (Ravindra et al., 2008). Unlike the other PAHs measured, which exhibit nighttime enhancement and are mostly split between Factors 3, 8 and 9, pyrene shows only minor nighttime enhancement even though it has an atmospheric lifetime with respect to reaction with OH of only a few hours (Atkinson and Arey, 1994), suggesting a continuous source. It is unclear why pyrene's diurnal profile differs from the other PAHs.

Factor 10 and Factor 1 have several compounds in common, such as the grass burning tracers, trihalomethanes (CIs 115–117), phthalimide (CI 100), *o*-dichlorobenzene and to a lesser extent phthalates. They also share weak diurnal variability, though the variability they do have is opposite. However, Factor 1 completely lacks any contribution from pyrene and the diesel markers. It seems likely that both Factor 1 and Factor 10 represent some stable background level of long-lived or continuously emitted compounds spanning the volatility range from VOCs to SVOCs, but that Factor 10 includes an additional continuous combustion related source that was absent in the beginning of the campaign.

4.3.12 Factor 11: Early morning cooking/diesel event

Factor 11 consists nearly exclusively of a 14 April 03:00 spike in concentration of some cooking and diesel tracers as well as a few other compounds. It includes 20–30% of the mass of cooking tracers palmitic acid (CI 57), stearic acid (CI 59), azelaic acid (CI 60) and nonanal (CI 62) and 10–25% of the mass of the diesel tracers C₁₀–C₁₉ alkanes, pristane and phytane (CIs 22, 30–40). 1-Tridecene (CI 102) and isophorone (CI 122) have their highest mass fraction in this factor (27% and 21% respectively). Winds were calm ($\leq 1 \text{ m s}^{-1}$) and from the northeast during this event (Figure 4.5).

Palmitic acid, stearic acid and azelaic acid are cooking tracers as discussed in the Factor 4 description, though the concentration variations captured in that factor are more likely to come

from a difference source. Nonanal has biogenic (Kirstine et al., 1998) and secondary (Atkinson, 2000; Fruekilde et al., 1998; Moise and Rudich, 2002) sources, but is also emitted in significant quantities from cooking (Rogge et al., 1991; Schauer et al., 1999a, 2002a), the likely source for this event. With northeast winds, one or more of the restaurants in the shopping center 100 m to the north could be the source of the cooking and diesel activity.

Isophorone is a solvent for resins, polymers, wax, oil, pesticides, paints and printing inks (International Programme on Chemical Safety, 1995; Samimi, 1982). While it has been detected at low levels in foods (Sasaki et al., 2005; Kataoka et al., 2007), it is not detected in food cooking emissions (Rogge et al., 1991; Schauer et al., 1999a, 2002a), so isophorone likely arises from a separate and temporally coincident source.

While little information is available about sources of 1-tridecene specifically, lower molecular weight alkenes come from mostly anthropogenic origin in urban areas, specifically mobile sources (Luecken et al., 2012). In this data set, 1-tridecene correlates better with diesel tracers ($r \approx 0.7$) than gasoline tracers ($r \approx 0.55$), though it is not specifically mentioned in speciated diesel composition studies (Rogge et al., 1993a; Schauer et al., 1999b; Gentner et al., 2013b). Even at its peak, the 1-tridecene concentration is less than 4 ng m^{-3} (0.5 ppt).

4.3.13 Factor 12: Isoprene

Factor 12 contains 73% of the mass of isoprene (CI 63), and no more than 10% of the mass of any other compound. The concentration is elevated between the early morning hours and late evening hours, with a peak in the early evening (18:00 LT) and a much smaller peak in the morning (04:00 to 06:00 LT). When the concentration of this factor is high, wind speeds are typically elevated and from the west (Figure 4.5).

Isoprene is predominantly of biogenic origin and its emission is light- and temperature-dependent (Guenther, 1997). Seasonal output varies greatly, with maximum emission in the summer months (Palmer et al., 2006; Liakakou et al., 2007). Summertime diurnal concentration profiles of isoprene typically increase from morning to a midday maximum, declining again by nightfall, in accordance with its sensitivity to light and temperature. In wintertime when biogenic production is low, isoprene has been observed to correlate with pollutants of known vehicle traffic origin in urban areas and is inferred to originate from that source (Reimann et al., 2000; Borbon et al., 2001; Lee and Wang, 2006; Hellén et al., 2012; Kaltsonoudis et al., 2016).

As spring represents a transition from winter to summer conditions, evidence of both anthropogenic and biogenic isoprene is present in Livermore. The small early morning peak is unlikely to be of biogenic origin since it occurs when temperatures are coldest and before the sun rises. The peak coincides with those of the traffic markers; restricted to the hours of 22:00 to 05:30 LT, isoprene correlates with benzene and several other gasoline markers (methylcyclopentane through p-diethylbenzene in Table 4.1 and Figure 4.4). The correlation between benzene and isoprene is shown in Figure 4.8. A linear regression of the data puts the intercept within error of the origin, suggesting no additional sources for isoprene or benzene overnight. The slope, which represents an average ratio, is 0.22. Analysis of vehicle emissions measured during dynamometer tests performed in 2014 (Drozd et al., 2016) show a median

isoprene to benzene ratio of 0.18 with 50% of the data between 0.14 – 0.34 (Figure B.7), providing independent support for attributing these isoprene emissions to anthropogenic sources.

In contrast, the late afternoon or early evening peaks roughly correlate with the maximum afternoon temperature, though the peaks occur a few hours after the temperature maximum. Midday concentrations may be depressed by reaction with the hydroxyl radical as well as dilution from the heightened boundary layer and high winds. In the early evening there is a narrow window of time when the sun has set (and therefore hydroxyl radical production has ceased), but isoprene emission continues. The lowering boundary layer and lower wind speeds may also contribute to the heightened isoprene concentrations. Later in the evening, emission ceases and isoprene is rapidly lost to reaction with nitrate radical and ozone (Steinbacher et al., 2005).

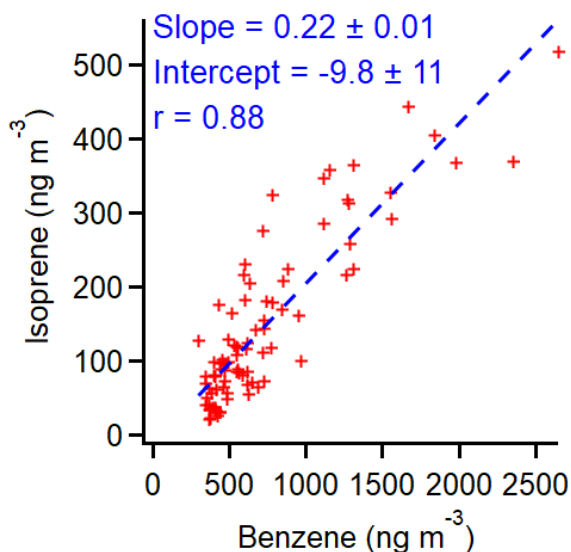


Figure 4.8. Correlation of isoprene and benzene between 22:00 and 05:30 LT, when biogenic production of isoprene is expected to be negligible.

4.3.14 Factor 13: Possible jet fuel event

Factor 13 captures a short episode of heightened gasoline tracer concentrations at 23:00 on 13 April. It is not associated with a sudden shift in wind patterns, but more likely represents a transient source. Around 20% of the mass of C₆–C₁₀ linear, branched and aromatic hydrocarbons (CIs 1-29) is included in this factor, with smaller contributions out to C₁₄ (CIs 30-33). Compositionally, Factor 13 differs from Factor 3 (gasoline) in its lack of other compound classes; Factor 3 additionally contains contributions from PAHs, palmitoleic acid and D4 and D5 siloxanes. Since D5 originates from personal care products likely applied in the morning hours, its absence in Factor 13 is not surprising. Similarly, as mentioned in the Factor 3 discussion, palmitoleic acid and D4 coincide temporally with regular morning gasoline emissions but do not come from gasoline, so are not expected in Factor 13 either. The PAH presence in Factor 3 was ascribed to gasoline exhaust, so its absence in this factor is inconsistent with a gasoline source. One possibility is that Factor 13 captures a low jet aircraft flyover, since the carbon number range of jet fuel approximately matches the factor's chemical profile (Masiol and Harrison, 2014) but jet

fuel is depleted in PAHs compared to gasoline (Shumway, 2000). The likely origin or destination of the aircraft is Livermore Municipal Airport, located approximately 3 km away from the sampling site.

4.4 Conclusion

For the first time on a single instrument, hourly measurements were successfully carried out of over 160 organic compounds in the ambient air ranging from C₅ to C₂₇ alkane equivalent volatility in both gas and particle phases. Measurements took place in Livermore, California between 11 April and 21 April 2018 with the cTAG. PMF was applied to a subset of the measured compounds to elucidate the major sources of pollution in Livermore in the springtime.

Major factors observed to contribute significantly included gasoline emissions, consumer product emissions, emissions from evaporative (temperature-dependent) sources, biomass burning, secondary oxidation, background emissions from continuously emitting sources or long-lived pollutants, and several factors associated with single compounds or specific events during the campaign described by a unique compositional profile. The gasoline factor had a morning maximum, but lacked the evening enhancement observed in other studies, likely due to the residential area of our sampling location and emissions from modern vehicles being concentrated in cold starts, in addition to afternoon meteorological conditions that favor dilution and oxidation of emitted pollutants. Monoterpenoid compounds were associated with the personal care product factor more than any other factor, highlighting the dominance in urbanized areas of anthropogenic sources for some compounds normally from biogenic sources. No clear diesel factor emerged; rather, diesel tracers were split between three different factors primarily associated with distinct single events. Isoprene's dual biogenic and vehicle exhaust sources combined with atmospheric chemistry suppressing midday concentrations forced it into its own factor. While PCBTF and isophorone are both industrial chemicals associated with solvents, they exhibit extremely distinct temporal profiles and are present in different factors, suggesting distinct sources. The clearly separated biomass burning factor demonstrates that residential wood burning is still an important source of organic emissions even in the springtime.

This analysis underscores the increasing importance of anthropogenic petroleum-derived VOCs from non-mobile sources in a suburban environment, an emerging topic of interest in recent years (McDonald et al., 2018). The ability to resolve individual isomers at high time resolution proved crucial, as it allowed for (1) the separation of the monoterpenes between consumer product emissions and a suspected biogenic source, and (2) the distinct categorization and interpretation of the nitrophenol and dichlorobenzene isomers. Including VOCs, IVOCs and SVOCs together in a single analysis expanded the profiles of some sources dominated by VOCs, such as the IVOCs methyl salicylate and α -isomethyl ionone being included in the consumer product factor. Similarly, the secondary oxidation/persistent personal care product emissions factor included a mix of SVOCs, stable VOCs and oxygenated VOCs, constituting a unique profile distinct from fresh personal care product emissions. Measurement of compounds over a wide range of volatilities and oxidation states can allow for more detailed source characterization and tracking of atmospheric processes than focusing on VOCs or particulate matter alone.

4.5 Acknowledgments

The Livermore Area Recreation and Park District (LARPD) provided the site and infrastructure in Livermore for the spring 2018 field deployment. The authors would like to especially thank Bruce Aizawa and Steve Sommers of LARPD for enabling us to do measurements at the site. Hourly temperature, wind speed and direction, and ozone measured approximately 100 m away from our site were provided by the Bay Area Air Quality Management District. cTAG development, including the field deployment in Livermore, was supported by the US Department of Energy SBIR/STTR under grant DE-SC0011397. Rebecca A. Wernis was supported by the US Environmental Protection Agency (EPA) Science To Achieve Results (STAR) fellowship assistance agreement no. FP-91778401-0.

Disclaimer: This publication has not been formally reviewed by the EPA. The views expressed in this publication are solely those of the authors, and the EPA does not endorse any products or commercial services mentioned in this publication.

5 Future work

This work advances our understanding of complex atmospheric organic mixtures and our ability to measure them. The ideas discussed below range from instrument development opportunities to gaps in the scientific literature and future research directions to maximize the potential of cTAG.

While cTAG has expanded the range of organic carbon that can be detected in a single instrument, there are still compound classes that it cannot measure. Like its cousin and predecessor SV-TAG, cTAG circumvents the tradeoff of nonpolar vs polar chromatography column optimization on the SVOC channel by using a derivatization agent to convert polar species into nonpolar ones, allowing a nonpolar GC column to elute both nonpolar and polar analytes. With some laboratory development this should be possible on the I/VOC channel as well, expanding the observable compound range to include highly oxygenated VOCs in addition to low-polarity ones. This was attempted during the development of cTAG. The main obstacle we ran into was the lack of a derivatization agent we could introduce that did not interfere with the volatility range of ambient compounds we sought to observe, since excess derivatization agent needs to be discarded before the sample reaches the GC column to avoid rapid GC column and MS ion source degradation.

While the analysis in Chapter 4 contained some secondary species and at least one secondary source category, most of the compounds included in the analysis were primary, reflecting their greater abundances, availability in commercial standard mixtures and more extensive prior research. Future deployments of cTAG should aim to characterize more of the oxygenated (and therefore likely secondary) mass on the SVOC channel, coupled with candidate precursors on the I/VOC channel to track the oxidation process and possibly connect newly identified secondary product tracers to likely precursor compounds.

To aid in the process of characterizing more oxygenated compounds found in ambient data sets, some recent tools developed by my colleagues in the Goldstein group could be of use. For compound identification, mass spectral libraries of compounds present in laboratory biomass burning and terpene oxidation experiments (UCB GLOBES Mass Spectral Libraries (<https://nature.berkeley.edu/ahg/data/MSLibrary/>): Jen et al., 2019; Yee et al., 2018) complement the NIST Mass Spectral Database (NIST Standard Reference Database 1A, 2022) with more atmospherically relevant sets of compounds. Where identification is not possible and to more accurately calibrate compounds without authentic standards, future data sets could benefit from application of the model described in Franklin et al. (2022), which uses machine learning on a test set of data to predict the chemical properties of observed compounds based on GC retention time and mass spectral information.

As discussed in Chapter 1 and Section 3.4, recent review literature underscores the need for more speciated IVOC and SVOC measurements in atmospherically diverse contexts to improve our understanding of SOA formation and of the importance of different pollution sources locally and globally (Shrivastava et al., 2017; Heald and Kroll, 2020). Climate change and changing policy and land use patterns will continue to alter the dominant sources of pollution on

all spatial scales, making ongoing measurements crucial. cTAG is well-suited to make meaningful contributions in this area, with deployment in urban, suburban, agricultural/rural and remote contexts likely to yield new insights.

Measurement of speciated VOCs, IVOCs and SVOCs would be far less powerful without the enormous existing body of research on the sources, atmospheric behavior and physical and chemical properties of specific compounds. However, gaps in this crucial research area remain. Chemical isomers can have different physical and chemical characteristics or sources, underscoring the need for widespread use of measurement techniques capable of distinguishing between them. The nitrophenol isomers discussed in sections 4.3.5 and 4.3.10 are a striking example of this, with one isomer having a lower vapor pressure by about 2 orders of magnitude (U.S. EPA, 2022); other examples included in or adjacent to this work include the dichlorobenzene isomers (different sources), mono-, sesqui- and diterpenes (highly species-dependent isomer emission), and levoglucosan and its isomers mannosan and galactosan (emitted from BB in different ratios depending on the source fuel and burning conditions) (Suciu et al., 2019). The lack of prior studies distinguishing nitrophenol isomers, for example, limited the interpretation of the nitrophenol observations in Chapter 4.

Similarly, many known marker compounds, particularly IVOCs and SVOCs, lack studies on their atmospheric reaction kinetics. Among BB markers, mannosan, galactosan, 4-hydroxybenzoic acid, syringaldehyde and syringic acid are all expected to have appreciable mass that could contribute to SOA from BB (**Error! Reference source not found.**). No gas-phase reaction rate estimate for 4-nitrophenol with OH radical exists despite it being observed overwhelmingly in the gas-phase in this study (Section 4.3.5) and others (Yuan et al., 2016; Wang et al., 2020). Studies on the reaction kinetics of these and other important tracers with common atmospheric oxidants would enhance SOA formation estimates and inform interpretations of concentration measurements such as those gathered using cTAG.

Finally, the advancement of low-cost sensors for air pollution monitoring over the past decade has been exciting, with huge potential still for this emerging field. Existing low-cost sensors measure small gases (e.g. CO₂, CO) or bulk properties of particulate matter (e.g. black carbon, fine particulate matter), but measurement of most speciated organics remains the domain of more complex and expensive instrumentation. While there are technological hurdles to overcome, the combined power of a ubiquitous, distributed low-cost sensor network with targeted measurement of important SVOC tracer compounds is compelling to imagine. Such a network could allow researchers and monitoring organizations to definitively apportion measured black carbon between biomass burning and diesel emissions on a citywide scale, for example, since tracer compounds can separately capture the extreme variability of each source on seasonal, weekly, daily and hourly timescales. Personal use could allow consumers to identify volatile toxic chemicals in residences or other indoor environments in which they spend the majority of their time. The potential applications and areas of future research described here are just a limited subset of the possibilities for speciated measurement of atmospheric reactive organic carbon.

Appendix A: Miniature gas chromatograph development

cTAG uses dual miniature gas chromatographs (GCs) to preserve compactness and independent temperature control. Figure A.1 shows a schematic of the final design and a photo of a GC hub on the instrument. Having reproducible temperature ramps is critical for batch chromatogram analysis, since the exact elution time of each compound is dependent upon the column temperature. Figure A.2 shows that we can run a consistent, repeatable temperature program using PID control on the mini-GCs.

(a)

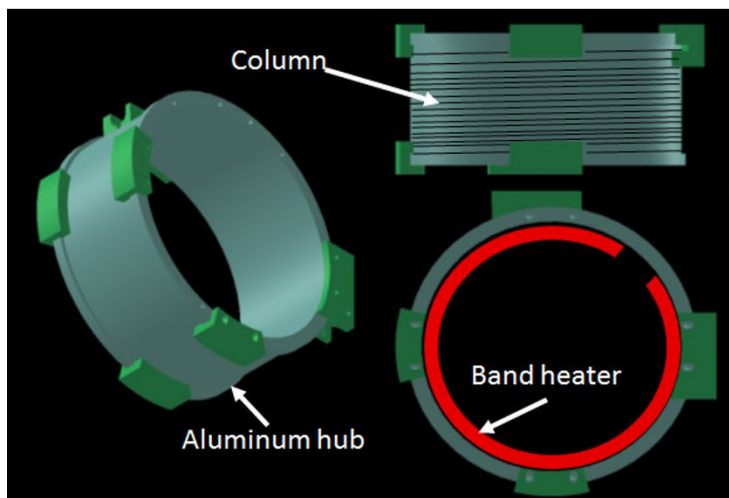


Figure A.1. Schematic and photo of miniature gas chromatographs. Clamps on the edges of the rim of the hub hold the chromatography column in place at each end. An aluminium sheet is wrapped around the outside of the hub over the column to further ensure even heating of the column itself.

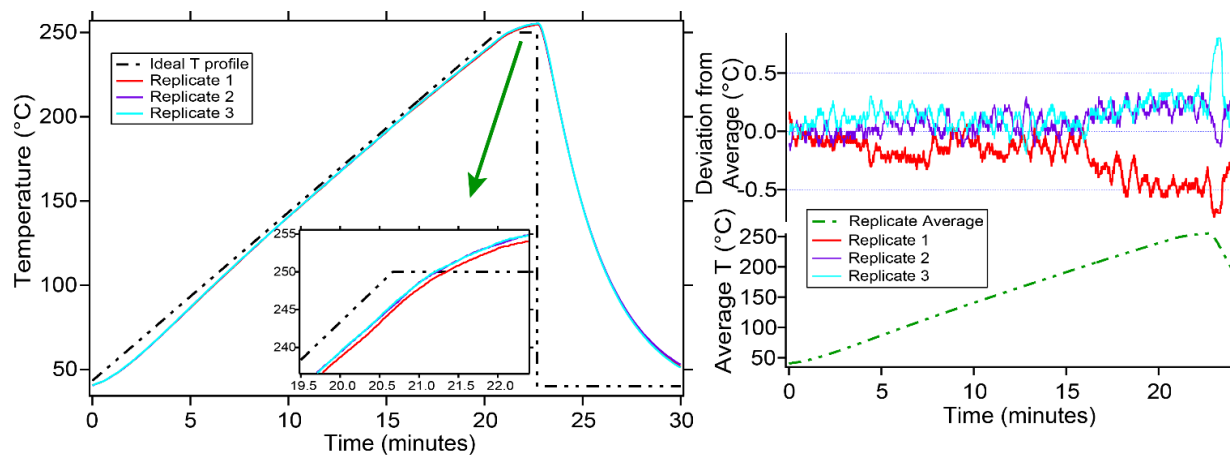


Figure A.2. Demonstration of reproducibility of temperature ramps on the miniature gas chromatographs. This leads to consistent elution times of compounds of interest, streamlining batch peak integration.

Appendix B: Supporting information for source apportionment of VOCs, IVOCs and SVOCs in Livermore

B.1 Precision uncertainty histograms

Precision uncertainty is discussed in Section 4.2.2.3.2.

Figure B.1 shows the relative standard deviations of the internal standard ratios for all internal standards used for normalization in this analysis. Hydrocarbons between *n*-tetradecane (C₁₄) and pyrene (elutes just before *n*-docosane (C₂₂)) all correlate closely. Additionally, the distribution of internal standard ratios across samples is approximately normal (e.g., Figure B.2 (a)). We thus infer that any ambient hydrocarbon observed in this volatility range could be normalized by any of the internal standards in this range with 10% or less precision uncertainty introduced. Though transfer efficiency suffers for hydrocarbons with lower volatility than *n*-docosane, leading to greater sensitivity of internal standard choice, 10% is still a satisfactory precision uncertainty for ambient compounds in this volatility range provided the analyte and internal standard retention indices differ by less than about 200. (In later deployments of cTAG, transfer efficiency remains high up to *n*-triacontane.) The best hydrocarbon pairings have a relative standard deviation of less than 5%. From this observation we conservatively estimate that compounds normalized by an isotopologue incur 5% precision uncertainty.

On the high volatility side, deuterated tridecane was lost in the refocusing step during occasional periods of high ambient temperature, causing its measured signal to drop near zero. Ambient compounds in this volatility range are therefore normalized by tetradecane with an assigned precision uncertainty of 25% based on the RSD of the tridecane-tetradecane ratio. The distribution of ratios is somewhat skewed (Figure B.2 (b)); a few data points should likely be assigned a higher uncertainty and many could be assigned a lower uncertainty, but 25% represents an appropriate overall estimate for the most volatile compounds.

Oxygenated compounds exhibit greater RSD values regardless of whether they are paired with hydrocarbons or other oxygenates. Deuterated syringic acid, which elutes just before eicosane (C₂₀), produces an RSD of about 30% when paired with most other compounds, oxygenated or not, and an approximately normally distributed set of ratios (Figure B.2 (c)). Ambient oxygenates are normalized by the nearest deuterated oxygenate in volatility if their retention indices are within 200 and the nearest hydrocarbon otherwise; in both cases the assigned precision uncertainty is 30%. Table B.1 summarizes the categories of precision uncertainty assigned to ambient compounds for this analysis.

Denominator → Numerator ↓	Hydrocarbons												Oxygenates			
	d-Tridecane	d-Tetradecane	d-Hexadecane	d-Octadecane	d-Phenanthrene	d-Eicosane	d-Pyrene	d-Docosane	d-Tetracosane	d-Hexacosane	d-Chrysene	d-Octacosane	d-Vanillic Acid	d-Pentadecanol	d-Syringic Acid	d-Antraquinone
d-Tridecane	0.00	0.27	0.27	0.28	0.29	0.29	0.28	0.32	0.40	0.56	0.70	0.71	0.34	0.26	0.46	0.33
d-Tetradecane	1.89	0.00	0.02	0.05	0.08	0.08	0.06	0.14	0.26	0.45	0.58	0.63	0.17	0.18	0.34	0.15
d-Hexadecane	1.92	0.02	0.00	0.04	0.07	0.06	0.04	0.12	0.25	0.44	0.57	0.61	0.16	0.19	0.32	0.14
d-Octadecane	1.95	0.04	0.03	0.00	0.06	0.05	0.04	0.11	0.23	0.41	0.54	0.59	0.15	0.20	0.31	0.12
d-Phenanthrene	1.96	0.07	0.06	0.06	0.00	0.07	0.06	0.12	0.24	0.41	0.47	0.58	0.16	0.21	0.31	0.13
d-Eicosane	2.02	0.07	0.06	0.05	0.07	0.00	0.04	0.06	0.19	0.37	0.51	0.54	0.12	0.22	0.27	0.09
d-Pyrene	1.97	0.06	0.04	0.04	0.06	0.04	0.00	0.09	0.22	0.40	0.52	0.58	0.12	0.19	0.29	0.10
d-Docosane	2.17	0.13	0.12	0.10	0.11	0.06	0.09	0.00	0.13	0.31	0.48	0.48	0.09	0.27	0.22	0.07
d-Tetracosane	2.46	0.26	0.25	0.23	0.23	0.19	0.22	0.13	0.00	0.19	0.45	0.37	0.14	0.38	0.14	0.16
d-Hexacosane	2.83	0.43	0.42	0.40	0.40	0.36	0.38	0.30	0.18	0.00	0.39	0.19	0.30	0.54	0.20	0.32
d-Chrysene	2.16	0.31	0.30	0.29	0.27	0.27	0.29	0.26	0.29	0.33	0.00	0.43	0.30	0.39	0.32	0.27
d-Octacosane	2.92	0.62	0.61	0.59	0.59	0.56	0.57	0.50	0.37	0.20	0.46	0.00	0.48	0.67	0.38	0.50
d-Vanillic Acid	2.34	0.17	0.16	0.15	0.16	0.12	0.13	0.09	0.14	0.32	0.50	0.50	0.00	0.27	0.19	0.10
d-Pentadecanol	1.43	0.17	0.17	0.17	0.21	0.18	0.16	0.21	0.30	0.48	0.68	0.65	0.20	0.00	0.36	0.20
d-Syringic Acid	2.72	0.34	0.33	0.32	0.31	0.28	0.30	0.22	0.13	0.18	0.42	0.34	0.18	0.44	0.00	0.24
d-Antraquinone	2.08	0.14	0.13	0.11	0.13	0.08	0.10	0.07	0.15	0.31	0.43	0.47	0.10	0.24	0.23	0.00

Figure B.1. Relative standard deviations of all internal standard ratios used in this study. Green = 0; red = 0.7 or greater.

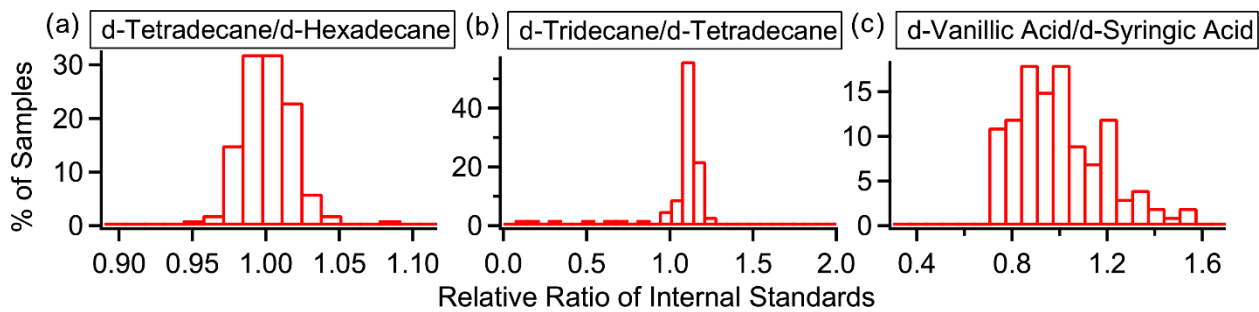


Figure B.2. Example distribution of relative ratios of internal standards for (a) two hydrocarbons with a retention index difference of 200, (b) tridecane and tetradecane and (c) two oxygenated compounds.

Table B.1. Summary of internal standard assignments for normalization of ambient compounds in this analysis and the precision uncertainty incurred from each assignment. Because the precision uncertainty is the only source of uncertainty that varies from sample to sample, it is the only uncertainty assigned to individual compounds as input to the PMF model.

Ambient Compound Category	Precision Uncertainty Assigned
Compounds with isotopologue internal standards	5%
Hydrocarbons with retention index at or above 1400 (no isotopologue)	10%
Compounds with retention index below 1400 (no isotopologue)	25%
Compounds that do not fall into any of the above categories, including most oxygenates	30%

B.2 PMF evaluation of different factor solutions

B.2.1 Q/Q_{exp}

A common consideration for deciding which solution best explains the data is to compare Q/Q_{exp} for solutions with different numbers of factors (Ulbrich et al., 2009). The expected value of Q , or Q_{exp} , is calculated for m compounds, n sample times and p factors as:

$$Q_{exp} = mn - p(m + n) \quad (B1)$$

Q/Q_{exp} is expected to decrease as the number of factors increases, as more of the data is able to be fit. A relatively large decrease in Q/Q_{exp} between successive solutions suggests the additional factor explains more of the data than would be expected and thus should be included. This effectively sets a minimum number of factors for the final chosen solution.

Q/Q_{exp} and the percent reduction in Q/Q_{exp} between successive solutions is shown in Figure B.3. Unusually large percent reductions are present with the addition of the 8th factor and, especially, with the addition of the 13th factor. This is one reason the 13 factor solution was chosen.

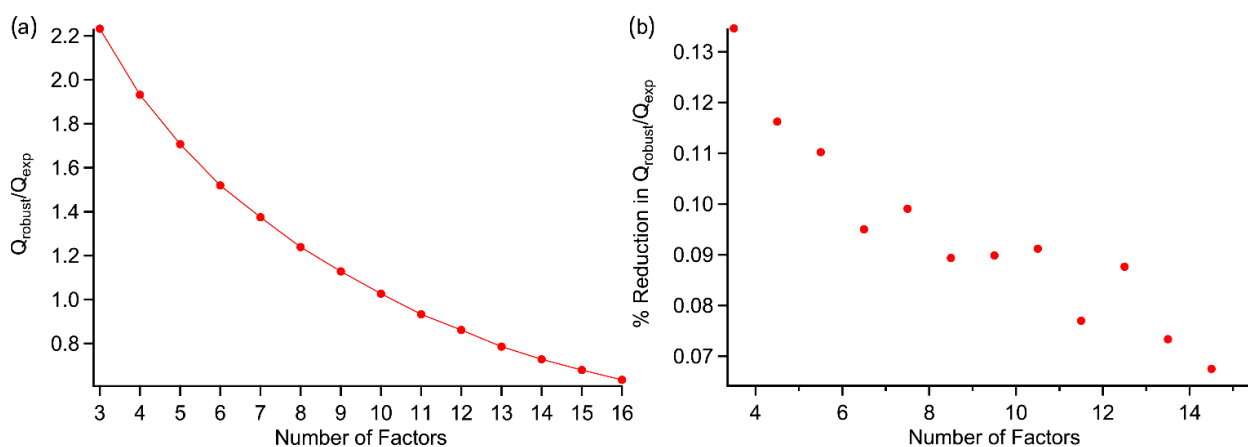


Figure B.3. (a) Q/Q_{exp} for different numbers of factors. (b) % reduction in Q/Q_{exp} as the number of factors is increased.

B.2.2 Beyond 13 factors: bootstrapping results

The 14 factor solution and beyond were ultimately rejected because the new factors contained low fractions of compounds from many factors, taking mass away from the other factors. Additionally, the factor timelines for 14th, 15th, and 16th factors were not very distinct from existing factors, as reflected in the decreasing average bootstrapping self-mapping fraction (89.77% for 13 factors, 88.21% for 14 factors, 86.07% for 15 factors and 87.19% for 16 factors). Finally, the additional factors had no clear physical interpretations that were distinct from factors present in the 13 factor solution.

B.2.3 FPEAK rotation

FPEAK exploration is discussed in Section 4.3.1.

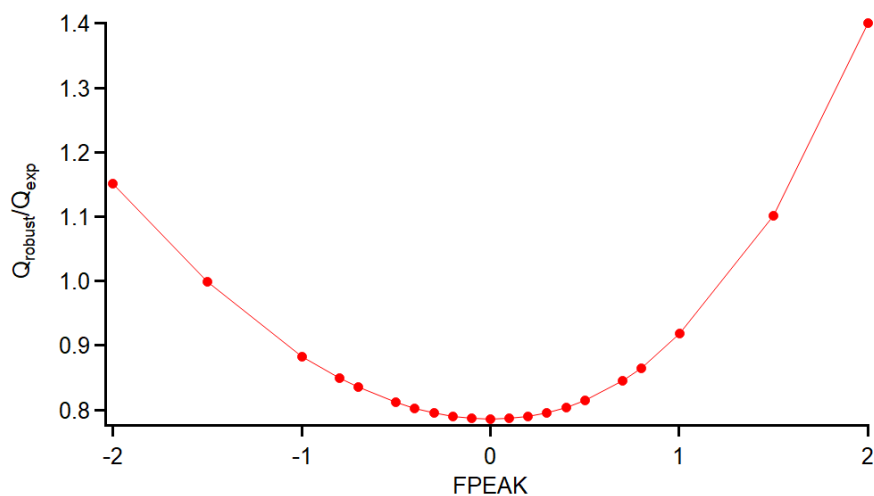


Figure B.4. Q/Q_{exp} for different values of the FPEAK parameter. The minimum value is at FPEAK = 0.

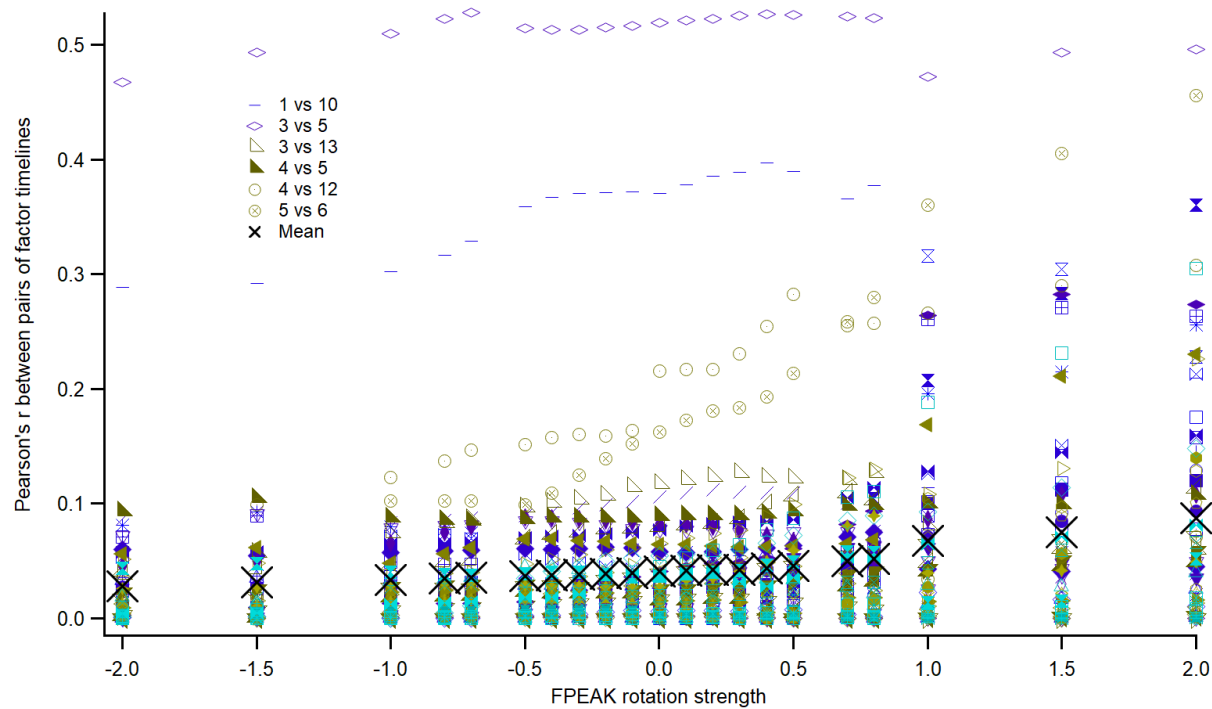


Figure B.5. Pearson's r for the cross correlation between every pair of factors in the 13 factor solution, along with the mean r for each FPEAK value. Since there are a total of 78 pairings, only outliers are included in the legend. Negative values of FPEAK provide modest improvements (i.e. decreases) in r values, but not enough to outweigh the optimization of Q/Q_{exp} at FPEAK = 0 (Figure B.4).

B.3 Factor apportionment of VOCs, IVOCs and SVOCs

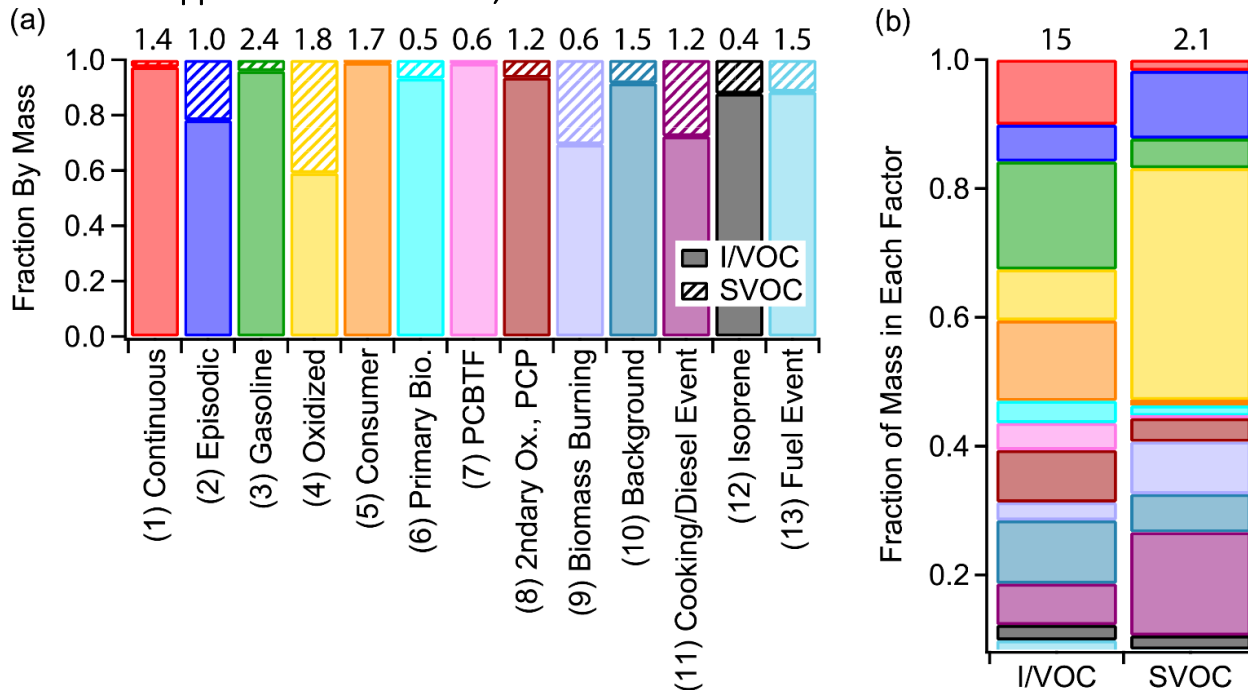


Figure B.6. (a) Fraction of average mass from each cTAG measurement channel in each factor. (b) Fraction of the average total mass of compounds measured on each channel found in each factor. The numbers at the top represent the average total mass for (a) that factor or (b) that class of compounds in $\mu\text{g m}^{-3}$.

B.4 Isoprene to benzene emission factors in gasoline exhaust

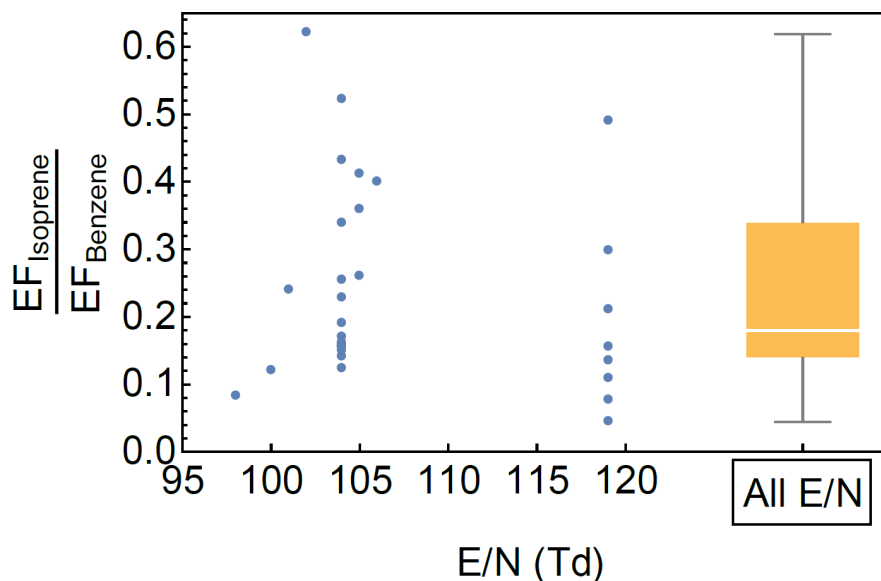


Figure B.7. The ratio of isoprene to benzene emission factors (EF) (mg (kg Fuel)^{-1}) for cold-start emissions for a wide range of vehicle classes, showing a mean value of 0.18. Observed ratios are sorted by the E/N (electric field density ratio) used in measurements made by a quadrupole proton transfer reaction mass spectrometer. Vehicles span model year 1990 - 2014 and Pre-LEV to SULEV emissions categories. There is no trend with E/N , suggesting a minimal effect of substituted cyclohexanes on isoprene measurements (Gueneron et al., 2015).

References

Dichlorobenzenes | Toxicological Profile | ATSDR:
<https://wwwn.cdc.gov/TSP/ToxProfiles/ToxProfiles.aspx?id=704&tid=126>, last access: 13 April 2022.

Aiken, A. C., DeCarlo, P. F., Kroll, J. H., Worsnop, D. R., Huffman, J. A., Docherty, K. S., Ulbrich, I. M., Mohr, C., Kimmel, J. R., Sueper, D., Sun, Y., Zhang, Q., Trimborn, A., Northway, M., Ziemann, P. J., Canagaratna, M. R., Onasch, T. B., Alfarra, M. R., Prevot, A. S. H., Dommen, J., Duplissy, J., Metzger, A., Baltensperger, U., and Jimenez, J. L.: O/C and OM/OC Ratios of Primary, Secondary, and Ambient Organic Aerosols with High-Resolution Time-of-Flight Aerosol Mass Spectrometry, *Environ. Sci. Technol.*, 42, 4478–4485, <https://doi.org/10.1021/es703009q>, 2008.

Akagi, S. K., Yokelson, R. J., Wiedinmyer, C., and Wennberg, P. O.: Emission factors for open and domestic biomass burning for use in atmospheric models, *Atmos. Chem. Phys.*, 35, <https://doi.org/10.5194/acp-11-4039-2011>, 2011.

Akherati, A., He, Y., Coggon, M. M., Koss, A. R., Hodshire, A. L., Sekimoto, K., Warneke, C., de Gouw, J., Yee, L., Seinfeld, J. H., Onasch, T. B., Herndon, S. C., Knighton, W. B., Cappa, C. D., Kleeman, M. J., Lim, C. Y., Kroll, J. H., Pierce, J. R., and Jathar, S. H.: Oxygenated Aromatic Compounds are Important Precursors of Secondary Organic Aerosol in Biomass-Burning Emissions, *Environ. Sci. Technol.*, 54, 8568–8579, <https://doi.org/10.1021/acs.est.0c01345>, 2020.

Allan, J. D., Williams, P. I., Morgan, W. T., Martin, C. L., Flynn, M. J., Lee, J., Nemitz, E., Phillips, G. J., Gallagher, M. W., and Coe, H.: Contributions from transport, solid fuel burning and cooking to primary organic aerosols in two UK cities, *Atmos. Chem. Phys.*, 10, 647–668, <https://doi.org/10.5194/acp-10-647-2010>, 2010.

Alves, E. G., Jardine, K., Tota, J., Jardine, A., Yáñez-Serrano, A. M., Karl, T., Tavares, J., Nelson, B., Gu, D., Stavrou, T., Martin, S., Artaxo, P., Manzi, A., and Guenther, A.: Seasonality of isoprenoid emissions from a primary rainforest in central Amazonia, *Atmos. Chem. Phys.*, 16, 3903–3925, <https://doi.org/10.5194/acp-16-3903-2016>, 2016.

Anderson, J. O., Thundiyil, J. G., and Stolbach, A.: Clearing the Air: A Review of the Effects of Particulate Matter Air Pollution on Human Health, *J. Med. Toxicol.*, 8, 166–175, <https://doi.org/10.1007/s13181-011-0203-1>, 2012.

Anderson, W. A. C. and Castle, L.: Benzophenone in cartonboard packaging materials and the factors that influence its migration into food, *Food Addit. Contam.*, 20, 607–618, <https://doi.org/10.1080/0265203031000109486>, 2003.

Andreae, M. O. and Merlet, P.: Emission of trace gases and aerosols from biomass burning, *Global Biogeochem. Cycles*, 15, 955–966, <https://doi.org/10.1029/2000GB001382>, 2001.

Andreae, M. O., Rosenfeld, D., Artaxo, P., Costa, A. A., Frank, G. P., Longo, K. M., and Silva-Dias, M. A. F.: Smoking Rain Clouds over the Amazon, *Science*, 303, 1337–1342, <https://doi.org/10.1126/science.1092779>, 2004.

United States Census Data: <https://data.census.gov/cedsci/>, last access: 17 March 2022.

IBGE: Instituto Brasileiro de Geografia e Estatística: <https://cidades.ibge.gov.br/>, last access: 25 April 2022.

INMET: Instituto Nacional de Meteorologia: <https://portal.inmet.gov.br/>, last access: 29 June 2022.

Artaxo, P., Gerab, F., Yamasoe, M. A., and Martins, J. V.: Fine mode aerosol composition at three long-term atmospheric monitoring sites in the Amazon Basin, *J. Geophys. Res.*, 99, 22857–22868, <https://doi.org/10.1029/94JD01023>, 1994.

Artaxo, P., Martins, J. V., Yamasoe, M. A., Procópio, A. S., Pauliquevis, T. M., Andreae, M. O., Guyon, P., Gatti, L. V., and Leal, A. M. C.: Physical and chemical properties of aerosols in the wet and dry seasons in Rondônia, Amazonia, *J. Geophys. Res. Atmos.*, 107, LBA 49-1-LBA 49-14, <https://doi.org/10.1029/2001JD000666>, 2002.

Artaxo, P., Rizzo, L. V., Brito, J. F., Barbosa, H. M. J., Arana, A., Sena, E. T., Cirino, G. G., Bastos, W., Martin, S. T., and Andreae, M. O.: Atmospheric aerosols in Amazonia and land use change: from natural biogenic to biomass burning conditions, *Faraday Discuss.*, 165, 203–235, <https://doi.org/10.1039/c3fd00052d>, 2013.

Atkinson, R.: Atmospheric chemistry of VOCs and NO_x, *Atmos. Environ.*, 34, 2063–2101, [https://doi.org/10.1016/S1352-2310\(99\)00460-4](https://doi.org/10.1016/S1352-2310(99)00460-4), 2000.

Atkinson, R. and Arey, J.: Lifetimes and fates of toxic air contaminants in California's atmosphere, June 1993. Final report, California Air Resources Board Research Division, 1993.

Atkinson, R. and Arey, J.: Atmospheric chemistry of gas-phase polycyclic aromatic hydrocarbons: formation of atmospheric mutagens., *Environ. Health Perspect.*, 102, 10, 1994.

Atkinson, R. and Arey, J.: Atmospheric Degradation of Volatile Organic Compounds, *Chem. Rev.*, 103, 4605–4638, <https://doi.org/10.1021/cr0206420>, 2003.

ATSDR: Toxicological Profile for Dichlorobenzenes, U.S. Department of Health and Human Services, Public Health Service, Agency for Toxic Substances and Disease Registry, 500 pp., 2006.

Aumont, B., Camredon, M., Mouchel-Vallon, C., La, S., Ouzebidou, F., Valorso, R., Lee-Taylor, J., and Madronich, S.: Modeling the influence of alkane molecular structure on secondary organic aerosol formation, *Faraday Discuss.*, 165, 105–122, <https://doi.org/10.1039/C3FD00029J>, 2013.

Baek, S. O., Field, R. A., Goldstone, M. E., Kirk, P. W., Lester, J. N., and Perry, R.: A review of atmospheric polycyclic aromatic hydrocarbons: Sources, fate and behavior, *Water Air Soil Pollut*, 60, 279–300, <https://doi.org/10.1007/BF00282628>, 1991.

Bay Area Air Quality Management District: Understanding Particulate Matter, 2012.

Bay Area Air Quality Management District: Wood Smoke Pollution: <https://www.baaqmd.gov/rules-and-compliance/wood-smoke>, last access: 28 July 2022.

Bertrand, A., Stefenelli, G., Jen, C. N., Pieber, S. M., Bruns, E. A., Ni, H., Temime-Roussel, B., Slowik, J. G., Goldstein, A. H., El Haddad, I., Baltensperger, U., Prévôt, A. S. H., Wortham, H., and Marchand, N.: Evolution of the chemical fingerprint of biomass burning organic aerosol during aging, *Atmos. Chem. Phys.*, 18, 7607–7624, <https://doi.org/10.5194/acp-18-7607-2018>, 2018.

Why is air quality so bad in the winter? How wood-smoke pollution and “temperature inversions” work in the Bay Area: <https://www.sfchronicle.com/projects/2021/winter-air-pollution/>, last access: 30 March 2022.

Bhattacharai, H., Saikawa, E., Wan, X., Zhu, H., Ram, K., Gao, S., Kang, S., Zhang, Q., Zhang, Y., Wu, G., Wang, X., Kawamura, K., Fu, P., and Cong, Z.: Levoglucosan as a tracer of biomass burning: Recent progress and perspectives, *Atmos. Res.*, 220, 20–33, <https://doi.org/10.1016/j.atmosres.2019.01.004>, 2019.

Bond, T. C., Streets, D. G., Yarber, K. F., Nelson, S. M., Woo, J.-H., and Klimont, Z.: A technology-based global inventory of black and organic carbon emissions from combustion, *J. Geophys. Res. Atmos.*, 109, <https://doi.org/10.1029/2003JD003697>, 2004.

Borbon, A., Fontaine, H., Veillerot, M., Locoge, N., Galloo, J. C., and Guillermo, R.: An investigation into the traffic-related fraction of isoprene at an urban location, *Atmos. Environ.*, 35, 3749–3760, [https://doi.org/10.1016/S1352-2310\(01\)00170-4](https://doi.org/10.1016/S1352-2310(01)00170-4), 2001.

Boreddy, S. K. R., Haque, Md. M., Kawamura, K., Fu, P., and Kim, Y.: Homologous series of n-alkanes (C19-C35), fatty acids (C12-C32) and n-alcohols (C8-C30) in atmospheric aerosols from central Alaska: Molecular distributions, seasonality and source indices, *Atmos. Environ.*, 184, 87–97, <https://doi.org/10.1016/j.atmosenv.2018.04.021>, 2018.

Bouvier-Brown, N. C., Goldstein, A. H., Gilman, J. B., Kuster, W. C., and de Gouw, J. A.: In-situ ambient quantification of monoterpenes, sesquiterpenes, and related oxygenated compounds during BEARPEX 2007: implications for gas- and particle-phase chemistry, *Atmos. Chem. Phys.*, 9, 5505–5518, <https://doi.org/10.5194/acp-9-5505-2009>, 2009.

Brito, J., Rizzo, L. V., Morgan, W. T., Coe, H., Johnson, B., Haywood, J., Longo, K., Freitas, S., Andreae, M. O., and Artaxo, P.: Ground-based aerosol characterization during the South American Biomass Burning Analysis (SAMBBA) field experiment, *Atmos. Chem. Phys.*, 14, 12069–12083, <https://doi.org/10.5194/acp-14-12069-2014>, 2014.

Brown, S. G., Frankel, A., and Hafner, H. R.: Source apportionment of VOCs in the Los Angeles area using positive matrix factorization, *Atmos. Environ.*, 41, 227–237, <https://doi.org/10.1016/j.atmosenv.2006.08.021>, 2007.

Brunekreef, B. and Holgate, S. T.: Air pollution and health, *The Lancet*, 360, 1233–1242, [https://doi.org/10.1016/S0140-6736\(02\)11274-8](https://doi.org/10.1016/S0140-6736(02)11274-8), 2002.

Bui, T. T., Giovanoulis, G., Cousins, A. P., Magnér, J., Cousins, I. T., and de Wit, C. A.: Human exposure, hazard and risk of alternative plasticizers to phthalate esters, *Sci. Total Environ.*, 541, 451–467, <https://doi.org/10.1016/j.scitotenv.2015.09.036>, 2016.

Cahill, T. M., Seaman, V. Y., Charles, M. J., Holzinger, R., and Goldstein, A. H.: Secondary organic aerosols formed from oxidation of biogenic volatile organic compounds in the Sierra Nevada Mountains of California, *J. Geophys. Res. Atmos.*, 111, <https://doi.org/10.1029/2006JD007178>, 2006.

Calogirou, A., Larsen, B. R., Brussol, C., Duane, M., and Kotzias, D.: Decomposition of Terpenes by Ozone during Sampling on Tenax, *Anal. Chem.*, 68, 1499–1506, <https://doi.org/10.1021/ac950803i>, 1996.

Canagaratna, M. r., Jayne, J. t., Jimenez, J. l., Allan, J. d., Alfarra, M. r., Zhang, Q., Onasch, T. b., Drewnick, F., Coe, H., Middlebrook, A., Delia, A., Williams, L. r., Trimborn, A. m., Northway, M. j., DeCarlo, P. f., Kolb, C. e., Davidovits, P., and Worsnop, D. r.: Chemical and microphysical characterization of ambient aerosols with the aerodyne aerosol mass spectrometer, *Mass Spectrom. Rev.*, 26, 185–222, <https://doi.org/10.1002/mas.20115>, 2007.

Canagaratna, M. R., Jimenez, J. L., Kroll, J. H., Chen, Q., Kessler, S. H., Massoli, P., Hildebrandt Ruiz, L., Fortner, E., Williams, L. R., Wilson, K. R., Surratt, J. D., Donahue, N. M., Jayne, J. T., and Worsnop, D. R.: Elemental ratio measurements of organic compounds using aerosol mass spectrometry: characterization, improved calibration, and implications, *Atmospheric Chemistry and Physics*, 15, 253–272, <https://doi.org/10.5194/acp-15-253-2015>, 2015.

Cao, X.-L. and Hewitt, C. N.: Build-up of artifacts on adsorbents during storage and its effect on passive sampling and gas chromatography-flame ionization detection of low concentrations of volatile organic compounds in air, *J. Chromatogr. A*, 688, 368–374, [https://doi.org/10.1016/0021-9673\(94\)00908-2](https://doi.org/10.1016/0021-9673(94)00908-2), 1994.

Caravaggio, G. A., Charland, J.-P., Macdonald, P., and Graham, L.: n-Alkane Profiles of Engine Lubricating Oil and Particulate Matter by Molecular Sieve Extraction, *Environ. Sci. Technol.*, 41, 3697–3701, <https://doi.org/10.1021/es062233h>, 2007.

Carneiro, R. G. and Fisch, G.: Observational analysis of the daily cycle of the planetary boundary layer in the central Amazon during a non-El Niño year and El Niño year (GoAmazon project 2014/5), *Atmos. Chem. Phys.*, 20, 5547–5558, <https://doi.org/10.5194/acp-20-5547-2020>, 2020.

Carpenter, L. J. and Liss, P. S.: On temperate sources of bromoform and other reactive organic bromine gases, *J. Geophys. Res. Atmos.*, 105, 20539–20547, <https://doi.org/10.1029/2000JD900242>, 2000.

Cecinato, A., Di Palo, V., Pomata, D., Tomasi Scianò, M. C., and Possanzini, M.: Measurement of phase-distributed nitrophenols in Rome ambient air, *Chemosphere*, 59, 679–683, <https://doi.org/10.1016/j.chemosphere.2004.10.045>, 2005.

Chan, A. W. H., Kautzman, K. E., Chhabra, P. S., Surratt, J. D., Chan, M. N., Crouse, J. D., Kürten, A., Wennberg, P. O., Flagan, R. C., and Seinfeld, J. H.: Secondary organic aerosol formation from photooxidation of naphthalene and alkylnaphthalenes: implications for oxidation of intermediate volatility organic compounds (IVOCs), *Atmospheric Chemistry and Physics*, 9, 3049–3060, 2009a.

Chan, A. W. H., Kautzman, K. E., Chhabra, P. S., Surratt, J. D., Chan, M. N., Crouse, J. D., Kürten, A., Wennberg, P. O., Flagan, R. C., and Seinfeld, J. H.: Secondary organic aerosol formation from photooxidation of naphthalene and alkylnaphthalenes: implications for oxidation of intermediate volatility organic compounds (IVOCs), *Atmos. Chem. Phys.*, 9, 3049–3060, <https://doi.org/10.5194/acp-9-3049-2009>, 2009b.

Chan, A. W. H., Kreisberg, N. M., Hohaus, T., Campuzano-Jost, P., Zhao, Y., Day, D. A., Kaser, L., Karl, T., Hansel, A., Teng, A. P., Ruehl, C. R., Sueper, D. T., Jayne, J. T., Worsnop, D. R., Jimenez, J. L., Hering, S. V., and Goldstein, A. H.: Speciated measurements of semivolatile and intermediate volatility organic compounds (S/IVOCs) in a pine forest during BEACHON-RoMBAS 2011, *Atmos. Chem. Phys.*, 16, 1187–1205, <https://doi.org/10.5194/acp-16-1187-2016>, 2016.

Chan, M. N., Surratt, J. D., Claeys, M., Edgerton, E. S., Tanner, R. L., Shaw, S. L., Zheng, M., Knipping, E. M., Eddingsaas, N. C., Wennberg, P. O., and Seinfeld, J. H.: Characterization and Quantification of Isoprene-Derived Epoxydiols in Ambient Aerosol in the Southeastern United States, *Environ. Sci. Technol.*, 44, 4590–4596, <https://doi.org/10.1021/es100596b>, 2010.

Chebbi, A. and Carlier, P.: Carboxylic acids in the troposphere, occurrence, sources, and sinks: A review, *Atmos. Environ.*, 30, 4233–4249, [https://doi.org/10.1016/1352-2310\(96\)00102-1](https://doi.org/10.1016/1352-2310(96)00102-1), 1996.

Chen, J., Wenger, J. C., and Venables, D. S.: Near-Ultraviolet Absorption Cross Sections of Nitrophenols and Their Potential Influence on Tropospheric Oxidation Capacity, *J. Phys. Chem. A*, 115, 12235–12242, <https://doi.org/10.1021/jp206929r>, 2011.

Cheng, X., Chen, Q., Li, Y., Huang, G., Liu, Y., Lu, S., Zheng, Y., Qiu, W., Lu, K., Qiu, X., Bianchi, F., Yan, C., Yuan, B., Shao, M., Wang, Z., Canagaratna, M. R., Zhu, T., Wu, Y., and Zeng, L.: Secondary Production of Gaseous Nitrated Phenols in Polluted Urban Environments, *Environ. Sci. Technol.*, 55, 4410–4419, <https://doi.org/10.1021/acs.est.0c07988>, 2021.

Chin, J.-Y., Godwin, C., Jia, C., Robins, T., Lewis, T., Parker, E., Max, P., and Batterman, S.: Concentrations and risks of p-dichlorobenzene in indoor and outdoor air, *Indoor Air*, 23, 40–49, <https://doi.org/10.1111/j.1600-0668.2012.00796.x>, 2013.

Chung, M. Y., Maris, C., Krischke, U., Meller, R., and Paulson, S. E.: An investigation of the relationship between total non-methane organic carbon and the sum of speciated hydrocarbons and carbonyls measured by standard GC/FID: measurements in the Los Angeles air basin, *Atmospheric Environment*, 37, 159–170, [https://doi.org/10.1016/S1352-2310\(03\)00388-1](https://doi.org/10.1016/S1352-2310(03)00388-1), 2003.

Claeys, M., Szmigielski, R., Kourtchev, I., Van der Veken, P., Vermeylen, R., Maenhaut, W., Jaoui, M., Kleindienst, T. E., Lewandowski, M., Offenberg, J. H., and Edney, E. O.: Hydroxydicarboxylic Acids: Markers for Secondary Organic Aerosol from the Photooxidation of α -Pinene, *Environ. Sci. Technol.*, 41, 1628–1634, <https://doi.org/10.1021/es0620181>, 2007.

Claeys, M., Iinuma, Y., Szmigielski, R., Surratt, J. D., Blockhuys, F., Van Alsenoy, C., Böge, O., Sierau, B., Gómez-González, Y., Vermeylen, R., Van der Veken, P., Shahgholi, M., Chan, A. W. H., Herrmann, H., Seinfeld, J. H., and Maenhaut, W.: Terpenylic Acid and Related Compounds from the Oxidation of α -Pinene: Implications for New Particle Formation and Growth above Forests, *Environ. Sci. Technol.*, 43, 6976–6982, <https://doi.org/10.1021/es9007596>, 2009.

Claeys, M., Kourtchev, I., Pashynska, V., Vas, G., Vermeylen, R., Wang, W., Cafmeyer, J., Chi, X., Artaxo, P., Andreae, M. O., and Maenhaut, W.: Polar organic marker compounds in atmospheric aerosols during the LBA-SMOCC 2002 biomass burning experiment in Rondônia, Brazil: sources and source processes, time series, diel variations and size distributions, *Atmos. Chem. Phys.*, 10, 9319–9331, <https://doi.org/10.5194/acp-10-9319-2010>, 2010.

Claeys, M., Vermeylen, R., Yasmeen, F., Gómez-González, Y., Chi, X., Maenhaut, W., Mészáros, T., Salma, I., Claeys, M., Vermeylen, R., Yasmeen, F., Gómez-González, Y., Chi, X., Maenhaut, W., Mészáros, T., and Salma, I.: Chemical characterisation of humic-like substances from urban, rural and tropical biomass burning environments using liquid chromatography with UV/vis photodiode array detection and electrospray ionisation mass spectrometry, *Environ. Chem.*, 9, 273–284, <https://doi.org/10.1071/EN11163>, 2012.

Clausen, P. A., Liu, Z., Kofoed-Sørensen, V., Little, J., and Wolkoff, P.: Influence of Temperature on the Emission of Di-(2-ethylhexyl)phthalate (DEHP) from PVC Flooring in the Emission Cell FLEC, *Environ. Sci. Technol.*, 46, 909–915, <https://doi.org/10.1021/es2035625>, 2012.

Coeur-Tourneur, C., Cassez, A., and Wenger, J. C.: Rate Coefficients for the Gas-Phase Reaction of Hydroxyl Radicals with 2-Methoxyphenol (Guaiacol) and Related Compounds, *J. Phys. Chem. A*, 114, 11645–11650, <https://doi.org/10.1021/jp1071023>, 2010.

Coggon, M. M., McDonald, B. C., Vlasenko, A., Veres, P. R., Bernard, F., Koss, A. R., Yuan, B., Gilman, J. B., Peischl, J., Aikin, K. C., DuRant, J., Warneke, C., Li, S.-M., and de Gouw, J. A.: Diurnal Variability and Emission Pattern of Decamethylcyclopentasiloxane (D5) from the Application of Personal Care Products in Two North American Cities, *Environ. Sci. Technol.*, 52, 5610–5618, <https://doi.org/10.1021/acs.est.8b00506>, 2018.

Coggon, M. M., Gkatzelis, G. I., McDonald, B. C., Gilman, J. B., Schwantes, R. H., Abuhassan, N., Aikin, K. C., Arend, M. F., Berkoff, T. A., Brown, S. S., Campos, T. L., Dickerson, R. R., Gronoff, G.,

Hurley, J. F., Isaacman-VanWertz, G., Koss, A. R., Li, M., McKeen, S. A., Moshary, F., Peischl, J., Pospisilova, V., Ren, X., Wilson, A., Wu, Y., Trainer, M., and Warneke, C.: Volatile chemical product emissions enhance ozone and modulate urban chemistry, *Proc. Natl. Acad. Sci. U.S.A.*, 118, e2026653118, <https://doi.org/10.1073/pnas.2026653118>, 2021.

Column/Fan Modules for Fast GC: <https://www.vici.com/gc/column-fan-modules.php>, last access: 6 October 2020.

Corchnoy, S. B. and Atkinson, R.: Kinetics of the gas-phase reactions of hydroxyl and nitrogen oxide (NO₃) radicals with 2-carene, 1,8-cineole, p-cymene, and terpinolene, *Environ. Sci. Technol.*, 24, 1497–1502, <https://doi.org/10.1021/es00080a007>, 1990.

Cousins, I. T. and Mackay, D.: Gas–Particle Partitioning of Organic Compounds and Its Interpretation Using Relative Solubilities, *Environ. Sci. Technol.*, 35, 643–647, <https://doi.org/10.1021/es001123m>, 2001.

Cropper, P. M., Overson, D. K., Cary, R. A., Eatough, D. J., Chow, J. C., and Hansen, J. C.: Development of the GC-MS organic aerosol monitor (GC-MS OAM) for in-field detection of particulate organic compounds, *Atmos. Environ.*, 169, 258–266, <https://doi.org/10.1016/j.atmosenv.2017.09.019>, 2017.

Dall’Osto, M., Paglione, M., Decesari, S., Facchini, M. C., O’Dowd, C., Plass-Duellmer, C., and Harrison, R. M.: On the Origin of AMS “Cooking Organic Aerosol” at a Rural Site, *Environ. Sci. Technol.*, 49, 13964–13972, <https://doi.org/10.1021/acs.est.5b02922>, 2015.

Davidson, E. A., de Araújo, A. C., Artaxo, P., Balch, J. K., Brown, I. F., C. Bustamante, M. M., Coe, M. T., DeFries, R. S., Keller, M., Longo, M., Munger, J. W., Schroeder, W., Soares-Filho, B. S., Souza, C. M., and Wofsy, S. C.: The Amazon basin in transition, *Nature*, 481, 321–328, <https://doi.org/10.1038/nature10717>, 2012.

De Gouw, J. and Jimenez, J. L.: Organic Aerosols in the Earth’s Atmosphere, *Environ. Sci. Technol.*, 43, 7614–7618, <https://doi.org/10.1021/es9006004>, 2009.

DeCarlo, P. F., Kimmel, J. R., Trimborn, A., Northway, M. J., Jayne, J. T., Aiken, A. C., Gonin, M., Fuhrer, K., Horvath, T., Docherty, K. S., Worsnop, D. R., and Jimenez, J. L.: Field-Deployable, High-Resolution, Time-of-Flight Aerosol Mass Spectrometer, *Anal. Chem.*, 78, 8281–8289, <https://doi.org/10.1021/ac061249n>, 2006.

Decesari, S., Fuzzi, S., Facchini, M. C., Mircea, M., Emblico, L., Cavalli, F., Maenhaut, W., Chi, X., Schkolnik, G., Falkovich, A., Rudich, Y., Claeys, M., Pashynska, V., Vas, G., Kourtchev, I., Vermeylen, R., Hoffer, A., Andreae, M. O., Tagliavini, E., Moretti, F., and Artaxo, P.: Characterization of the organic composition of aerosols from Rondônia, Brazil, during the LBA-SMOCC 2002 experiment and its representation through model compounds, *Atmos. Chem. Phys.*, 6, 375–402, <https://doi.org/10.5194/acp-6-375-2006>, 2006.

Docherty, K. S., Stone, E. A., Ulbrich, I. M., DeCarlo, P. F., Snyder, D. C., Schauer, J. J., Peltier, R. E., Weber, R. J., Murphy, S. M., Seinfeld, J. H., Grover, B. D., Eatough, D. J., and Jimenez, J. L.: Apportionment of Primary and Secondary Organic Aerosols in Southern California during the 2005 Study of Organic Aerosols in Riverside (SOAR-1), *Environ. Sci. Technol.*, **42**, 7655–7662, <https://doi.org/10.1021/es8008166>, 2008.

Donahue, N. M., Robinson, A. L., and Pandis, S. N.: Atmospheric organic particulate matter: From smoke to secondary organic aerosol, *Atmos. Environ.*, **43**, 94–106, <https://doi.org/10.1016/j.atmosenv.2008.09.055>, 2009.

Donahue, N. M., Epstein, S. A., Pandis, S. N., and Robinson, A. L.: A two-dimensional volatility basis set: 1. organic-aerosol mixing thermodynamics, *Atmos. Chem. Phys.*, **11**, 3303–3318, <https://doi.org/10.5194/acp-11-3303-2011>, 2011.

Donahue, N. M., Henry, K. M., Mentel, T. F., Kiendler-Scharr, A., Spindler, C., Bohn, B., Brauers, T., Dorn, H. P., Fuchs, H., Tillmann, R., Wahner, A., Saathoff, H., Naumann, K.-H., Möhler, O., Leisner, T., Müller, L., Reinnig, M.-C., Hoffmann, T., Salo, K., Hallquist, M., Frosch, M., Bilde, M., Tritscher, T., Barmet, P., Praplan, A. P., DeCarlo, P. F., Dommen, J., Prévôt, A. S. H., and Baltensperger, U.: Aging of biogenic secondary organic aerosol via gas-phase OH radical reactions, *Proc. Natl. Acad. Sci. U.S.A.*, **109**, 13503–13508, <https://doi.org/10.1073/pnas.1115186109>, 2012.

Donaldson, K. and Tran, C. L.: Inflammation Caused by Particles and Fibers, *Inhal. Toxicol.*, **14**, 5–27, <https://doi.org/10.1080/089583701753338613>, 2002.

Downs, C. A., DiNardo, J. C., Stien, D., Rodrigues, A. M. S., and Lebaron, P.: Benzophenone Accumulates over Time from the Degradation of Octocrylene in Commercial Sunscreen Products, *Chem. Res. Toxicol.*, **34**, 1046–1054, <https://doi.org/10.1021/acs.chemrestox.0c00461>, 2021.

Drozd, G. T., Zhao, Y., Saliba, G., Frodin, B., Maddox, C., Weber, R. J., Chang, M.-C. O., Maldonado, H., Sardar, S., Robinson, A. L., and Goldstein, A. H.: Time Resolved Measurements of Speciated Tailpipe Emissions from Motor Vehicles: Trends with Emission Control Technology, Cold Start Effects, and Speciation, *Environ. Sci. Technol.*, **50**, 13592–13599, <https://doi.org/10.1021/acs.est.6b04513>, 2016.

Drozd, G. T., Zhao, Y., Saliba, G., Frodin, B., Maddox, C., Oliver Chang, M.-C., Maldonado, H., Sardar, S., Weber, R. J., Robinson, A. L., and Goldstein, A. H.: Detailed Speciation of Intermediate Volatility and Semivolatile Organic Compound Emissions from Gasoline Vehicles: Effects of Cold-Starts and Implications for Secondary Organic Aerosol Formation, *Environ. Sci. Technol.*, **53**, 1706–1714, <https://doi.org/10.1021/acs.est.8b05600>, 2019.

Drozd, G. T., Weber, R. J., and Goldstein, A. H.: Highly Resolved Composition during Diesel Evaporation with Modeled Ozone and Secondary Aerosol Formation: Insights into Pollutant Formation from Evaporative Intermediate Volatility Organic Compound Sources, *Environ. Sci. Technol.*, **55**, 5742–5751, <https://doi.org/10.1021/acs.est.0c08832>, 2021.

Camphor (Professional Patient Advice): <https://www.drugs.com/ppa/camphor.html>, last access: 28 March 2022.

Duhl, T. R., Helmig, D., and Guenther, A.: Sesquiterpene emissions from vegetation: a review, *Biogeosciences*, 5, 761–777, <https://doi.org/10.5194/bg-5-761-2008>, 2008.

Engel, A., Rigby, M., Burkholder, J. B., Fernandez, R. P., Froidevaux, L., Hall, B. D., Hossaini, R., Saito, T., Vollmer, M. K., and Yao, B.: Update on Ozone-Depleting Substances (ODSs) and Other Gases of Interest to the Montreal Protocol, Chapter 1 in *Scientific Assessment of Ozone Depletion: 2018, Global Ozone Research and Monitoring Project - Report No. 58*, World Meteorological Organization, Geneva, Switzerland, 2018.

Ervens, B., Turpin, B. J., and Weber, R. J.: Secondary organic aerosol formation in cloud droplets and aqueous particles (aqSOA): a review of laboratory, field and model studies, *Atmos. Chem. Phys.*, 11, 11069–11102, <https://doi.org/10.5194/acp-11-11069-2011>, 2011.

2-Methoxynaphthalene Information: <https://echa.europa.eu/substance-information/-/substanceinfo/100.002.013>, last access: 12 April 2022.

Fantuzzi, G., Righi, E., Predieri, G., Ceppelli, G., Gobba, F., and Aggazzotti, G.: Occupational exposure to trihalomethanes in indoor swimming pools, *Sci. Total Environ.*, 264, 257–265, [https://doi.org/10.1016/S0048-9697\(00\)00722-1](https://doi.org/10.1016/S0048-9697(00)00722-1), 2001.

Finewax, Z., de Gouw, J. A., and Ziemann, P. J.: Identification and Quantification of 4-Nitrocatechol Formed from OH and NO₃ Radical-Initiated Reactions of Catechol in Air in the Presence of NO_x: Implications for Secondary Organic Aerosol Formation from Biomass Burning, *Environ. Sci. Technol.*, 52, 1981–1989, <https://doi.org/10.1021/acs.est.7b05864>, 2018.

Fisch, G., Tota, J., Machado, L. A. T., Silva Dias, M. A. F., da F. Lyra, R. F., Nobre, C. A., Dolman, A. J., and Gash, J. H. C.: The convective boundary layer over pasture and forest in Amazonia, *Theor. Appl. Climatol.*, 78, 47–59, <https://doi.org/10.1007/s00704-004-0043-x>, 2004.

Flagg, M., Hoag, K., and Lapka, J.: 2020 Air Monitoring Network Plan, 2020.

Foley, J. P. and Dorsey, J. G.: Clarification of the limit of detection in chromatography, *Chromatographia*, 18, 503–511, <https://doi.org/10.1007/BF02267236>, 1984.

Franklin, E. B., Yee, L. D., Aumont, B., Weber, R. J., Grigas, P., and Goldstein, A. H.: Ch3MS-RF: a random forest model for chemical characterization and improved quantification of unidentified atmospheric organics detected by chromatography–mass spectrometry techniques, *Atmospheric Measurement Techniques*, 15, 3779–3803, <https://doi.org/10.5194/amt-15-3779-2022>, 2022.

Fraser, M. P., Cass, G. R., Simoneit, B. R. T., and Rasmussen, R. A.: Air Quality Model Evaluation Data for Organics. 4. C₂–C₃₆ Non-Aromatic Hydrocarbons, *Environ. Sci. Technol.*, 31, 2356–2367, <https://doi.org/10.1021/es960980g>, 1997.

Fraser, M. P., Cass, G. R., Simoneit, B. R. T., and Rasmussen, R. A.: Air Quality Model Evaluation Data for Organics. 5. C₆–C₂₂ Nonpolar and Semipolar Aromatic Compounds, *Environ. Sci. Technol.*, 32, 1760–1770, <https://doi.org/10.1021/es970349v>, 1998.

Fruekilde, P., Hjorth, J., Jensen, N. R., Kotzias, D., and Larsen, B.: Ozonolysis at vegetation surfaces: a source of acetone, 4-oxopentanal, 6-methyl-5-hepten-2-one, and geranyl acetone in the troposphere, *Atmos. Environ.*, 32, 1893–1902, [https://doi.org/10.1016/S1352-2310\(97\)00485-8](https://doi.org/10.1016/S1352-2310(97)00485-8), 1998.

Fu, P., Kawamura, K., Chen, J., and Miyazaki, Y.: Secondary Production of Organic Aerosols from Biogenic VOCs over Mt. Fuji, Japan, *Environ. Sci. Technol.*, 48, 8491–8497, <https://doi.org/10.1021/es500794d>, 2014.

Fuentes, J. D., Chamecki, M., Santos, R. M. N. dos, Randow, C. V., Stoy, P. C., Katul, G., Fitzjarrald, D., Manzi, A., Gerken, T., Trowbridge, A., Freire, L. S., Ruiz-Plancarte, J., Maia, J. M. F., Tóta, J., Dias, N., Fisch, G., Schumacher, C., Acevedo, O., Mercer, J. R., and Yañez-Serrano, A. M.: Linking Meteorology, Turbulence, and Air Chemistry in the Amazon Rain Forest, *Bull. Amer. Meteor.*, 97, 2329–2342, <https://doi.org/10.1175/BAMS-D-15-00152.1>, 2016.

Fujii, M., Shinohara, N., Lim, A., Otake, T., Kumagai, K., and Yanagisawa, Y.: A study on emission of phthalate esters from plastic materials using a passive flux sampler, *Atmos. Environ.*, 37, 5495–5504, <https://doi.org/10.1016/j.atmosenv.2003.09.026>, 2003.

Fuzzi, S., Decesari, S., Facchini, M. C., Cavalli, F., Emblico, L., Mircea, M., Andreae, M. O., Trebs, I., Hoffer, A., Guyon, P., Artaxo, P., Rizzo, L. V., Lara, L. L., Pauliquevis, T., Maenhaut, W., Raes, N., Chi, X., Mayol-Bracero, O. L., Soto-García, L. L., Claeys, M., Kourtchev, I., Rissler, J., Swietlicki, E., Tagliavini, E., Schkolnik, G., Falkovich, A. H., Rudich, Y., Fisch, G., and Gatti, L. V.: Overview of the inorganic and organic composition of size-segregated aerosol in Rondônia, Brazil, from the biomass-burning period to the onset of the wet season, *J. Geophys. Res. Atmos.*, 112, <https://doi.org/10.1029/2005JD006741>, 2007.

Gao, G., Chen, H., Chai, Y., Jin, L., Liu, X., and Lu, C.: A method based on precolumn derivatization and ultra high performance liquid chromatography with high-resolution mass spectrometry for the simultaneous determination of phthalimide and phthalic acid in tea, *J. Sep. Sci.*, 42, 1304–1311, <https://doi.org/10.1002/jssc.201801128>, 2019.

Garneau, F.-X., Collin, G., Gagnon, H., and Pichette, A.: Chemical Composition of the Hydrosol and the Essential Oil of Three Different Species of the Pinaceae Family : *Picea glauca* (Moench) Voss., *Picea mariana* (Mill.) B.S.P., and *Abies balsamea* (L.) Mill., *Journal of Essential Oil Bearing Plants*, 15, 227–236, <https://doi.org/10.1080/0972060X.2012.10644040>, 2012.

Gentner, D. R., Isaacman, G., Worton, D. R., Chan, A. W. H., Dallmann, T. R., Davis, L., Liu, S., Day, D. A., Russell, L. M., Wilson, K. R., Weber, R., Guha, A., Harley, R. A., and Goldstein, A. H.: Elucidating secondary organic aerosol from diesel and gasoline vehicles through detailed

characterization of organic carbon emissions, *Proc. Natl. Acad. Sci. U.S.A.*, 109, 18318–18323, <https://doi.org/10.1073/pnas.1212272109>, 2012.

Gentner, D. R., Worton, D. R., Isaacman, G., Davis, L. C., Dallmann, T. R., Wood, E. C., Herndon, S. C., Goldstein, A. H., and Harley, R. A.: Chemical Composition of Gas-Phase Organic Carbon Emissions from Motor Vehicles and Implications for Ozone Production, *Environ. Sci. Technol.*, 47, 11837–11848, <https://doi.org/10.1021/es401470e>, 2013a.

Gentner, D. R., Worton, D. R., Isaacman, G., Davis, L. C., Dallmann, T. R., Wood, E. C., Herndon, S. C., Goldstein, A. H., and Harley, R. A.: Chemical Composition of Gas-Phase Organic Carbon Emissions from Motor Vehicles and Implications for Ozone Production, *Environ. Sci. Technol.*, 47, 11837–11848, <https://doi.org/10.1021/es401470e>, 2013b.

Gkatzelis, G. I., Coggon, M. M., McDonald, B. C., Peischl, J., Aikin, K. C., Gilman, J. B., Trainer, M., and Warneke, C.: Identifying Volatile Chemical Product Tracer Compounds in U.S. Cities, *Environ. Sci. Technol.*, 55, 188–199, <https://doi.org/10.1021/acs.est.0c05467>, 2021.

Goldan, P. D., Kuster, W. C., Williams, E., Murphy, P. C., Fehsenfeld, F. C., and Meagher, J.: Nonmethane hydrocarbon and oxy hydrocarbon measurements during the 2002 New England Air Quality Study, *J. Geophys. Res. Atmos.*, 109, 1–14, <https://doi.org/10.1029/2003JD004455>, 2004.

Goldstein, A. H. and Galbally, I. E.: Known and Unexplored Organic Constituents in the Earth's Atmosphere, *Environ. Sci. Technol.*, 41, 1514–1521, <https://doi.org/10.1021/es072476p>, 2007.

Goldstein, A. H., Daube, B. C., Munger, J. W., and Wofsy, S. C.: Automated in-situ monitoring of atmospheric non-methane hydrocarbon concentrations and gradients, *J Atmos Chem*, 21, 43–59, <https://doi.org/10.1007/BF00712437>, 1995.

de Gouw, J. A., Middlebrook, A. M., Warneke, C., Ahmadov, R., Atlas, E. L., Bahreini, R., Blake, D. R., Brock, C. A., Brioude, J., Fahey, D. W., Fehsenfeld, F. C., Holloway, J. S., Le Henaff, M., Lueb, R. A., McKeen, S. A., Meagher, J. F., Murphy, D. M., Paris, C., Parrish, D. D., Perring, A. E., Pollack, I. B., Ravishankara, A. R., Robinson, A. L., Ryerson, T. B., Schwarz, J. P., Spackman, J. R., Srinivasan, A., and Watts, L. A.: Organic aerosol formation downwind from the Deepwater Horizon oil spill, *Science*, 331, 1295–1299, <https://doi.org/10.1126/science.1200320>, 2011.

Graham, B., Mayol-Bracero, O. L., Guyon, P., Roberts, G. C., Decesari, S., Facchini, M. C., Artaxo, P., Maenhaut, W., Köll, P., and Andreae, M. O.: Water-soluble organic compounds in biomass burning aerosols over Amazonia 1. Characterization by NMR and GC-MS, *J. Geophys. Res. Atmos.*, 107, LBA 14-1-LBA 14-16, <https://doi.org/10.1029/2001JD000336>, 2002.

Gueneron, M., Erickson, M. H., VanderSchelden, G. S., and Jobson, B. T.: PTR-MS fragmentation patterns of gasoline hydrocarbons, *International Journal of Mass Spectrometry*, 379, 97–109, <https://doi.org/10.1016/j.ijms.2015.01.001>, 2015.

Guenther, A.: Seasonal and Spatial Variations in Natural Volatile Organic Compound Emissions, *Ecol. Appl.*, 7, 34–45, [https://doi.org/10.1890/1051-0761\(1997\)007\[0034:SASVIN\]2.0.CO;2](https://doi.org/10.1890/1051-0761(1997)007[0034:SASVIN]2.0.CO;2), 1997.

Hallquist, M., Wenger, J. C., Baltensperger, U., Rudich, Y., Simpson, D., Claeys, M., Dommen, J., Donahue, N. M., George, C., Goldstein, A. H., Hamilton, J. F., Herrmann, H., Hoffmann, T., Iinuma, Y., Jang, M., Jenkin, M. E., Jimenez, J. L., Kiendler-Scharr, A., Maenhaut, W., McFiggans, G., Mentel, Th. F., Monod, A., Prévôt, A. S. H., Seinfeld, J. H., Surratt, J. D., Szmigielski, R., and Wildt, J.: The formation, properties and impact of secondary organic aerosol: current and emerging issues, *Atmos. Chem. Phys.*, 9, 5155–5235, 2009.

Ham, J. E.: Rate Constants for the Gas-Phase Reactions of Ozone and Nitrate Radicals with the Sesquiterpenes: Valencene and Farnesol: Gas-Phase Reactions of Ozone and Nitrate Radicals with the Sesquiterpenes, *Int. J. Chem. Kinet.*, 45, 508–514, <https://doi.org/10.1002/kin.20789>, 2013.

Han, D., Li, J., Cao, H., He, M., Hu, J., and Yao, S.: Theoretical investigation on the mechanisms and kinetics of OH-initiated photooxidation of dimethyl phthalate (DMP) in atmosphere, *Chemosphere*, 95, 50–57, <https://doi.org/10.1016/j.chemosphere.2013.07.087>, 2014.

Hand, J. L., Schichtel, B. A., Malm, W. C., and Frank, N. H.: Spatial and Temporal Trends in PM_{2.5} Organic and Elemental Carbon across the United States, *Adv. Meteorol.*, 2013, e367674, <https://doi.org/10.1155/2013/367674>, 2013.

Harrison, M. a. J., Heal, M. R., and Cape, J. N.: Evaluation of the pathways of tropospheric nitrophenol formation from benzene and phenol using a multiphase model, *Atmos. Chem. Phys.*, 5, 1679–1695, <https://doi.org/10.5194/acp-5-1679-2005>, 2005a.

Harrison, M. A. J., Barra, S., Borghesi, D., Vione, D., Arsene, C., and Iulian Olariu, R.: Nitrated phenols in the atmosphere: a review, *Atmos. Environ.*, 39, 231–248, <https://doi.org/10.1016/j.atmosenv.2004.09.044>, 2005b.

Hatch, L. E., Luo, W., Pankow, J. F., Yokelson, R. J., Stockwell, C. E., and Barsanti, K. C.: Identification and quantification of gaseous organic compounds emitted from biomass burning using two-dimensional gas chromatography–time-of-flight mass spectrometry, *Atmos. Chem. Phys.*, 15, 1865–1899, <https://doi.org/10.5194/acp-15-1865-2015>, 2015.

Hatch, L. E., Yokelson, R. J., Stockwell, C. E., Veres, P. R., Simpson, I. J., Blake, D. R., Orlando, J. J., and Barsanti, K. C.: Multi-instrument comparison and compilation of non-methane organic gas emissions from biomass burning and implications for smoke-derived secondary organic aerosol precursors, *Atmos. Chem. Phys.*, 17, 1471–1489, <https://doi.org/10.5194/acp-17-1471-2017>, 2017.

Heald, C. L. and Kroll, J. H.: The fuel of atmospheric chemistry: Toward a complete description of reactive organic carbon, *Sci. Adv.*, 6, eaay8967, <https://doi.org/10.1126/sciadv.aay8967>, 2020.

Heald, C. L., Henze, D. K., Horowitz, L. W., Feddema, J., Lamarque, J.-F., Guenther, A., Hess, P. G., Vitt, F., Seinfeld, J. H., Goldstein, A. H., and Fung, I.: Predicted change in global secondary organic aerosol concentrations in response to future climate, emissions, and land use change, *J. Geophys. Res. Atmos.*, 113, <https://doi.org/10.1029/2007JD009092>, 2008.

Hellén, H., Tykkä, T., and Hakola, H.: Importance of monoterpenes and isoprene in urban air in northern Europe, *Atmos. Environ.*, 59, 59–66, <https://doi.org/10.1016/j.atmosenv.2012.04.049>, 2012.

Helmig, D.: Ozone removal techniques in the sampling of atmospheric volatile organic trace gases, *Atmospheric Environment*, 31, 3635–3651, [https://doi.org/10.1016/S1352-2310\(97\)00144-1](https://doi.org/10.1016/S1352-2310(97)00144-1), 1997.

Hennigan, C. J., Sullivan, A. P., Collett, J. L., and Robinson, A. L.: Levoglucosan stability in biomass burning particles exposed to hydroxyl radicals, *Geophys. Res. Lett.*, 37, <https://doi.org/10.1029/2010GL043088>, 2010.

Hodzic, A., Jimenez, J. L., Madronich, S., Canagaratna, M. R., DeCarlo, P. F., Kleinman, L., and Fast, J.: Modeling organic aerosols in a megacity: potential contribution of semi-volatile and intermediate volatility primary organic compounds to secondary organic aerosol formation, *Atmospheric Chemistry and Physics*, 10, 5491–5514, <https://doi.org/10.5194/acp-10-5491-2010>, 2010.

Hoeve, J. E. T., Remer, L. A., Correia, A. L., and Jacobson, M. Z.: Recent shift from forest to savanna burning in the Amazon Basin observed by satellite, *Environ. Res. Lett.*, 7, 024020, <https://doi.org/10.1088/1748-9326/7/2/024020>, 2012.

Hoffer, A., Gelencsér, A., Blazsó, M., Guyon, P., Artaxo, P., and Andreae, M. O.: Diel and seasonal variations in the chemical composition of biomass burning aerosol, *Atmos. Chem. Phys.*, 6, 3505–3515, <https://doi.org/10.5194/acp-6-3505-2006>, 2006.

Hoffmann, D., Iinuma, Y., and Herrmann, H.: Development of a method for fast analysis of phenolic molecular markers in biomass burning particles using high performance liquid chromatography/atmospheric pressure chemical ionisation mass spectrometry, *J. Chromatogr. A*, 1143, 168–175, <https://doi.org/10.1016/j.chroma.2007.01.035>, 2007.

Hoffmann, D., Tilgner, A., Iinuma, Y., and Herrmann, H.: Atmospheric stability of levoglucosan: a detailed laboratory and modeling study, *Environ. Sci. Technol.*, 44, 694–699, <https://doi.org/10.1021/es902476f>, 2010.

Holben, B. N., Setzer, A., Eck, T. F., Pereira, A., and Slutsker, I.: Effect of dry-season biomass burning on Amazon basin aerosol concentrations and optical properties, 1992–1994, *J. Geophys. Res. Atmos.*, 101, 19465–19481, <https://doi.org/10.1029/96JD01114>, 1996.

Hopke, P. K.: Review of receptor modeling methods for source apportionment, *J. Air Waste Manag. Assoc.*, 66, 237–259, <https://doi.org/10.1080/10962247.2016.1140693>, 2016.

Hopkins, J. R., Lewis, A. C., and Read, K. A.: A two-column method for long-term monitoring of non-methane hydrocarbons (NMHCs) and oxygenated volatile organic compounds (o-VOCs), *J. Environ. Monit.*, 5, 8–13, <https://doi.org/10.1039/B202798D>, 2003.

Horii, Y. and Kannan, K.: Survey of Organosilicone Compounds, Including Cyclic and Linear Siloxanes, in Personal-Care and Household Products, *Arch. Environ. Contam. Toxicol.*, 55, 701, <https://doi.org/10.1007/s00244-008-9172-z>, 2008.

Hosseini, S., Urbanski, S. P., Dixit, P., Qi, L., Burling, I. R., Yokelson, R. J., Johnson, T. J., Shrivastava, M., Jung, H. S., Weise, D. R., Miller, J. W., and Cocker III, D. R.: Laboratory characterization of PM emissions from combustion of wildland biomass fuels, *J. Geophys. Res. Atmos.*, 118, 9914–9929, <https://doi.org/10.1002/jgrd.50481>, 2013.

Howsam, M. and Jones, K. C.: Sources of PAHs in the Environment, in: PAHs and Related Compounds: Chemistry, edited by: Neilson, A. H., Springer, Berlin, Heidelberg, 137–174, https://doi.org/10.1007/978-3-540-49697-7_4, 1998.

Hunter, J. F., Day, D. A., Palm, B. B., Yatavelli, R. L. N., Chan, A. W. H., Kaser, L., Cappellin, L., Hayes, P. L., Cross, E. S., Carrasquillo, A. J., Campuzano-Jost, P., Stark, H., Zhao, Y., Hohaus, T., Smith, J. N., Hansel, A., Karl, T., Goldstein, A. H., Guenther, A., Worsnop, D. R., Thornton, J. A., Heald, C. L., Jimenez, J. L., and Kroll, J. H.: Comprehensive characterization of atmospheric organic carbon at a forested site, *Nat. Geosci.*, 10, 748–753, <https://doi.org/10.1038/ngeo3018>, 2017.

Hurteau, M. D., Westerling, A. L., Wiedinmyer, C., and Bryant, B. P.: Projected Effects of Climate and Development on California Wildfire Emissions through 2100, *Environ. Sci. Technol.*, 48, 2298–2304, <https://doi.org/10.1021/es4050133>, 2014.

Iinuma, Y., Brüggemann, E., Gnauk, T., Müller, K., Andreae, M. O., Helas, G., Parmar, R., and Herrmann, H.: Source characterization of biomass burning particles: The combustion of selected European conifers, African hardwood, savanna grass, and German and Indonesian peat, *J. Geophys. Res.*, 112, D08209, <https://doi.org/10.1029/2006JD007120>, 2007.

Inomata, S., Tanimoto, H., Fujitani, Y., Sekimoto, K., Sato, K., Fushimi, A., Yamada, H., Hori, S., Kumazawa, Y., Shimono, A., and Hikida, T.: On-line measurements of gaseous nitro-organic compounds in diesel vehicle exhaust by proton-transfer-reaction mass spectrometry, *Atmos. Environ.*, 73, 195–203, <https://doi.org/10.1016/j.atmosenv.2013.03.035>, 2013.

International Programme on Chemical Safety: Environmental Health Criteria 174 Isophorone, World Health Organization, Geneva, Switzerland, 1995.

Isaacman, G., Kreisberg, N. M., Worton, D. R., Hering, S. V., and Goldstein, A. H.: A versatile and reproducible automatic injection system for liquid standard introduction: application to in-situ calibration, *Atmos. Meas. Tech.*, 4, 1937–1942, <https://doi.org/10.5194/amt-4-1937-2011>, 2011.

Isaacman, G., Chan, A. W. H., Nah, T., Worton, D. R., Ruehl, C. R., Wilson, K. R., and Goldstein, A. H.: Heterogeneous OH Oxidation of Motor Oil Particles Causes Selective Depletion of Branched

and Less Cyclic Hydrocarbons, *Environ. Sci. Technol.*, 46, 10632–10640, <https://doi.org/10.1021/es302768a>, 2012a.

Isaacman, G., Wilson, K. R., Chan, A. W. H., Worton, D. R., Kimmel, J. R., Nah, T., Hohaus, T., Gonin, M., Kroll, J. H., Worsnop, D. R., and Goldstein, A. H.: Improved Resolution of Hydrocarbon Structures and Constitutional Isomers in Complex Mixtures Using Gas Chromatography-Vacuum Ultraviolet-Mass Spectrometry, *Anal. Chem.*, 84, 2335–2342, <https://doi.org/10.1021/ac2030464>, 2012b.

Isaacman, G., Kreisberg, N. M., Yee, L. D., Worton, D. R., Chan, A. W. H., Moss, J. A., Hering, S. V., and Goldstein, A. H.: Online derivatization for hourly measurements of gas- and particle-phase semi-volatile oxygenated organic compounds by thermal desorption aerosol gas chromatography (SV-TAG), *Atmos. Meas. Tech.*, 7, 4417–4429, <https://doi.org/10.5194/amt-7-4417-2014>, 2014.

Isaacman-VanWertz, G., Sueper, D. T., Aikin, K. C., Lerner, B. M., Gilman, J. B., de Gouw, J. A., Worsnop, D. R., and Goldstein, A. H.: Automated single-ion peak fitting as an efficient approach for analyzing complex chromatographic data, *J. Chromatogr. A*, 1529, 81–92, <https://doi.org/10.1016/j.chroma.2017.11.005>, 2017.

Isaacman-VanWertz, G., Massoli, P., O'Brien, R., Lim, C., Franklin, J. P., Moss, J. A., Hunter, J. F., Nowak, J. B., Canagaratna, M. R., Misztal, P. K., Arata, C., Roscioli, J. R., Herndon, S. T., Onasch, T. B., Lambe, A. T., Jayne, J. T., Su, L., Knopf, D. A., Goldstein, A. H., Worsnop, D. R., and Kroll, J. H.: Chemical evolution of atmospheric organic carbon over multiple generations of oxidation, *Nat. Chem.*, 10, 462–468, <https://doi.org/10.1038/s41557-018-0002-2>, 2018.

Jaoui, M., Kleindienst, T. E., Lewandowski, M., Offenberg, J. H., and Edney, E. O.: Identification and Quantification of Aerosol Polar Oxygenated Compounds Bearing Carboxylic or Hydroxyl Groups. 2. Organic Tracer Compounds from Monoterpenes, *Environ. Sci. Technol.*, 39, 5661–5673, <https://doi.org/10.1021/es048111b>, 2005.

Jaoui, M., Lewandowski, M., Kleindienst, T. E., Offenberg, J. H., and Edney, E. O.: β -caryophyllinic acid: An atmospheric tracer for β -caryophyllene secondary organic aerosol, *Geophys. Res. Lett.*, 34, <https://doi.org/10.1029/2006GL028827>, 2007.

Jardine, K. J., Henderson, W. M., Huxman, T. E., Abrell, L., and Shartsis, T.: Dynamic Solution Injection: a new method for preparing pptv-ppbv standard atmospheres of volatile organic compounds, *Atmos. Meas. Tech.*, 3, 3047–3066, 2010.

Jen, C. N., Hatch, L. E., Selimovic, V., Yokelson, R. J., Weber, R., Fernandez, A. E., Kreisberg, N. M., Barsanti, K. C., and Goldstein, A. H.: Speciated and total emission factors of particulate organics from burning western US wildland fuels and their dependence on combustion efficiency, *Atmos. Chem. Phys.*, 19, 1013–1026, <https://doi.org/10.5194/acp-19-1013-2019>, 2019.

Jimenez, J. L., Canagaratna, M. R., Donahue, N. M., Prevot, A. S. H., Zhang, Q., Kroll, J. H., DeCarlo, P. F., Allan, J. D., Coe, H., Ng, N. L., Aiken, A. C., Docherty, K. S., Ulbrich, I. M., Grieshop, A. P.,

Robinson, A. L., Duplissy, J., Smith, J. D., Wilson, K. R., Lanz, V. A., Hueglin, C., Sun, Y. L., Tian, J., Laaksonen, A., Raatikainen, T., Rautiainen, J., Vaattovaara, P., Ehn, M., Kulmala, M., Tomlinson, J. M., Collins, D. R., Cubison, M. J., E, Dunlea, J., Huffman, J. A., Onasch, T. B., Alfarra, M. R., Williams, P. I., Bower, K., Kondo, Y., Schneider, J., Drewnick, F., Borrmann, S., Weimer, S., Demerjian, K., Salcedo, D., Cottrell, L., Griffin, R., Takami, A., Miyoshi, T., Hatakeyama, S., Shimojo, A., Sun, J. Y., Zhang, Y. M., Dzepina, K., Kimmel, J. R., Sueper, D., Jayne, J. T., Herndon, S. C., Trimborn, A. M., Williams, L. R., Wood, E. C., Middlebrook, A. M., Kolb, C. E., Baltensperger, U., and Worsnop, D. R.: Evolution of Organic Aerosols in the Atmosphere, *Science*, 326, 1525–1529, <https://doi.org/10.1126/science.1180353>, 2009.

Kaltsonoudis, C., Kostenidou, E., Florou, K., Psichoudaki, M., and Pandis, S. N.: Temporal variability and sources of VOCs in urban areas of the eastern Mediterranean, *Atmos. Chem. Phys.*, 16, 14825–14842, <https://doi.org/10.5194/acp-16-14825-2016>, 2016.

Kanakidou, M., Seinfeld, J. H., Pandis, S. N., Barnes, I., Dentener, F. J., Facchini, M. C., Van Dingenen, R., Ervens, B., Nenes, A., Nielsen, C. J., Swietlicki, E., Putaud, J. P., Balkanski, Y., Fuzzi, S., Horth, J., Moortgat, G. K., Winterhalter, R., Myhre, C. E. L., Tsigaridis, K., Vignati, E., Stephanou, E. G., and Wilson, J.: Organic aerosol and global climate modelling: a review, *Atmos. Chem. Phys.*, 5, 1053–1123, <https://doi.org/10.5194/acp-5-1053-2005>, 2005.

Karbiwnyk, C. M., Mills, C. S., Helmig, D., and Birks, J. W.: Use of Chlorofluorocarbons as Internal Standards for the Measurement of Atmospheric Non-Methane Volatile Organic Compounds Sampled onto Solid Adsorbent Cartridges, *Environ. Sci. Technol.*, 37, 1002–1007, <https://doi.org/10.1021/es025910q>, 2003.

Kataoka, H., Terada, Y., Inoue, R., and Mitani, K.: Determination of isophorone in food samples by solid-phase microextraction coupled with gas chromatography–mass spectrometry, *J. Chromatogr. A*, 1155, 100–104, <https://doi.org/10.1016/j.chroma.2007.04.005>, 2007.

Kawamura, K. and Bikina, S.: A review of dicarboxylic acids and related compounds in atmospheric aerosols: Molecular distributions, sources and transformation, *Atmospheric Research*, 170, 140–160, <https://doi.org/10.1016/j.atmosres.2015.11.018>, 2016.

Kawamura, K., Steinberg, S., and Kaplan, I. R.: Homologous series of C1–C10 monocarboxylic acids and C1–C6 carbonyls in Los Angeles air and motor vehicle exhausts, *Atmos. Environ.*, 34, 4175–4191, [https://doi.org/10.1016/S1352-2310\(00\)00212-0](https://doi.org/10.1016/S1352-2310(00)00212-0), 2000.

Kawamura, K., Ishimura, Y., and Yamazaki, K.: Four years' observations of terrestrial lipid class compounds in marine aerosols from the western North Pacific, *Global Biogeochem. Cycles*, 17, 3-1-3–19, <https://doi.org/10.1029/2001GB001810>, 2003.

Kawamura, Kimitaka., Ng, L. Ling., and Kaplan, I. R.: Determination of organic acids (C1–C10) in the atmosphere, motor exhausts, and engine oils, *Environ. Sci. Technol.*, 19, 1082–1086, <https://doi.org/10.1021/es00141a010>, 1985.

Kenny, L. C., Gussman, R., and Meyer, M.: Development of a Sharp-Cut Cyclone for Ambient Aerosol Monitoring Applications, *Aerosol Sci. Technol.*, 32, 338–358, <https://doi.org/10.1080/027868200303669>, 2000.

Kerger, B. D., Schmidt, C. E., and Paustenbach, D. J.: Assessment of Airborne Exposure to Trihalomethanes from Tap Water in Residential Showers and Baths, *Risk Anal.*, 20, 637–652, <https://doi.org/10.1111/0272-4332.205058>, 2000.

Khare, P., Machesky, J., Soto, R., He, M., Presto, A. A., and Gentner, D. R.: Asphalt-related emissions are a major missing nontraditional source of secondary organic aerosol precursors, *Sci. Adv.*, 6, eabb9785, <https://doi.org/10.1126/sciadv.abb9785>, 2020.

Kim, K.-H., Kabir, E., and Kabir, S.: A review on the human health impact of airborne particulate matter, *Environ. Int.*, 74, 136–143, <https://doi.org/10.1016/j.envint.2014.10.005>, 2015.

Kirstine, W., Galbally, I., Ye, Y., and Hooper, M.: Emissions of volatile organic compounds (primarily oxygenated species) from pasture, *J. Geophys. Res. Atmos.*, 103, 10605–10619, <https://doi.org/10.1029/97JD03753>, 1998.

Kitanovski, Z., Grgić, I., Vermeylen, R., Claeys, M., and Maenhaut, W.: Liquid chromatography tandem mass spectrometry method for characterization of monoaromatic nitro-compounds in atmospheric particulate matter, *J. Chromatogr. A*, 1268, 35–43, <https://doi.org/10.1016/j.chroma.2012.10.021>, 2012.

Kjällstrand, J. and Petersson, G.: Phenolic antioxidants in alder smoke during industrial meat curing, *Food Chem.*, 74, 85–89, [https://doi.org/10.1016/S0308-8146\(01\)00102-9](https://doi.org/10.1016/S0308-8146(01)00102-9), 2001a.

Kjällstrand, J. and Petersson, G.: Phenolic antioxidants in wood smoke, *Sci. Total Environ.*, 277, 69–75, [https://doi.org/10.1016/S0048-9697\(00\)00863-9](https://doi.org/10.1016/S0048-9697(00)00863-9), 2001b.

Kleindienst, T. E., Jaoui, M., Lewandowski, M., Offenber, J. H., and Docherty, K. S.: The formation of SOA and chemical tracer compounds from the photooxidation of naphthalene and its methyl analogs in the presence and absence of nitrogen oxides, *Atmos. Chem. Phys.*, 12, 8711–8726, <https://doi.org/10.5194/acp-12-8711-2012>, 2012.

Kniss, V. M. L., Gioia, J., and Ronen, H.: 2017 Clean Air Plan, Bay Area Air Quality Management District, 268, 2017.

Knoderer, C., Nguyen, D., and Alrick, D.: 2017 Air Monitoring Network Plan, Bay Area Air Quality Management District, 2018.

Knote, C., Hodzic, A., and Jimenez, J. L.: The effect of dry and wet deposition of condensable vapors on secondary organic aerosols concentrations over the continental US, *Atmos. Chem. Phys.*, 15, 1–18, <https://doi.org/10.5194/acp-15-1-2015>, 2015.

Koren, I., Martins, J. V., Remer, L. A., and Afargan, H.: Smoke Invigoration Versus Inhibition of Clouds over the Amazon, *Science*, 321, 946–949, <https://doi.org/10.1126/science.1159185>, 2008.

Krasner, S. W., McGuire, M. J., Jacangelo, J. G., Patania, N. L., Reagan, K. M., and Aieta, E. M.: The Occurrence of Disinfection By-products in US Drinking Water, *J. Am. Water Works Assoc.*, 81, 41–53, <https://doi.org/10.1002/j.1551-8833.1989.tb03258.x>, 1989.

Kreisberg, N. M., Worton, D. R., Zhao, Y., Isaacman, G., Goldstein, A. H., and Hering, S. V.: Development of an automated high-temperature valveless injection system for online gas chromatography, *Atmos. Meas. Tech.*, 7, 4431–4444, <https://doi.org/10.5194/amt-7-4431-2014>, 2014.

Kroll, J. H. and Seinfeld, J. H.: Chemistry of secondary organic aerosol: Formation and evolution of low-volatility organics in the atmosphere, *Atmos. Environ.*, 42, 3593–3624, <https://doi.org/10.1016/j.atmosenv.2008.01.003>, 2008.

Lai, C., Liu, Y., Ma, J., Ma, Q., and He, H.: Degradation kinetics of levoglucosan initiated by hydroxyl radical under different environmental conditions, *Atmos. Environ.*, 91, 32–39, <https://doi.org/10.1016/j.atmosenv.2014.03.054>, 2014.

Lamanna, M. S. and Goldstein, A. H.: In situ measurements of C2–C10 volatile organic compounds above a Sierra Nevada ponderosa pine plantation, *J. Geophys. Res. Atmos.*, 104, 21247–21262, <https://doi.org/10.1029/1999JD900289>, 1999.

Lapczynski, A., Jones, L., McGinty, D., Bhatia, S. P., Letizia, C. S., and Api, A. M.: Fragrance material review on methyl salicylate, *Food Chem. Toxicol.*, 45, S428–S452, <https://doi.org/10.1016/j.fct.2007.09.053>, 2007.

Lauraguais, A., Coeur-Tourneur, C., Cassez, A., and Seydi, A.: Rate constant and secondary organic aerosol yields for the gas-phase reaction of hydroxyl radicals with syringol (2,6-dimethoxyphenol), *Atmos. Environ.*, 55, 43–48, <https://doi.org/10.1016/j.atmosenv.2012.02.027>, 2012.

Lee, B. and Wang, J.: Concentration variation of isoprene and its implications for peak ozone concentration, *Atmos. Environ.*, 40, 5486–5495, <https://doi.org/10.1016/j.atmosenv.2006.03.035>, 2006.

Lerner, B. M., Gilman, J. B., Aikin, K. C., Atlas, E. L., Goldan, P. D., Graus, M., Hendershot, R., Isaacman-VanWertz, G. A., Koss, A., Kuster, W. C., Lueb, R. A., McLaughlin, R. J., Peischl, J., Sueper, D., Ryerson, T. B., Tokarek, T. W., Warneke, C., Yuan, B., and de Gouw, J. A.: An improved, automated whole air sampler and gas chromatography mass spectrometry analysis system for volatile organic compounds in the atmosphere, *Atmos. Meas. Tech.*, 10, 291–313, <https://doi.org/10.5194/amt-10-291-2017>, 2017.

Li, R., Wang, Q., He, X., Zhu, S., Zhang, K., Duan, Y., Fu, Q., Qiao, L., Wang, Y., Huang, L., Li, L., and Yu, J. Z.: Source apportionment of PM_{2.5} in Shanghai based on hourly organic molecular markers and other source tracers, *Atmos. Chem. Phys.*, 20, 12047–12061, <https://doi.org/10.5194/acp-20-12047-2020>, 2020.

Li, W., Ge, P., Chen, M., Tang, J., Cao, M., Cui, Y., Hu, K., and Nie, D.: Tracers from Biomass Burning Emissions and Identification of Biomass Burning, *Atmosphere*, 12, 1401, <https://doi.org/10.3390/atmos12111401>, 2021.

Li, X., Jiang, L., Hoa, L. P., Lyu, Y., Xu, T., Yang, X., Iinuma, Y., Chen, J., and Herrmann, H.: Size distribution of particle-phase sugar and nitrophenol tracers during severe urban haze episodes in Shanghai, *Atmos. Environ.*, 145, 115–127, <https://doi.org/10.1016/j.atmosenv.2016.09.030>, 2016.

Liakakou, E., Vrekoussis, M., Bonsang, B., Donousis, Ch., Kanakidou, M., and Mihalopoulos, N.: Isoprene above the Eastern Mediterranean: Seasonal variation and contribution to the oxidation capacity of the atmosphere, *Atmos. Environ.*, 41, 1002–1010, <https://doi.org/10.1016/j.atmosenv.2006.09.034>, 2007.

Liang, Y. and Xu, Y.: Emission of Phthalates and Phthalate Alternatives from Vinyl Flooring and Crib Mattress Covers: The Influence of Temperature, *Environ. Sci. Technol.*, 48, 14228–14237, <https://doi.org/10.1021/es504801x>, 2014.

Lim, L. H., Harrison, R. M., and Harrad, S.: The Contribution of Traffic to Atmospheric Concentrations of Polycyclic Aromatic Hydrocarbons, *Environ. Sci. Technol.*, 33, 3538–3542, <https://doi.org/10.1021/es990392d>, 1999.

Lim, Y. B. and Ziemann, P. J.: Effects of Molecular Structure on Aerosol Yields from OH Radical-Initiated Reactions of Linear, Branched, and Cyclic Alkanes in the Presence of NO_x, *Environ. Sci. Technol.*, 43, 2328–2334, <https://doi.org/10.1021/es803389s>, 2009.

Lin, G., Penner, J. E., and Zhou, C.: How will SOA change in the future?, *Geophys. Res. Lett.*, 43, 1718–1726, <https://doi.org/10.1002/2015GL067137>, 2016a.

Lin, P., Aiona, P. K., Li, Y., Shiraiwa, M., Laskin, J., Nizkorodov, S. A., and Laskin, A.: Molecular Characterization of Brown Carbon in Biomass Burning Aerosol Particles, *Environ. Sci. Technol.*, 50, 11815–11824, <https://doi.org/10.1021/acs.est.6b03024>, 2016b.

Lippmann, M. and Chen, L.-C.: Health effects of concentrated ambient air particulate matter (CAPs) and its components, *Crit. Rev. Toxicol.*, 39, 865–913, <https://doi.org/10.3109/10408440903300080>, 2009.

Liu, Z. and Little, J. C.: 5 - Semivolatile organic compounds (SVOCs): phthalates and flame retardants, in: *Toxicity of Building Materials*, edited by: Pacheco-Torgal, F., Jalali, S., and Fucic, A., Woodhead Publishing, 122–137, <https://doi.org/10.1533/9780857096357.122>, 2012.

Logue, J. M., McKone, T. E., Sherman, M. H., and Singer, B. C.: Hazard assessment of chemical air contaminants measured in residences, *Indoor Air*, 21, 92–109, <https://doi.org/10.1111/j.1600-0668.2010.00683.x>, 2011.

Lopez-Hilfiker, F. D., Mohr, C., Ehn, M., Rubach, F., Kleist, E., Wildt, J., Mentel, T. F., Lutz, A., Hallquist, M., Worsnop, D., and Thornton, J. A.: A novel method for online analysis of gas and particle composition: description and evaluation of a Filter Inlet for Gases and AEROSols (FIGAERO), *Atmos. Meas. Tech.*, 7, 983–1001, <https://doi.org/10.5194/amt-7-983-2014>, 2014.

Loscos, N., Hernandez-Orte, P., Cacho, J., and Ferreira, V.: Release and Formation of Varietal Aroma Compounds during Alcoholic Fermentation from Nonfloral Grape Odorless Flavor Precursors Fractions, *J. Agric. Food Chem.*, 55, 6674–6684, <https://doi.org/10.1021/jf0702343>, 2007.

Lu, K., Fuchs, H., Hofzumahaus, A., Tan, Z., Wang, H., Zhang, L., Schmitt, S. H., Rohrer, F., Bohn, B., Broch, S., Dong, H., Gkatzelis, G. I., Hohaus, T., Holland, F., Li, X., Liu, Y., Liu, Y., Ma, X., Novelli, A., Schlag, P., Shao, M., Wu, Y., Wu, Z., Zeng, L., Hu, M., Kiendler-Scharr, A., Wahner, A., and Zhang, Y.: Fast Photochemistry in Wintertime Haze: Consequences for Pollution Mitigation Strategies, *Environ. Sci. Technol.*, 53, 10676–10684, <https://doi.org/10.1021/acs.est.9b02422>, 2019.

Luecken, D. J., Hutzell, W. T., Strum, M. L., and Pouliot, G. A.: Regional sources of atmospheric formaldehyde and acetaldehyde, and implications for atmospheric modeling, *Atmos. Environ.*, 47, 477–490, <https://doi.org/10.1016/j.atmosenv.2011.10.005>, 2012.

Lüttke, J., Scheer, V., Levsen, K., Wünsch, G., Neil Cape, J., Hargreaves, K. J., Storeton-West, R. L., Acker, K., Wieprecht, W., and Jones, B.: Occurrence and formation of nitrated phenols in and out of cloud, *Atmos. Environ.*, 31, 2637–2648, [https://doi.org/10.1016/S1352-2310\(96\)00229-4](https://doi.org/10.1016/S1352-2310(96)00229-4), 1997.

Lüttke, J., Levsen, K., Acker, K., Wieprecht, W., and Möller, D.: Phenols and Nitrated Phenols in Clouds at Mount Brocken, *Int. J. Environ. Anal. Chem.*, 74, 69–89, <https://doi.org/10.1080/03067319908031417>, 1999.

Manley, S. L., Goodwin, K., and North, W. J.: Laboratory production of bromoform, methylene bromide, and methyl iodide by macroalgae and distribution in nearshore southern California waters, *Limnol. Oceanogr.*, 37, 1652–1659, <https://doi.org/10.4319/lo.1992.37.8.1652>, 1992.

Mao, D., Weghe, H. V. D., Lookman, R., Vanermen, G., Brucker, N. D., and Diels, L.: Resolving the unresolved complex mixture in motor oils using high-performance liquid chromatography followed by comprehensive two-dimensional gas chromatography, *Fuel*, 88, 312–318, <https://doi.org/10.1016/j.fuel.2008.08.021>, 2009.

van Marle, M. J. E., Field, R. D., van der Werf, G. R., Estrada de Wagt, I. A., Houghton, R. A., Rizzo, L. V., Artaxo, P., and Tsigaridis, K.: Fire and deforestation dynamics in Amazonia (1973–2014), *Global Biogeochem. Cycles*, 31, 24–38, <https://doi.org/10.1002/2016GB005445>, 2017.

Martin, S. T., Artaxo, P., Machado, L. a. T., Manzi, A. O., Souza, R. a. F., Schumacher, C., Wang, J., Andreae, M. O., Barbosa, H. M. J., Fan, J., Fisch, G., Goldstein, A. H., Guenther, A., Jimenez, J. L., Pöschl, U., Silva Dias, M. A., Smith, J. N., and Wendisch, M.: Introduction: Observations and Modeling of the Green Ocean Amazon (GoAmazon2014/5), *Atmos. Chem. Phys.*, 16, 4785–4797, <https://doi.org/10.5194/acp-16-4785-2016>, 2016.

Martinez, R. E., Williams, B. J., Zhang, Y., Hagan, D., Walker, M., Kreisberg, N. M., Hering, S. V., Hohaus, T., Jayne, J. T., and Worsnop, D. R.: Development of a volatility and polarity separator (VAPS) for volatility- and polarity-resolved organic aerosol measurement, *Aerosol Sci. Technol.*, 50, 255–271, <https://doi.org/10.1080/02786826.2016.1147645>, 2016.

Masiol, M. and Harrison, R. M.: Aircraft engine exhaust emissions and other airport-related contributions to ambient air pollution: A review, *Atmos. Environ.*, 95, 409–455, <https://doi.org/10.1016/j.atmosenv.2014.05.070>, 2014.

Mason, S. A., Field, R. J., Yokelson, R. J., Kochivar, M. A., Tinsley, M. R., Ward, D. E., and Hao, W. M.: Complex effects arising in smoke plume simulations due to inclusion of direct emissions of oxygenated organic species from biomass combustion, *J. Geophys. Res. Atmos.*, 106, 12527–12539, <https://doi.org/10.1029/2001JD900003>, 2001.

McDonald, B. C., Gentner, D. R., Goldstein, A. H., and Harley, R. A.: Long-Term Trends in Motor Vehicle Emissions in U.S. Urban Areas, *Environ. Sci. Technol.*, 47, 10022–10031, <https://doi.org/10.1021/es401034z>, 2013.

McDonald, B. C., Gouw, J. A. de, Gilman, J. B., Jathar, S. H., Akherati, A., Cappa, C. D., Jimenez, J. L., Lee-Taylor, J., Hayes, P. L., McKeen, S. A., Cui, Y. Y., Kim, S.-W., Gentner, D. R., Isaacman-VanWertz, G., Goldstein, A. H., Harley, R. A., Frost, G. J., Roberts, J. M., Ryerson, T. B., and Trainer, M.: Volatile chemical products emerging as largest petrochemical source of urban organic emissions, *Science*, 359, 760–764, <https://doi.org/10.1126/science.aag0524>, 2018.

Medcraft, C. and Schnell, M.: A Comparative Study of Two Bicyclic Ethers, Eucalyptol and 1,4-Cineole, by Broadband Rotational Spectroscopy, *Z. Phys. Chem. (N F)*, 230, 1–14, <https://doi.org/10.1515/zpch-2015-0643>, 2016.

Meek, M. E., Giddings, M., and Gomes, R.: 1,2-Dichlorobenzene: Evaluation of risks to health from environmental exposure in Canada, *J. Environ. Sci. Health C*, 12, 269–275, <https://doi.org/10.1080/10590509409373445>, 1994.

Millet, D. B., Donahue, N. M., Pandis, S. N., Polidori, A., Stanier, C. O., Turpin, B. J., and Goldstein, A. H.: Atmospheric volatile organic compound measurements during the Pittsburgh Air Quality Study: Results, interpretation, and quantification of primary and secondary contributions, *Journal*

of Geophysical Research: Atmospheres, 110, D07S07, <https://doi.org/10.1029/2004JD004601>, 2005.

Mohr, C., DeCarlo, P. F., Heringa, M. F., Chirico, R., Slowik, J. G., Richter, R., Reche, C., Alastuey, A., Querol, X., Seco, R., Peñuelas, J., Jiménez, J. L., Crippa, M., Zimmermann, R., Baltensperger, U., and Prévôt, A. S. H.: Identification and quantification of organic aerosol from cooking and other sources in Barcelona using aerosol mass spectrometer data, *Atmos. Chem. Phys.*, 12, 1649–1665, <https://doi.org/10.5194/acp-12-1649-2012>, 2012.

Mohr, C., Lopez-Hilfiker, F. D., Zotter, P., Prévôt, A. S. H., Xu, L., Ng, N. L., Herndon, S. C., Williams, L. R., Franklin, J. P., Zahniser, M. S., Worsnop, D. R., Knighton, W. B., Aiken, A. C., Gorkowski, K. J., Dubey, M. K., Allan, J. D., and Thornton, J. A.: Contribution of Nitrated Phenols to Wood Burning Brown Carbon Light Absorption in Detling, United Kingdom during Winter Time, *Environ. Sci. Technol.*, 47, 6316–6324, <https://doi.org/10.1021/es400683v>, 2013.

Moise, T. and Rudich, Y.: Reactive Uptake of Ozone by Aerosol-Associated Unsaturated Fatty Acids: Kinetics, Mechanism, and Products, *J. Phys. Chem. A*, 106, 6469–6476, <https://doi.org/10.1021/jp025597e>, 2002.

Montemayor, B. P., Price, B. B., and van Egmond, R. A.: Accounting for intended use application in characterizing the contributions of cyclopentasiloxane (D5) to aquatic loadings following personal care product use: Antiperspirants, skin care products and hair care products, *Chemosphere*, 93, 735–740, <https://doi.org/10.1016/j.chemosphere.2012.10.043>, 2013.

Mudge, S. M., DeLeo, P. C., and Dyer, S. D.: Quantifying the anthropogenic fraction of fatty alcohols in a terrestrial environment, *Environ. Toxicol. Chem.*, 31, 1209–1222, <https://doi.org/10.1002/etc.1808>, 2012.

Murphy, D. M., Cziczo, D. J., Froyd, K. D., Hudson, P. K., Matthew, B. M., Middlebrook, A. M., Peltier, R. E., Sullivan, A., Thomson, D. S., and Weber, R. J.: Single-particle mass spectrometry of tropospheric aerosol particles, *J. Geophys. Res. Atmos.*, 111, <https://doi.org/10.1029/2006JD007340>, 2006.

Myhre, G., Shindell, D., Bréon, F.-M., Collins, W., Fuglestad, J., Huang, J., Koch, D., Lamarque, J.-F., Lee, D., Mendoza, B., Nakajima, T., Robock, A., Stephens, G., Zhang, H., Aamaas, B., Boucher, O., Dalsøren, S. B., Daniel, J. S., Forster, P., Granier, C., Haigh, J., Hodnebrog, Ø., Kaplan, J. O., Marston, G., Nielsen, C. J., O'Neill, B. C., Peters, G. P., Pongratz, J., Ramaswamy, V., Roth, R., Rotstayn, L., Smith, S. J., Stevenson, D., Vernier, J.-P., Wild, O., Young, P., Jacob, D., Ravishankara, A. R., and Shine, K.: Anthropogenic and Natural Radiative Forcing. In: *Climate Change 2013: The Physical Science Basis. Contribution of Working Group I to the Fifth Assessment Report of the Intergovernmental Panel on Climate Change* [Stocker, T.F., D. Qin, G.-K. Plattner, M. Tignor, S. K. Allen, J. Boschung, A. Nauels, Y. Xia, V. Bex and P. M. Midgley (eds.)], Cambridge University Press, Cambridge, United Kingdom and New York, NY, USA, 82, 2013.

NIST Standard Reference Database 1A: <https://www.nist.gov/srd/nist-standard-reference-database-1a>, last access: 19 April 2022.

National Research Council: Rethinking the Ozone Problem in Urban and Regional Air Pollution, National Academies Press, 525 pp., 1992.

Navea, J. G., Young, M. A., Xu, S., Grassian, V. H., and Stanier, C. O.: The atmospheric lifetimes and concentrations of cyclic methylsiloxanes octamethylcyclotetrasiloxane (D4) and decamethylcyclopentasiloxane (D5) and the influence of heterogeneous uptake, *Atmos. Environ.*, 45, 3181–3191, <https://doi.org/10.1016/j.atmosenv.2011.02.038>, 2011.

Nel, A.: Air Pollution-Related Illness: Effects of Particles, *Science*, 308, 804–806, <https://doi.org/10.1126/science.1108752>, 2005.

Ng, N. L., Chhabra, P. S., Chan, A. W. H., Surratt, J. D., Kroll, J. H., Kwan, A. J., McCabe, D. C., Wennberg, P. O., Sorooshian, A., Murphy, S. M., Dalleska, N. F., Flagan, R. C., and Seinfeld, J. H.: Effect of NO_x level on secondary organic aerosol (SOA) formation from the photooxidation of terpenes, *Atmos. Chem. Phys.*, 16, 2007.

del Nogal Sánchez, M., Pérez-Pavón, J. L., and Moreno Cordero, B.: Determination of suspected allergens in cosmetic products by headspace-programmed temperature vaporization–fast gas chromatography–quadrupole mass spectrometry, *Anal. Bioanal. Chem.*, 397, 2579–2591, <https://doi.org/10.1007/s00216-010-3803-8>, 2010.

Nojima, K., Kawaguchi, A., Ohya, T., Kanno, S., and Hirobe, M.: Studies on Photochemical Reaction of Air Pollutants. X. Identification of Nitrophenols in Suspended Particulates, *Chem. Pharm. Bull.*, 31, 1047–1051, <https://doi.org/10.1248/cpb.31.1047>, 1983.

Nolte, C. G., Schauer, J. J., Cass, G. R., and Simoneit, B. R. T.: Highly Polar Organic Compounds Present in Meat Smoke, *Environ. Sci. Technol.*, 33, 3313–3316, <https://doi.org/10.1021/es990122v>, 1999.

Nolte, C. G., Schauer, J. J., Cass, G. R., and Simoneit, B. R. T.: Highly Polar Organic Compounds Present in Wood Smoke and in the Ambient Atmosphere, *Environ. Sci. Technol.*, 35, 1912–1919, <https://doi.org/10.1021/es001420r>, 2001a.

Nolte, C. G., Schauer, J. J., Cass, G. R., and Simoneit, B. R. T.: Highly Polar Organic Compounds Present in Wood Smoke and in the Ambient Atmosphere, *Environ. Sci. Technol.*, 35, 1912–1919, <https://doi.org/10.1021/es001420r>, 2001b.

Nolte, C. G., Schauer, J. J., Cass, G. R., and Simoneit, B. R. T.: Trimethylsilyl Derivatives of Organic Compounds in Source Samples and in Atmospheric Fine Particulate Matter, *Environ. Sci. Technol.*, 36, 4273–4281, <https://doi.org/10.1021/es020518y>, 2002.

Norris, G., Duvall, R., Brown, S., and Bai, S.: Positive Matrix Factorization (PMF) 5.0 Fundamentals and User Guide, U.S. Environmental Protection Agency, 2014.

Nurmatov, U. B., Tagieva, N., Semple, S., Devereux, G., and Sheikh, A.: Volatile organic compounds and risk of asthma and allergy: a systematic review and meta-analysis of observational and interventional studies, *Prim. Care Respir. J.*, 22, S9–S15, <https://doi.org/10.4104/pcrj.2013.00010>, 2013.

de Oliveira Alves, N., Brito, J., Caumo, S., Arana, A., de Souza Hacon, S., Artaxo, P., Hillamo, R., Teinilä, K., Batistuzzo de Medeiros, S. R., and de Castro Vasconcellos, P.: Biomass burning in the Amazon region: Aerosol source apportionment and associated health risk assessment, *Atmos. Environ.*, 120, 277–285, <https://doi.org/10.1016/j.atmosenv.2015.08.059>, 2015.

Oros, D. R. and Simoneit, B. R. T.: Identification and emission factors of molecular tracers in organic aerosols from biomass burning Part 1. Temperate climate conifers, *Appl. Geochemistry*, 32, [https://doi.org/10.1016/S0883-2927\(01\)00021-X](https://doi.org/10.1016/S0883-2927(01)00021-X), 2001a.

Oros, D. R. and Simoneit, B. R. T.: Identification and emission factors of molecular tracers in organic aerosols from biomass burning Part 2. Deciduous trees, *Appl. Geochemistry*, 21, [https://doi.org/10.1016/S0883-2927\(01\)00022-1](https://doi.org/10.1016/S0883-2927(01)00022-1), 2001b.

Oros, D. R., Abas, M. R. bin, Omar, N. Y. M. J., Rahman, N. A., and Simoneit, B. R. T.: Identification and emission factors of molecular tracers in organic aerosols from biomass burning: Part 3. Grasses, *Appl. Geochemistry*, 21, 919–940, <https://doi.org/10.1016/j.apgeochem.2006.01.008>, 2006.

Paatero, P. and Hopke, P. K.: Rotational tools for factor analytic models, *J. Chemom.*, 23, 91–100, <https://doi.org/10.1002/cem.1197>, 2009.

Paatero, P. and Tapper, U.: Positive matrix factorization: A non-negative factor model with optimal utilization of error estimates of data values, *Environmetrics*, 5, 111–126, <https://doi.org/10.1002/env.3170050203>, 1994.

Palmer, P. I., Abbot, D. S., Fu, T.-M., Jacob, D. J., Chance, K., Kurosu, T. P., Guenther, A., Wiedinmyer, C., Stanton, J. C., Pilling, M. J., Pressley, S. N., Lamb, B., and Sumner, A. L.: Quantifying the seasonal and interannual variability of North American isoprene emissions using satellite observations of the formaldehyde column, *J. Geophys. Res. Atmos.*, 111, <https://doi.org/10.1029/2005JD006689>, 2006.

Pollmann, J., Ortega, J., and Helmig, D.: Analysis of Atmospheric Sesquiterpenes: Sampling Losses and Mitigation of Ozone Interferences, *Environ. Sci. Technol.*, 39, 9620–9629, <https://doi.org/10.1021/es050440w>, 2005a.

Pollmann, J., Ortega, J., and Helmig, D.: Analysis of Atmospheric Sesquiterpenes: Sampling Losses and Mitigation of Ozone Interferences, *Environ. Sci. Technol.*, 39, 9620–9629, <https://doi.org/10.1021/es050440w>, 2005b.

Pope, C. A. and Dockery, D. W.: Health Effects of Fine Particulate Air Pollution: Lines that Connect, *J. Air Waste Manag. Assoc.*, 56, 709–742, <https://doi.org/10.1080/10473289.2006.10464485>, 2006.

Presto, A. A., Miracolo, M. A., Donahue, N. M., and Robinson, A. L.: Secondary Organic Aerosol Formation from High-NO_x Photo-Oxidation of Low Volatility Precursors: n-Alkanes, *Environ. Sci. Technol.*, 44, 2029–2034, <https://doi.org/10.1021/es903712r>, 2010.

Hazardous Substances Data Bank: <https://pubchem.ncbi.nlm.nih.gov/source/hsdb>, last access: 16 March 2022.

2-Cyclopenten-1-one: <https://pubchem.ncbi.nlm.nih.gov/compound/13588>, last access: 12 April 2022.

Ravindra, K., Sokhi, R., and Van Grieken, R.: Atmospheric polycyclic aromatic hydrocarbons: Source attribution, emission factors and regulation, *Atmos. Environ.*, 42, 2895–2921, <https://doi.org/10.1016/j.atmosenv.2007.12.010>, 2008.

Reimann, S., Calanca, P., and Hofer, P.: The anthropogenic contribution to isoprene concentrations in a rural atmosphere, *Atmos. Environ.*, 34, 109–115, [https://doi.org/10.1016/S1352-2310\(99\)00285-X](https://doi.org/10.1016/S1352-2310(99)00285-X), 2000.

Reissell, A., Arey, J., and Atkinson, R.: Atmospheric Chemistry of Camphor, *Int. J. Chem. Kinet.*, 33, 56–63, [https://doi.org/10.1002/1097-4601\(20010101\)33:1<56::AID-KIN7>3.0.CO;2-Y](https://doi.org/10.1002/1097-4601(20010101)33:1<56::AID-KIN7>3.0.CO;2-Y), 2001.

Ren, H., Xue, M., An, Z., Zhou, W., and Jiang, J.: Quartz filter-based thermal desorption gas chromatography mass spectrometry for in-situ molecular level measurement of ambient organic aerosols, *J. Chromatogr. A*, 1589, 141–148, <https://doi.org/10.1016/j.chroma.2019.01.010>, 2019.

Ren, Y., McGillen, M. R., Daële, V., Casas, J., and Mellouki, A.: The fate of methyl salicylate in the environment and its role as signal in multitrophic interactions, *Sci. Total Environ.*, 749, 141406, <https://doi.org/10.1016/j.scitotenv.2020.141406>, 2020.

Richardson, S. D., DeMarini, D. M., Kogevinas, M., Fernandez, P., Marco, E., Lourencetti, C., Ballest, é C., Heederik, D., Meliefste, K., McKague, A. B., Marcos, R., Font, -Ribera Laia, Grimalt, J. O., and Villanueva, C. M.: What's in the Pool? A Comprehensive Identification of Disinfection By-products and Assessment of Mutagenicity of Chlorinated and Brominated Swimming Pool Water, *Environ. Health Perspect.*, 118, 1523–1530, <https://doi.org/10.1289/ehp.1001965>, 2010.

Ridley, D. A., Heald, C. L., Ridley, K. J., and Kroll, J. H.: Causes and consequences of decreasing atmospheric organic aerosol in the United States, *Proc. Natl. Acad. Sci. U.S.A.*, 115, 290–295, <https://doi.org/10.1073/pnas.1700387115>, 2018.

Righi, E., Fantuzzi, G., Predieri, G., and Aggazzotti, G.: Bromate, chlorite, chlorate, haloacetic acids, and trihalomethanes occurrence in indoor swimming pool waters in Italy, *Microchem. J.*, 113, 23–29, <https://doi.org/10.1016/j.microc.2013.11.007>, 2014.

Rissler, J., Vestin, A., Swietlicki, E., Fisch, G., Zhou, J., Artaxo, P., and Andreae, M. O.: Size distribution and hygroscopic properties of aerosol particles from dry-season biomass burning in Amazonia, *Atmos. Chem. Phys.*, 6, 471–491, <https://doi.org/10.5194/acp-6-471-2006>, 2006.

Robinson, A. L., Subramanian, R., Donahue, N. M., Bernardo-Bricker, A., and Rogge, W. F.: Source Apportionment of Molecular Markers and Organic Aerosol. 3. Food Cooking Emissions, *Environ. Sci. Technol.*, 40, 7820–7827, <https://doi.org/10.1021/es060781p>, 2006.

Robinson, A. L., Donahue, N. M., Shrivastava, M. K., Weitkamp, E. A., Sage, A. M., Grieshop, A. P., Lane, T. E., Pierce, J. R., and Pandis, S. N.: Rethinking Organic Aerosols: Semivolatile Emissions and Photochemical Aging, *Science*, 315, 1259–1262, <https://doi.org/10.1126/science.1133061>, 2007a.

Robinson, A. L., Donahue, N. M., Shrivastava, M. K., Weitkamp, E. A., Sage, A. M., Grieshop, A. P., Lane, T. E., Pierce, J. R., and Pandis, S. N.: Rethinking Organic Aerosols: Semivolatile Emissions and Photochemical Aging, *Science*, 315, 1259–1262, 2007b.

Rogge, W. F., Hildemann, L. M., Mazurek, M. A., Cass, G. R., and Simoneit, B. R. T.: Sources of fine organic aerosol. 1. Charbroilers and meat cooking operations, *Environ. Sci. Technol.*, 25, 1112–1125, <https://doi.org/10.1021/es00018a015>, 1991.

Rogge, W. F., Hildemann, L. M., Mazurek, M. A., Cass, G. R., and Simoneit, B. R. T.: Sources of fine organic aerosol. 2. Noncatalyst and catalyst-equipped automobiles and heavy-duty diesel trucks, *Environ. Sci. Technol.*, 27, 636–651, <https://doi.org/10.1021/es00041a007>, 1993a.

Rogge, W. F., Hildemann, L. M., Mazurek, M. A., Cass, G. R., and Simoneit, B. R. T.: Sources of fine organic aerosol. 4. Particulate abrasion products from leaf surfaces of urban plants, *Environ. Sci. Technol.*, 27, 2700–2711, <https://doi.org/10.1021/es00049a008>, 1993b.

Rogge, W. F., Hildemann, L. M., Mazurek, M. A., Cass, G. R., and Simoneit, B. R. T.: Mathematical modeling of atmospheric fine particle-associated primary organic compound concentrations, *J. Geophys. Res. Atmos.*, 101, 19379–19394, <https://doi.org/10.1029/95JD02050>, 1996.

Rogge, W. F., Hildemann, L. M., Mazurek, M. A., Cass, G. R., and Simoneit, B. R. T.: Sources of Fine Organic Aerosol. 7. Hot Asphalt Roofing Tar Pot Fumes, *Environ. Sci. Technol.*, 31, 2726–2730, <https://doi.org/10.1021/es960525k>, 1997.

Rogge, W. F., Hildemann, L. M., Mazurek, M. A., and Cass, G. R.: Sources of Fine Organic Aerosol. 9. Pine, Oak, and Synthetic Log Combustion in Residential Fireplaces, *Environ. Sci. Technol.*, 32, 13–22, <https://doi.org/10.1021/es960930b>, 1998.

Roman, C., Arsene, C., Bejan, I. G., and Olariu, R. I.: Investigations into the gas-phase photolysis and OH radical kinetics of nitrocatechols: implications of intramolecular interactions on their atmospheric behaviour, *Atmos. Chem. Phys.*, 22, 2203–2219, <https://doi.org/10.5194/acp-22-2203-2022>, 2022.

de Sá, S. S., Palm, B. B., Campuzano-Jost, P., Day, D. A., Newburn, M. K., Hu, W., Isaacman-VanWertz, G., Yee, L. D., Thalman, R., Brito, J., Carbone, S., Artaxo, P., Goldstein, A. H., Manzi, A. O., Souza, R. A. F., Mei, F., Shilling, J. E., Springston, S. R., Wang, J., Surratt, J. D., Alexander, M. L., Jimenez, J. L., and Martin, S. T.: Influence of urban pollution on the production of organic particulate matter from isoprene epoxydiols in central Amazonia, *Atmos. Chem. Phys.*, **17**, 6611–6629, <https://doi.org/10.5194/acp-17-6611-2017>, 2017.

de Sá, S. S., Palm, B. B., Campuzano-Jost, P., Day, D. A., Hu, W., Isaacman-VanWertz, G., Yee, L. D., Brito, J., Carbone, S., Ribeiro, I. O., Cirino, G. G., Liu, Y., Thalman, R., Sedlacek, A., Funk, A., Schumacher, C., Shilling, J. E., Schneider, J., Artaxo, P., Goldstein, A. H., Souza, R. A. F., Wang, J., McKinney, K. A., Barbosa, H., Alexander, M. L., Jimenez, J. L., and Martin, S. T.: Urban influence on the concentration and composition of submicron particulate matter in central Amazonia, *Atmos. Chem. Phys.*, **18**, 12185–12206, <https://doi.org/10.5194/acp-18-12185-2018>, 2018.

de Sá, S. S., Rizzo, L. V., Palm, B. B., Campuzano-Jost, P., Day, D. A., Yee, L. D., Wernis, R., Isaacman-VanWertz, G., Brito, J., Carbone, S., Liu, Y. J., Sedlacek, A., Springston, S., Goldstein, A. H., Barbosa, H. M. J., Alexander, M. L., Artaxo, P., Jimenez, J. L., and Martin, S. T.: Contributions of biomass-burning, urban, and biogenic emissions to the concentrations and light-absorbing properties of particulate matter in central Amazonia during the dry season, *Atmos. Chem. Phys.*, **19**, 7973–8001, <https://doi.org/10.5194/acp-19-7973-2019>, 2019.

Salvador, C. M. G., Tang, R., Priestley, M., Li, L., Tsiligiannis, E., Le Breton, M., Zhu, W., Zeng, L., Wang, H., Yu, Y., Hu, M., Guo, S., and Hallquist, M.: Ambient nitro-aromatic compounds – biomass burning versus secondary formation in rural China, *Atmos. Chem. Phys.*, **21**, 1389–1406, <https://doi.org/10.5194/acp-21-1389-2021>, 2021.

Samimi, B.: Exposure to isophorone and other organic solvents in a screen printing plant, *American Industrial Hygiene Association Journal*, **43**, 43–48, <https://doi.org/10.1080/15298668291409343>, 1982.

Sander, R.: Compilation of Henry's law constants (version 4.0) for water as solvent, *Atmos. Chem. Phys.*, **15**, 4399–4981, <https://doi.org/10.5194/acp-15-4399-2015>, 2015.

Sangwan, M. and Zhu, L.: Role of Methyl-2-nitrophenol Photolysis as a Potential Source of OH Radicals in the Polluted Atmosphere: Implications from Laboratory Investigation, *J. Phys. Chem. A*, **122**, 1861–1872, <https://doi.org/10.1021/acs.jpca.7b11235>, 2018.

Sasaki, K., Tagata, H., Kawakami, H., Nagasaki, T., Nemoto, S., and Maitani, T.: Determination of Isophorone in Foods, *J. Food Hyg. Soc. Jpn*, **46**, 28–32, <https://doi.org/10.3358/shokueishi.46.28>, 2005.

Schauer, J. J., Rogge, W. F., Hildemann, L. M., Mazurek, M. A., Cass, G. R., and Simoneit, B. R. T.: Source apportionment of airborne particulate matter using organic compounds as tracers, *Atmos. Environ.*, **30**, 3837–3855, [https://doi.org/10.1016/1352-2310\(96\)00085-4](https://doi.org/10.1016/1352-2310(96)00085-4), 1996.

Schauer, J. J., Kleeman, M. J., Cass, G. R., and Simoneit, B. R. T.: Measurement of Emissions from Air Pollution Sources. 1. C1 through C29 Organic Compounds from Meat Charbroiling, *Environ. Sci. Technol.*, 33, 1566–1577, <https://doi.org/10.1021/es980076j>, 1999a.

Schauer, J. J., Kleeman, M. J., Cass, G. R., and Simoneit, B. R. T.: Measurement of Emissions from Air Pollution Sources. 2. C1 through C30 Organic Compounds from Medium Duty Diesel Trucks, *Environ. Sci. Technol.*, 33, 1578–1587, <https://doi.org/10.1021/es980081n>, 1999b.

Schauer, J. J., Kleeman, M. J., Cass, G. R., and Simoneit, B. R. T.: Measurement of Emissions from Air Pollution Sources. 3. C1–C29 Organic Compounds from Fireplace Combustion of Wood, *Environ. Sci. Technol.*, 35, 1716–1728, <https://doi.org/10.1021/es001331e>, 2001.

Schauer, J. J., Kleeman, M. J., Cass, G. R., and Simoneit, B. R. T.: Measurement of Emissions from Air Pollution Sources. 4. C1–C27 Organic Compounds from Cooking with Seed Oils, *Environ. Sci. Technol.*, 36, 567–575, <https://doi.org/10.1021/es002053m>, 2002a.

Schauer, J. J., Kleeman, M. J., Cass, G. R., and Simoneit, B. R. T.: Measurement of Emissions from Air Pollution Sources. 5. C1–C32 Organic Compounds from Gasoline-Powered Motor Vehicles, *Environ. Sci. Technol.*, 36, 1169–1180, <https://doi.org/10.1021/es0108077>, 2002b.

Schkolnik, G., Falkovich, A. H., Rudich, Y., Maenhaut, W., and Artaxo, P.: New Analytical Method for the Determination of Levoglucosan, Polyhydroxy Compounds, and 2-Methylerythritol and Its Application to Smoke and Rainwater Samples, *Environ. Sci. Technol.*, 39, 2744–2752, <https://doi.org/10.1021/es048363c>, 2005.

Definition of Breakthrough Volumes: <https://www.sisweb.com/index/referenc/resin3.htm>, last access: 29 September 2020.

Tenax® TA Breakthrough Volume Data: <https://www.sisweb.com/index/referenc/tenaxta.htm>, last access: 20 March 2020.

Seinfeld, J. H. and Pankow, J. F.: Organic Atmospheric Particulate Material, *Annu. Rev. Phys. Chem.*, 54, 121–140, <https://doi.org/10.1146/annurev.physchem.54.011002.103756>, 2003.

Shi, S., Cao, J., Zhang, Y., and Zhao, B.: Emissions of Phthalates from Indoor Flat Materials in Chinese Residences, *Environ. Sci. Technol.*, 52, 13166–13173, <https://doi.org/10.1021/acs.est.8b03580>, 2018.

Shrivastava, M., Cappa, C. D., Fan, J., Goldstein, A. H., Guenther, A. B., Jimenez, J. L., Kuang, C., Laskin, A., Martin, S. T., Ng, N. L., Petaja, T., Pierce, J. R., Rasch, P. J., Roldin, P., Seinfeld, J. H., Shilling, J., Smith, J. N., Thornton, J. A., Volkamer, R., Wang, J., Worsnop, D. R., Zaveri, R. A., Zelenyuk, A., and Zhang, Q.: Recent advances in understanding secondary organic aerosol: Implications for global climate forcing, *Rev. Geophys.*, 55, 509–559, <https://doi.org/10.1002/2016RG000540>, 2017.

Shumway, L. A.: Trace Element and Polycyclic Aromatic Hydrocarbon Analyses of Jet Engine Fuels: Jet A, JP5, and JP8, SPAWAR Systems Center, San Diego, CA, <https://doi.org/10.21236/ADA390641>, 2000.

Simoneit, B. R. T.: Organic matter of the troposphere — V: Application of molecular marker analysis to biogenic emissions into the troposphere for source reconciliations, *J. Atmos. Chem.*, 8, 251–275, <https://doi.org/10.1007/BF00051497>, 1989.

Simoneit, B. R. T.: A review of biomarker compounds as source indicators and tracers for air pollution, *Environ. Sci. & Pollut. Res.*, 6, 159–169, <https://doi.org/10.1007/BF02987621>, 1999.

Simoneit, B. R. T.: Biomass burning — a review of organic tracers for smoke from incomplete combustion, *Appl. Geochemistry*, 17, 129–162, [https://doi.org/10.1016/S0883-2927\(01\)00061-0](https://doi.org/10.1016/S0883-2927(01)00061-0), 2002.

Simoneit, B. R. T.: Atmospheric Transport of Terrestrial Organic Matter to the Sea, in: *Marine Organic Matter: Biomarkers, Isotopes and DNA*, edited by: Volkman, J. K., Springer, Berlin, Heidelberg, 165–208, https://doi.org/10.1007/698_2_006, 2006.

Simoneit, B. R. T. and Mazurek, M. A.: Organic matter of the troposphere—II.**For Part I, see Simoneit et al. (1977). Natural background of biogenic lipid matter in aerosols over the rural western united states, *Atmos. Environ.*, 16, 2139–2159, [https://doi.org/10.1016/0004-6981\(82\)90284-0](https://doi.org/10.1016/0004-6981(82)90284-0), 1982.

Simoneit, B. R. T., Rogge, W. F., Mazurek, M. A., Standley, L. J., Hildemann, L. M., and Cass, G. R.: Lignin pyrolysis products, lignans, and resin acids as specific tracers of plant classes in emissions from biomass combustion, *Environ. Sci. Technol.*, 27, 2533–2541, <https://doi.org/10.1021/es00048a034>, 1993.

Simoneit, B. R. T., Schauer, J. J., Nolte, C. G., Oros, D. R., Elias, V. O., Fraser, M. P., Rogge, W. F., and Cass, G. R.: Levoglucosan, a tracer for cellulose in biomass burning and atmospheric particles, *Atmos. Environ.*, 33, 173–182, [https://doi.org/10.1016/S1352-2310\(98\)00145-9](https://doi.org/10.1016/S1352-2310(98)00145-9), 1999.

Srivastava, A., Joseph, A. E., Patil, S., More, A., Dixit, R. C., and M. Prakash: Air toxics in ambient air of Delhi, *Atmos. Environ.*, 39, 59–71, <https://doi.org/10.1016/j.atmosenv.2004.09.053>, 2005.

Steinbacher, M., Dommen, J., Ordonez, C., Reimann, S., Gruebler, F. C., Staehelin, J., Andreani-Aksoyoglu, S., and Prevot, A. S. H.: Volatile Organic Compounds in the Po Basin. Part B: Biogenic VOCs, *J. Atmos. Chem.*, 51, 293–315, <https://doi.org/10.1007/s10874-005-3577-0>, 2005.

Steinemann, A.: Volatile emissions from common consumer products, *Air. Qual. Atmos. Health*, 8, 273–281, <https://doi.org/10.1007/s11869-015-0327-6>, 2015.

Steinemann, A. C., MacGregor, I. C., Gordon, S. M., Gallagher, L. G., Davis, A. L., Ribeiro, D. S., and Wallace, L. A.: Fragranced consumer products: Chemicals emitted, ingredients unlisted, *Environ. Impact Assess. Rev.*, 31, 328–333, <https://doi.org/10.1016/j.eiar.2010.08.002>, 2011.

Stockwell, C. E., Coggon, M. M., Gkatzelis, G. I., Ortega, J., McDonald, B. C., Peischl, J., Aikin, K., Gilman, J. B., Trainer, M., and Warneke, C.: Volatile organic compound emissions from solvent- and water-borne coatings – compositional differences and tracer compound identifications, *Atmos. Chem. Phys.*, 21, 6005–6022, <https://doi.org/10.5194/acp-21-6005-2021>, 2021.

Sturges, W. T., Cota, G. F., and Buckley, P. T.: Bromoform emission from Arctic ice algae, *Nature*, 358, 660–662, <https://doi.org/10.1038/358660a0>, 1992.

Su, H.-J., Chao, C.-J., Chang, H.-Y., and Wu, P.-C.: The effects of evaporating essential oils on indoor air quality, *Atmos. Environ.*, 41, 1230–1236, <https://doi.org/10.1016/j.atmosenv.2006.09.044>, 2007.

Suciu, L. G., Masiello, C. A., and Griffin, R. J.: Anhydrosugars as tracers in the Earth system, *Biogeochemistry*, 146, 209–256, <https://doi.org/10.1007/s10533-019-00622-0>, 2019.

Suh, I., Zhang, R., Molina, L. T., and Molina, M. J.: Oxidation Mechanism of Aromatic Peroxy and Bicyclic Radicals from OH-Toluene Reactions, *J. Am. Chem. Soc.*, 125, 12655–12665, <https://doi.org/10.1021/ja0350280>, 2003.

Sun, Y., Liu, L., Li, M., Chen, X., and Xu, F.: Theoretical investigation on the mechanisms and kinetics of OH/NO₃-initiated atmospheric oxidation of vanillin and vanillic acid, *Chemosphere*, 288, 132544, <https://doi.org/10.1016/j.chemosphere.2021.132544>, 2022.

Tang, X., Misztal, P. K., Nazaroff, W. W., and Goldstein, A. H.: Siloxanes Are the Most Abundant Volatile Organic Compound Emitted from Engineering Students in a Classroom, *Environ. Sci. Technol. Lett.*, 2, 303–307, <https://doi.org/10.1021/acs.estlett.5b00256>, 2015.

Tremp, J., Mattrel, P., Fingler, S., and Giger, W.: Phenols and nitrophenols as tropospheric pollutants: Emissions from automobile exhausts and phase transfer in the atmosphere, *Water Air Soil Pollut.*, 68, 113–123, <https://doi.org/10.1007/BF00479396>, 1993.

Turpin, B. J., Saxena, P., and Andrews, E.: Measuring and simulating particulate organics in the atmosphere: problems and prospects, *Atmos. Environ.*, 34, 2983–3013, [https://doi.org/10.1016/S1352-2310\(99\)00501-4](https://doi.org/10.1016/S1352-2310(99)00501-4), 2000.

Ulbrich, I. M., Canagaratna, M. R., Zhang, Q., Worsnop, D. R., and Jimenez, J. L.: Interpretation of organic components from Positive Matrix Factorization of aerosol mass spectrometric data, *Atmos. Chem. Phys.*, 9, 2891–2918, <https://doi.org/10.5194/acp-9-2891-2009>, 2009.

U.S. EPA (Environmental Protection Agency) Comptox Chemicals Dashboard: 2-Methoxynaphthalene: <https://comptox.epa.gov/dashboard/chemical/details/DTXSID7044392>, last access: 12 April 2022.

U.S. EPA (Environmental Protection Agency) Comptox Chemicals Dashboard: 2-Nitrophenol: <https://comptox.epa.gov/dashboard/chemical/details/DTXSID1021790>, last access: 5 April 2022.

U.S. EPA (Environmental Protection Agency) Comptox Chemicals Dashboard: 4-Hydroxybenzoic Acid: <https://comptox.epa.gov/dashboard/chemical/details/DTXSID3026647>, last access: 12 April 2022.

U.S. EPA (Environmental Protection Agency) Comptox Chemicals Dashboard: 4-Nitrophenol: <https://comptox.epa.gov/dashboard/chemical/details/DTXSID0021834>, last access: 5 April 2022.

U.S. EPA (Environmental Protection Agency) Comptox Chemicals Dashboard: Benzophenone: <https://comptox.epa.gov/dashboard/chemical/details/DTXSID0021961>, last access: 28 March 2022.

U.S. EPA (Environmental Protection Agency) Comptox Chemicals Dashboard: p-Anisic Acid: <https://comptox.epa.gov/dashboard/chemical/details/DTXSID4059205>, last access: 14 April 2022.

U.S. EPA (Environmental Protection Agency) Comptox Chemicals Dashboard: Phthalimide: <https://comptox.epa.gov/dashboard/chemical/details/DTXSID3026514>, last access: 12 April 2022.

Vione, D., Maurino, V., Minero, C., Duncianu, M., Olariu, R.-I., Arsene, C., Sarakha, M., and Mailhot, G.: Assessing the transformation kinetics of 2- and 4-nitrophenol in the atmospheric aqueous phase. Implications for the distribution of both nitroisomers in the atmosphere, *Atmos. Environ.*, 43, 2321–2327, <https://doi.org/10.1016/j.atmosenv.2009.01.025>, 2009.

Wang, H., Gao, Y., Wang, S., Wu, X., Liu, Y., Li, X., Huang, D., Lou, S., Wu, Z., Guo, S., Jing, S., Li, Y., Huang, C., Tyndall, G. S., Orlando, J. J., and Zhang, X.: Atmospheric Processing of Nitrophenols and Nitrocresols From Biomass Burning Emissions, *J. Geophys. Res. Atmos.*, 125, e2020JD033401, <https://doi.org/10.1029/2020JD033401>, 2020.

Wang, L., Atkinson, R., and Arey, J.: Dicarbonyl Products of the OH Radical-Initiated Reactions of Naphthalene and the C1- and C2-Alkyl naphthalenes, *Environ. Sci. Technol.*, 41, 2803–2810, <https://doi.org/10.1021/es0628102>, 2007.

Wang, L., Wang, X., Gu, R., Wang, H., Yao, L., Wen, L., Zhu, F., Wang, W., Xue, L., Yang, L., Lu, K., Chen, J., Wang, T., Zhang, Y., and Wang, W.: Observations of fine particulate nitrated phenols in four sites in northern China: concentrations, source apportionment, and secondary formation, *Atmos. Chem. Phys.*, 18, 4349–4359, <https://doi.org/10.5194/acp-18-4349-2018>, 2018.

Wang, Q., Huang, X. H. H., Tam, F. C. V., Zhang, X., Liu, K. M., Yeung, C., Feng, Y., Cheng, Y. Y., Wong, Y. K., Ng, W. M., Wu, C., Zhang, Q., Zhang, T., Lau, N. T., Yuan, Z., Lau, A. K. H., and Yu, J. Z.: Source apportionment of fine particulate matter in Macao, China with and without organic tracers: A comparative study using positive matrix factorization, *Atmos. Environ.*, 198, 183–193, <https://doi.org/10.1016/j.atmosenv.2018.10.057>, 2019a.

Wang, R., Moody, R., Koniecki, D., and Zhu, J.: Low molecular weight cyclic volatile methylsiloxanes in cosmetic products sold in Canada: implication for dermal exposure., *Environ Int*, 35, 900–904, <https://doi.org/10.1016/j.envint.2009.03.009>, 2009.

Wang, X., Gu, R., Wang, L., Xu, W., Zhang, Y., Chen, B., Li, W., Xue, L., Chen, J., and Wang, W.: Emissions of fine particulate nitrated phenols from the burning of five common types of biomass, *Environ. Pollut.*, 230, 405–412, <https://doi.org/10.1016/j.envpol.2017.06.072>, 2017.

Wang, Y., Hu, M., Wang, Y., Zheng, J., Shang, D., Yang, Y., Liu, Y., Li, X., Tang, R., Zhu, W., Du, Z., Wu, Y., Guo, S., Wu, Z., Lou, S., Hallquist, M., and Yu, J. Z.: The formation of nitro-aromatic compounds under high NO_x and anthropogenic VOC conditions in urban Beijing, China, *Atmos. Chem. Phys.*, 19, 7649–7665, <https://doi.org/10.5194/acp-19-7649-2019>, 2019b.

Warneke, C., de Gouw, J. A., Holloway, J. S., Peischl, J., Ryerson, T. B., Atlas, E., Blake, D., Trainer, M., and Parrish, D. D.: Multiyear trends in volatile organic compounds in Los Angeles, California: Five decades of decreasing emissions, *J. Geophys. Res. Atmos.*, 117, <https://doi.org/10.1029/2012JD017899>, 2012.

Weitkamp, E. A., Sage, A. M., Pierce, J. R., Donahue, N. M., and Robinson, A. L.: Organic Aerosol Formation from Photochemical Oxidation of Diesel Exhaust in a Smog Chamber, *Environ. Sci. Technol.*, 41, 6969–6975, <https://doi.org/10.1021/es070193r>, 2007.

Westerling, A. L.: Increasing western US forest wildfire activity: sensitivity to changes in the timing of spring, *Phil. Trans. R. Soc. B*, 371, 20150178, <https://doi.org/10.1098/rstb.2015.0178>, 2016.

Westerlund, J., Bryngelsson, I.-L., Löfstedt, H., Eriksson, K., Westberg, H., and Graff, P.: Occupational exposure to trichloramine and trihalomethanes: adverse health effects among personnel in habilitation and rehabilitation swimming pools, *J. Occup. Environ. Hyg.*, 16, 78–88, <https://doi.org/10.1080/15459624.2018.1536825>, 2019.

Williams, B. J., Goldstein, A. H., Kreisberg, N. M., and Hering, S. V.: An In-Situ Instrument for Speciated Organic Composition of Atmospheric Aerosols: Thermal Desorption Aerosol GC/MS-FID (TAG), *Aerosol Sci. Technol.*, 40, 627–638, <https://doi.org/10.1080/02786820600754631>, 2006.

Williams, B. J., Goldstein, A. H., Kreisberg, N. M., Hering, S. V., Worsnop, D. R., Ulbrich, I. M., Docherty, K. S., and Jimenez, J. L.: Major components of atmospheric organic aerosol in southern California as determined by hourly measurements of source marker compounds, *Atmos. Chem. Phys.*, 10, 11577–11603, <https://doi.org/10.5194/acp-10-11577-2010>, 2010.

World Meteorological Organization, United States, National Oceanic and Atmospheric Administration, United States, National Aeronautics and Space Administration, United Nations Environment Programme, and European Commission: Scientific assessment of ozone depletion: 2018., 2019.

Yao, D., Lyu, X., Lu, H., Zeng, L., Liu, T., Chan, C. K., and Guo, H.: Characteristics, sources and evolution processes of atmospheric organic aerosols at a roadside site in Hong Kong, *Atmos. Environ.*, 252, 118298, <https://doi.org/10.1016/j.atmosenv.2021.118298>, 2021.

Yee, L. D., Isaacman-VanWertz, G., Wernis, R. A., Meng, M., Rivera, V., Kreisberg, N. M., Hering, S. V., Bering, M. S., Glasius, M., Upshur, M. A., Gray Bé, A., Thomson, R. J., Geiger, F. M., Offenberg, J. H., Lewandowski, M., Kourtchev, I., Kalberer, M., de Sá, S., Martin, S. T., Alexander, M. L., Palm, B. B., Hu, W., Campuzano-Jost, P., Day, D. A., Jimenez, J. L., Liu, Y., McKinney, K. A., Artaxo, P., Viegas, J., Manzi, A., Oliveira, M. B., de Souza, R., Machado, L. A. T., Longo, K., and Goldstein, A. H.: Observations of sesquiterpenes and their oxidation products in central Amazonia during the wet and dry seasons, *Atmos. Chem. Phys.*, 18, 10433–10457, <https://doi.org/10.5194/acp-18-10433-2018>, 2018.

Yee, L. D., Isaacman-VanWertz, G., Wernis, R. A., Kreisberg, N. M., Glasius, M., Riva, M., Surratt, J. D., de Sá, S. S., Martin, S. T., Alexander, M. L., Palm, Brett. B., Hu, W., Campuzano-Jost, P., Day, D. A., Jimenez, J. L., Liu, Y., Misztal, P. K., Artaxo, P., Viegas, J., Manzi, A., de Souza, R. A. F., Edgerton, E. S., Baumann, K., and Goldstein, A. H.: Natural and Anthropogenically Influenced Isoprene Oxidation in Southeastern United States and Central Amazon, *Environ. Sci. Technol.*, 54, 5980–5991, <https://doi.org/10.1021/acs.est.0c00805>, 2020.

Yokelson, R. J., Susott, R., Ward, D. E., Reardon, J., and Griffith, D. W. T.: Emissions from smoldering combustion of biomass measured by open-path Fourier transform infrared spectroscopy, *J. Geophys. Res. Atmos.*, 102, 18865–18877, <https://doi.org/10.1029/97JD00852>, 1997.

Yuan, B., Shao, M., de Gouw, J., Parrish, D. D., Lu, S., Wang, M., Zeng, L., Zhang, Q., Song, Y., Zhang, J., and Hu, M.: Volatile organic compounds (VOCs) in urban air: How chemistry affects the interpretation of positive matrix factorization (PMF) analysis, *J. Geophys. Res. Atmos.*, 117, <https://doi.org/10.1029/2012JD018236>, 2012.

Yuan, B., Liggio, J., Wentzell, J., Li, S.-M., Stark, H., Roberts, J. M., Gilman, J., Lerner, B., Warneke, C., Li, R., Leithead, A., Osthoff, H. D., Wild, R., Brown, S. S., and de Gouw, J. A.: Secondary formation of nitrated phenols: insights from observations during the Uintah Basin Winter Ozone Study (UBWOS) 2014, *Atmos. Chem. Phys.*, 16, 2139–2153, <https://doi.org/10.5194/acp-16-2139-2016>, 2016.

Yuan, Z., Lau, A. K. H., Shao, M., Louie, P. K. K., Liu, S. C., and Zhu, T.: Source analysis of volatile organic compounds by positive matrix factorization in urban and rural environments in Beijing, *J. Geophys. Res. Atmos.*, 114, <https://doi.org/10.1029/2008JD011190>, 2009.

Zhang, Q., Jimenez, J. L., Canagaratna, M. R., Allan, J. D., Coe, H., Ulbrich, I., Alfarra, M. R., Takami, A., Middlebrook, A. M., Sun, Y. L., Dzepina, K., Dunlea, E., Docherty, K., DeCarlo, P. F., Salcedo, D., Onasch, T., Jayne, J. T., Miyoshi, T., Shimonono, A., Hatakeyama, S., Takegawa, N., Kondo, Y., Schneider, J., Drewnick, F., Borrmann, S., Weimer, S., Demerjian, K., Williams, P., Bower, K., Bahreini, R., Cottrell, L., Griffin, R. J., Rautiainen, J., Sun, J. Y., Zhang, Y. M., and Worsnop, D. R.:

Ubiquity and dominance of oxygenated species in organic aerosols in anthropogenically-influenced Northern Hemisphere midlatitudes, *Geophys. Res. Lett.*, 34, L13801, <https://doi.org/10.1029/2007GL029979>, 2007.

Zhang, X., Zhang, C., Sun, X., Yang, J., and Zhu, C.: Mechanism and kinetic study of the reaction of benzoic acid with OH, NO₃ and SO₄ – radicals in the atmosphere, *RSC Adv.*, 9, 18971–18977, <https://doi.org/10.1039/C9RA02457C>, 2019.

Zhao, Y., Kreisberg, N. M., Worton, D. R., Teng, A. P., Hering, S. V., and Goldstein, A. H.: Development of an In Situ Thermal Desorption Gas Chromatography Instrument for Quantifying Atmospheric Semi-Volatile Organic Compounds, *Aerosol Sci. Technol.*, 47, 258–266, <https://doi.org/10.1080/02786826.2012.747673>, 2013.

Zhao, Y., Hennigan, C. J., May, A. A., Tkacik, D. S., de Gouw, J. A., Gilman, J. B., Kuster, W. C., Borbon, A., and Robinson, A. L.: Intermediate-Volatility Organic Compounds: A Large Source of Secondary Organic Aerosol, *Environ. Sci. Technol.*, 48, 13743–13750, <https://doi.org/10.1021/es5035188>, 2014.

Zota, A. R., Calafat, A. M., and Woodruff, T. J.: Temporal Trends in Phthalate Exposures: Findings from the National Health and Nutrition Examination Survey, 2001–2010, *Environ. Health Perspect.*, 122, 235–241, <https://doi.org/10.1289/ehp.1306681>, 2014.

Zwiener, C., Richardson, S. D., De Marini, D. M., Grummt, T., Glauner, T., and Frimmel, F. H.: Drowning in Disinfection Byproducts? Assessing Swimming Pool Water, *Environ. Sci. Technol.*, 41, 363–372, <https://doi.org/10.1021/es062367v>, 2007.